Molecular and functional characterisation of circadian clock regulated RNA-binding proteins from *Arabidopsis thaliana*

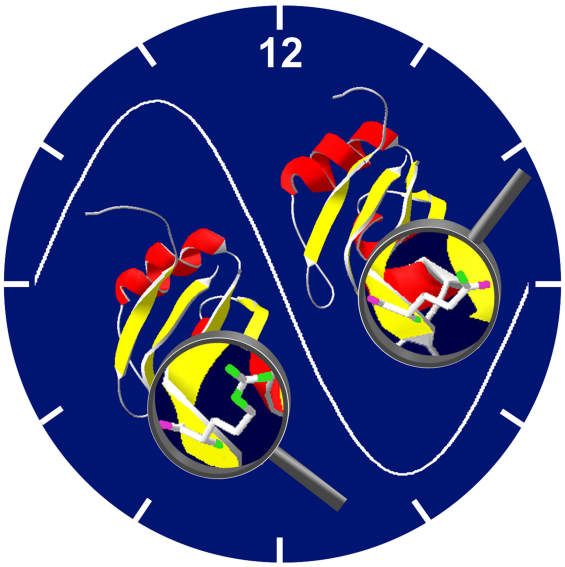

Dissertation

zur Erlangung des Akademischen Grades

Doktor der Naturwissenschaften

(Dr. rer. nat.)

vorgelegt von

Dipl.-Biotech. Jan Christoph Schöning

Fakultät für Biologie der Universität Bielefeld

Dezember 2007

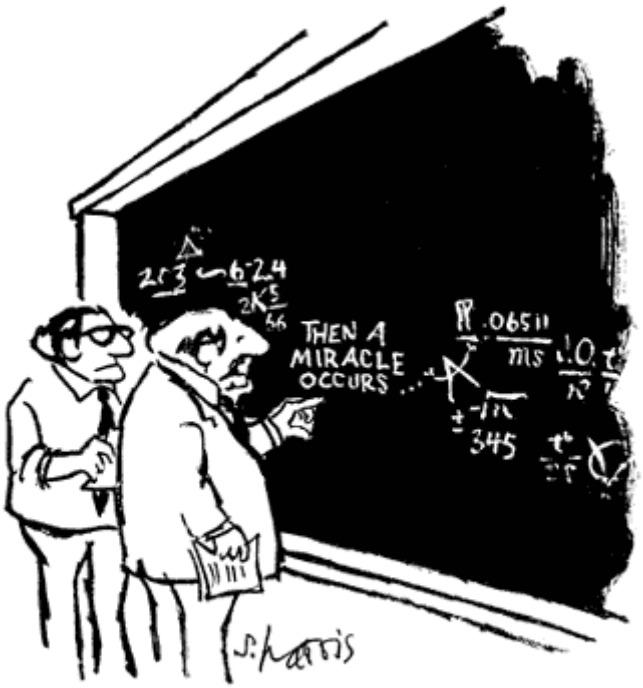

"I think you should be more explicit here in step two."

Table of Contents

1 Summary

The clock-regulated small RNA-binding protein *At*GRP7 (*Arabidopsis thaliana* glycine-rich RNA-binding protein) influences its own circadian oscillations by negative auto-regulation at the post-transcriptional level, presumably by binding to its own transcript. The present work analyses the RNA-binding mechanism of *At*GRP7 and its closest homologue *At*GRP8 at a molecular level. Definite binding sites within the *AtGRP7* and *AtGRP8* transcripts have been identified and binding of both proteins to these sequences has been demonstrated using synthetic oligoribonucleotides. Mutational analysis of the RNA and the proteins has uncovered nucleotides in the RNA targets and amino acids in the RNA recognition motif (RRM), respectively, that are crucial for binding affinity and specificity. Moreover, direct insights into the binding process have been obtained by the establishment of single molecule techniques such as fluorescence correlation spectroscopy and atomic force microscopy-based force spectroscopy. *At*GRP7 requires extended single-stranded regions for target recognition and has influence on the RNA secondary structure. The *At*GRP8 binding process exhibits two distinct steps since specific and unspecific binding events are detectable during target recognition.

In addition to the known regulation of *AtGRP8* by *At*GRP7, a reciprocal regulation of *At*GRP7 and *At*GRP8 *in vivo* has been demonstrated in transgenic plants overexpressing *At*GRP7 and *At*GRP8, respectively (*At*GRP-ox). Moreover, the *At*GRP-ox plants show that *At*GRP7 and *At*GRP8 share a number of downstream target transcripts. These findings extend the current picture of the *At*GRP7 slave oscillator by incorporating a second interdigitated feedback loop centred around *At*GRP8. Furthermore, the relevance of the *At*GRP7 RNA-binding activity for its *in vivo* function has been demonstrated. Mutation of a conserved RRM arginine ($R^{49}Q$) leads to a severe reduction in binding affinity *in vitro*. Overexpression of *At*GRP7, but not *At*GRP7-$R^{49}Q$ in transgenic *Arabidopsis* plants leads to alternative splicing and concomitant decay of endogenous *AtGRP7* transcript. This indicates that high affinity RNA binding is required for the negative auto-regulation of *At*GRP7 *in vivo*. This is the first example for an RNP1 mutation showing a direct correlation of binding affinity *in vitro* and function *in vivo*.

The alternatively spliced *AtGRP* transcripts have a premature termination codon and decay rapidly. To address the mechanism of this rapid degradation *upf1* and *upf3* mutant plants were analysed that are impaired in the nonsense-mediated decay (NMD) of RNAs. Indeed, the alternative *AtGRP* splice forms are increased in the *upf* mutant plants, indicating a previously unknown connection of the circadian clock and the NMD pathway.

1 Zusammenfassung

Das circadian regulierte RNA-Bindeprotein *At*GRP7 (*Arabidopsis thaliana* glycine-rich RNA-binding protein) ist Teil eines negativen Rückkopplungskreises, über den es seine eigene Expression durch Bildung eines alternativ gespleißten Transkripts reguliert. Diese post-transkriptionelle negative Autoregulation wird vermutlich durch eine Bindung des Proteins an sein eigenes Transkript initiiert. In dieser Arbeit wurden die RNA-Bindemechanismen von *At*GRP7 und dem nahe verwandten Protein *At*GRP8 molekularbiologisch charakterisiert. Es wurden spezifische Bindestellen innerhalb der *AtGRP7* und *AtGRP8* Transkripte identifiziert und eine Bindung von *At*GRP7 und *At*GRP8 an diese Sequenzen nachgewiesen. Durch die gezielte Mutation des Proteins und der RNA wurden wichtige Aminosäure-Reste im RRM und Basen in den RNA-Bindestellen für die Bindungsaffinität und Bindungsspezifität identifiziert. Die Etablierung von neuen Einzelmolekül-Techniken zur Analyse von RNA-Protein Interaktionen hat tiefer gehende Einblicke in den Bindeprozess selbst geliefert. Ein Einfluss von *At*GRP7 auf die Sekundärstruktur der RNA wurde mittels PET-FCS nachgewiesen. Die Untersuchung mit AFM zeigte, dass während der RNA-Bindung durch *At*GRP8 unterscheidbare Bindungsereignisse stattfinden.

In vivo Untersuchungen anhand von *At*GRP7 und *At*GRP8 Überexpressionslinien (*At*GRP-ox) haben eine reziproke Regulation von *At*GRP7 und *At*GRP8 gezeigt. Analog zur bereits bekannten negativen Regulation der *AtGRP7* und *AtGRP8* Transkripte in *At*GRP7-ox Pflanzen bewirkt die konstitutive Überexpression von *At*GRP8 ein alternatives Spleißen der endogenen *AtGRP* Transkripte. Die alternativ gespleißten Transkripte weisen ein vorzeitiges Stop-Codon auf und haben eine verringerte Halbwertszeit. Die Stabilität dieser Transkripte ist in *upf1* und *upf3* Pflanzen, in denen der NMD (*nonsense-mediated decay*) von RNAs gestört ist, deutlich erhöht. Dieses deutet auf eine Verbindung zwischen der circadianen Regulation und dem NMD-Pfad hin. Zusätzliche Untersuchungen zeigten, dass *At*GRP7 und *At*GRP8 identische *Target*-Transkripte in *Arabidopsis thaliana* regulieren.

Um einen Einfluss der RNA-Bindeaktivität auf die Auto- und *Target*-Regulation zu untersuchen, wurden transgene Pflanzen hergestellt, die ein mutiertes *At*GRP mit einer Punktmutation in der hoch konservierten RNP1 Region überexprimieren. Der Austausch von Arginin zu Glutamin (R→Q) hat eine starke Reduktion der Bindungsaffinität *in vitro* zur Folge. Die Überexpression von *At*GRP-RQ bewirkt *in vivo* weder eine negative Autoregulation noch eine Regulation von *Target*-Transkripten. Dieses deutet darauf hin, dass die Bindeaktivität essentiell für die Funktion der Proteine *in vivo* ist. Dieses ist das erste bekannte Beispiel für eine RNP1 Mutation, bei der die RNA-Bindeaktivität *in vitro* direkt mit einem Funktionsverlust des Proteins *in vivo* korreliert.

2 Introduction

RNA-binding proteins are involved in the post-transcriptional regulation of gene expression and thus are essential and global players in gene regulation. Throughout their life cycle RNAs are associated with different populations of RNA-binding proteins that control all steps of their life: RNA splicing and maturation, subcellular transport, translational control and RNA degradation (Siomi & Dreyfuss, 1997; Keene, 2001; Mata *et al.*, 2005). Thus, RNA-binding proteins (RBPs) have been studied extensively on the molecular level to gain insight into their binding mechanisms and their functions. During this process the involvement of RBPs has been assigned to different regulatory pathways in the cell. For a glycine-rich RNA-binding protein from *Arabidopsis thaliana*, *At*GRP7, it could be demonstrated that it is part of the circadian system and exerts its activity at the post-transcriptional level (Heintzen *et al.*, 1997). Up to that time regulation of clock components had been postulated to be mainly transcriptionally controlled. Thus, the *AtGRP7* feedback loop represents a new mechanism of clock associated posttranscriptional gene regulation. In the present work an in-depth functional characterisation of *At*GRP7 and the closely related *At*GRP8 protein both *in vitro* and *in vivo* has been performed.

2.1 Circadian clocks

Many environmental factors relevant for the physiology of an organism change periodically throughout the day. Most prominent among these are the rhythmic change of light and darkness and the alteration of temperature. An adaptation to these daily changes is obviously of advantage and thus, rhythmically regulated processes can be observed in nearly all organisms from cyanobacteria to humans (Golden & Canales, 2003; Roenneberg & Merrow, 2003; Dunlap & Loros, 2004; Dodd *et al.*, 2005; McClung, 2006; Wijnen *et al.*, 2006). Moreover, the rhythmic physiological, biochemical, and developmental patterns can not only be seen in light-dark cycles under entrainment conditions but also in constant light or darkness under free-running conditions. That means that the maintainance of rhythmicity must be achieved by an endogenous timekeeper, called the circadian clock. The term circadian is composed of the Latin words *circa* and *dies* and refers to the fact that in a constant environment the length of a period is not fixed exactly to 24 hours, but is always “about one day”. Today it is accepted that circadian clocks operate at the level of

single cells. A complex array of clock proteins regulates each other as well as downstream targets to maintain the 24 hour rhythm.

Circadian rhythms were first noticed in plants. The French astronomer de Mairan discovered that the opening and closing of *Mimosa pudica* leaves could also be observed in constant darkness, suggesting an intrinsic rhythm operating this process (de Mairan, 1729). About 100 years later these results could be verified also for constant light conditions by de Candolle who also showed that the free-running period differs from 24 hours (de Candolle, 1832). Although the existence of an endogenous clock thus had been demonstrated, it took until 1971 that a molecular basis for this clock mechanism was discovered. Konopka and Benzer mutagenised flies (*Drosophila melanogaster*) with ethyl methane sulfonate and screened the F1 generation for individuals with abnormal adult eclosion or locomotor activity (Konopka & Benzer, 1971). These screens were performed in constant darkness after entrainment in twelve hours light – twelve hours dark cycles (LD 12:12). They could identify flies with either short (19 hours) or long periods (28 hours) or with no rhythmicity in eclosion from pupal cases at all. Surprisingly, all phenotypes mapped to a single locus on the X-chromosome, *period* (*per*). Although a first clock component was now identified it took again about 20 years to find a direct hint how clock genes generate circadian rhythms. When the *per* locus was cloned in 1984 the molecular characterisation of circadian oscillations could be started (Reddy *et al.*, 1984). In 1990 Rosbash and colleagues demonstrated that *per* mRNA and PER protein have definite expression maxima in the course of a day and cycle in antiphase (Hardin *et al.*, 1990). Furthermore, they could demonstrate a negative feedback of the PER protein on the expression of its own mRNA, since the overexpression of PER resulted in a decline in endogenous *per* mRNA expression. These facts illustrated impressively the basic principles of molecular clocks that are valid until today: The timed expression of clock proteins on the one hand and the feedback of these proteins on their own expression on the other hand lead to the generation of self-sustained rhythms with a period of about 24 hours. Based on this idea a more complex scheme of molecular clocks was drawn.

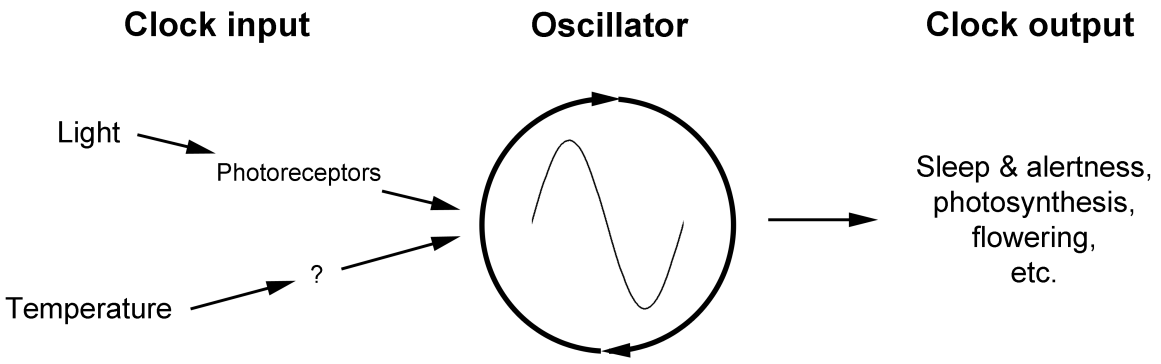

Figure 1. Schematic setup of circadian clocks. A central oscillator generates self-sustained rhythms of about 24 hours and hands them over to components of the clock output. By perception of light and temperature the intrinsic rhythm is synchronised with the environment (Schöning & Staiger, 2005).

Circadian clocks consist of three different parts: The central oscillator generating the intrinsic rhythms, the input pathway synchronising the rhythmicity of the endogenous oscillator to the outside world, and the output pathway translating the signals from the oscillator into physiological and biochemical processes visible in circadian behaviour (Figure 1).

2.1.1 The *Drosophila* clock – prime example for circadian oscillators

Although no direct homologies on the protein levels could be shown between animal, plant, fungal and cyanobacterial clocks, the basic principles of regulation are conserved and can be transferred from one organism to another. As *Drosophila* was the first organism clock genes could be identified in and still is the prime example for circadian regulatory processes, the main characteristics of circadian oscillators shall be explained on the basis of the *Drosophila* model.

Following the discovery of *period* a second *Drosophila* clock gene, *timeless* (*tim*), could be identified in 1994. Like *per*, *timeless* shows a diurnal expression with maximum expression during the night, and loss of function mutants resemble the arrhythmic phenotype of the per^0 mutants (Sehgal *et al.*, 1994). Moreover the loss of Timeless prevents the nuclear uptake of Period – a fact that is important for the regulation of the *Drosophila* clock (Vosshall *et al.*, 1994). For the generation of stable rhythms a few more factors had to be integrated into the model of the central oscillator. Especially factor(s) for the timed transcription of *per* and *tim* were lacking in the circadian system. These proteins were found in form of the two bHLH-PAS (basic helix-loop-helix-PER-ARNT-SIM) transcription factors dClock (dCLK) and Cycle (CYC) (Allada *et al.*, 1998; Darlington *et*

al., 1998; Rutila *et al.*, 1998). dCLK and CYC activate the expression of *per* and *tim* during the light phase leading to the observed high levels of PER and TIM around midnight. PER and TIM themselves feed back on their own expression by repressing the transcriptional activity of dCLK and CYC. Upon decline of PER and TIM the activity of dCLK and CYC is restored, and the loop of the central oscillator is closed (Figure 2).

2.1.1.1 Interlocking feedback loops shape circadian rhythms

The basic transcriptional feedback loop of the fly's clock had to be extended as it was found that the transcription of *dclk* itself is controlled by a second, interlocking feedback loop (Figure 2). This loop is comprised of two additional transcription factors named Vrille (VRI) and PAR Domain Protein 1 (PDP1). The expression of both factors at the end of the subjective day is enforced by dCLK itself. During the night both factors accumulate. First, VRI reaches its maximum and represses *dclk* transcription. After midnight the slower accumulating PDP1 reaches its peak and reactivates, in concert with the decline of the repressor PER, the transcription of *dclk* (Cyran et al. 2003, Glossop et al., 1999). The high degree of regulation of the *dclk* transcription and dCLK activity shows the importance of this factor for stable generation of period length and rhythmicity.

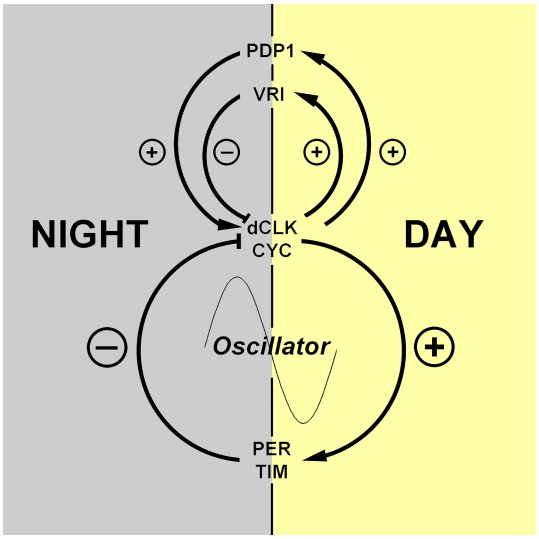

Figure 2. The central oscillator of *Drosophila melanogaster*. The expression of the clock genes *per* and *tim* is controlled by the transcription factors dCLK and CYC. The timed expression of *dclk* and *cyc* itself is controlled by the interlocking PDP1/VRI feedback loop (Schöning & Staiger, 2005).

2.1.1.2 Post-translational control is essential for the *Drosophila* clock

The regulation of PER and TIM activity is controlled post-translationally. Both, the accumulation of PER as well as the nuclear uptake of PER and TIM are controlled by two important classes of enzymes in the circadian system: kinases and phosphatases (Hardin, 2005). The kinase Double-Time (DBT) represses the accumulation of PER by phosphorylation. The phosphorylated form of PER is less stable as it is recognised by Supernumerary Limbs (SLMB), an E3 ubiquitin ligase, that targets PER by ubiquitination for the degradation via the proteasome pathway (Price *et al.*, 1998a). At the same time TIM is also degraded via the proteasome pathway due to a complex formation with the blue light photoreceptor Cryptochrome (CRY). The heterodimerisation of TIM and CRY relies on a light-induced conformational change of CRY (Lin *et al.*, 2001). Thus, after dusk TIM accumulates and stabilises PER by complex formation. Subsequently other kinases gain control over the complex. Casein Kinase II (CKII) and Shaggy (SGG) promote the nuclear uptake of the PER and TIM and the associated kinase DBT by phosphorylation (Harms *et al.*, 2004).

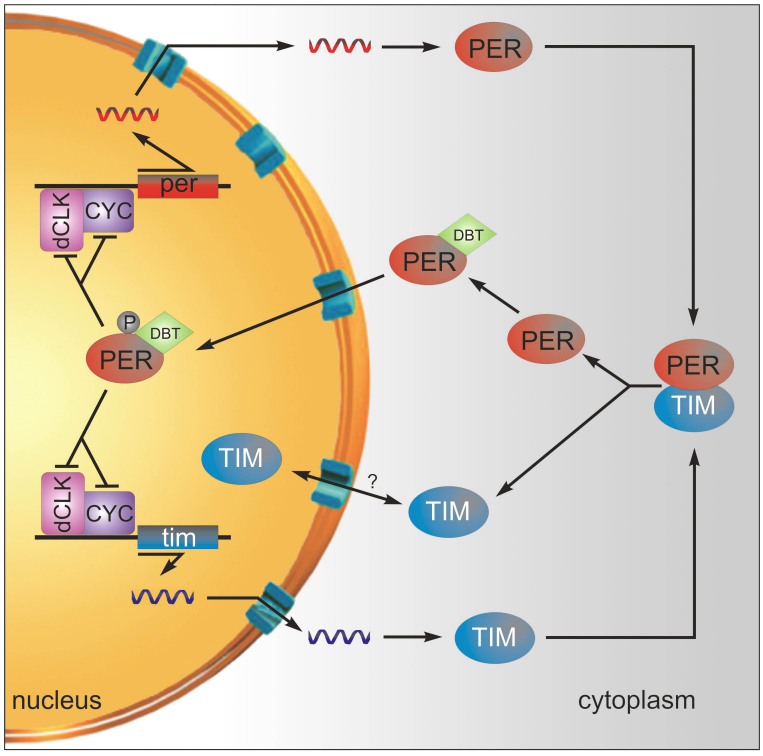

Figure 3: Post-translational regulation is essential for the *Drosophila* clock. Dimerisation and controlled (de-)phosphorylation of PER and TIM is necessary for the regulation of dCLK and CYC activity (Schöning & Staiger, 2006). See text for details.

Young and colleagues detected a cytoplasmic heterodimerisation of PER and TIM shortly after transcripional activation (Meyer *et al.*, 2006). Moreover, they demonstrated by FRET (flourescence resonance energy transfer) experiments that the PER/TIM complex dissociates upon nuclear uptake (Figure 3). Their results support a hypothesis recently suggested by the Rosbash group, proposing a TIM independent model for the circadian regulation of PER activity (Nawathean & Rosbash, 2004). Nawathean and Rosbash showed that the phosphorylated isoform of PER represses dCLK expression in the absence of TIM. Thus they suggest a model in which phosphorylation does not control the import and export of PER/TIM to regulate activity, but instead they conclude that the phosphorylation of PER directly determines its DNA-binding activity and thus its nuclear abundance. Despite this current discussion it is established that the nuclear PER, in association with DBT, hyperphosphorylates dCLK and thus interferes with its own transcription.

In principle the *Drosophila* oscillator consists of two interlocking feedback loops that drive the clock by transcriptional control, but post-transcriptional events like phosphorylation and complex formation stabilise and fine-tune it.

2.1.2 Circadian clocks in plants – the *Arabidopsis* model

Arabidopsis thaliana is the organsim of choice for the investigation of circadian clocks in plants. Although, the basic principles like the division into input, oscillator and output pathways (Figure 1) or the existence of transcriptional feedback loops are conserved in plants, none of the *Arabidopsis* clock proteins shows a significant homology to known clock components from *Drosophila*, mammals or fungi. This implies that the plant clock evolved independently, but in a convergent manner (Salome & McClung, 2004; Schöning & Staiger, 2005; McClung, 2006).

Like in flies the central oscillator of *Arabidopsis* comprises two transcription factors, CIRCADIAN CLOCK ASSOCIATED 1 (CCA1) and LATE ELONGATED HYPOCOTYL (LHY). Both show a circadian expression pattern with maximum abundance in the morning. CCA1 was first discovered in a screen for proteins binding to the promoter of the circadianly expressed LIGHT-HARVESTING CHLOROPHYLL a/b BINDING PROTEIN (LHCP) (Sun *et al.*, 1993). Constitutive overexpression of CCA1 leads to a loss of rhythmicity in endogenous *CCA1*, *LHCB*, *AtGRP7* and *CAT3* expression (Wang & Tobin, 1998). Interestingly, identical effects were observed in an *Arabidopsis* line carrying an insertion of a transposable element upstream of the *LHY* gene (Schaffer *et*

al., 1998). The strong overexpression due to the Cauliflower Mosaic Virus (CaMV) promoter within the transposon insertion further leads to a late flowering phenotype with an elongated hypocotyl.

Both, CCA1 and LHY are members of the Myb type class of transcription factors with a single DNA-binding Myb domain. This Myb domain binds to two closely related DNA motifs called CCA1 binding site (CBS) and evening element (EE). *CCA1* and *LHY* themselves harbour a CBS sequence in their promoter region. CCA1 is able to bind to these sequences and increasing amounts of CCA1 repress the transcription of *CCA1* and *LHY* (Wang & Tobin, 1998; Michael & McClung, 2002). Although CCA1 and LHY feed back on their own expression additional components were required to form a basic oscillator and to obtain a stable oscillation of the clock proteins.

A mutant line showing short period *LHCB* oscillations was the key for the identification of another gene of the central oscillator. The affected gene *TIMING OF CAB EXPRESSION 1* (*TOC1*) belongs to a class of pseudo-response regulators and shows circadian oscillations with peak abundance in the evening, opposite of the *CCA1* and *LHY* maxima (Millar *et al.*, 1995). Low levels in the *toc1* mutant result in a lower *CCA1* and *LHY* level indicating that TOC1 is a positive regulator of their expression. It is unlikely that TOC1 directly activates transcription as it shows no significant DNA binding properties (Strayer *et al.*, 2000). Nevertheless, TOC1 helps to close the loop of the core clockwork: It initiates the transcription of *CCA1* and *LHY* at the beginning of the night. Subsequently, these two transcription factors bind to an evening element within the *TOC1* promoter and repress its transcriptional activity. At the same time CCA1 and LHY also inhibit their own expression by binding to their own promoter (see above). The subsequent decay of CCA1 and LHY restores the expression of *TOC1* and a new cycle can be started (Alabadi *et al.*, 2001). To date no other factors for the timed expression of CCA1 and LHY have been identified on a molecular level. However, mathematical modelling of the *Arabidopsis* circadian system and analysis of a *cca1;lhy* double knock out mutant line have revealed some preference for GIGANTEA (GI) as the missing link (Locke *et al.*, 2005a; Locke *et al.*, 2005b). As predicted by the theoretical model for the *Arabidopsis* oscillator, *GI* mRNA is transiently expressed upon light induction at dawn but high CCA1 and LHY levels repress further *GI* accumulation until the end of the light phase. Afterwards, elevated GI levels are predicted to induce *TOC1* expression at dusk. Accumulation of TOC1 itself represses *GI* transcription and activates the transcription of *CCA1* and *LHY* in concert with an additional component X (Locke *et al.*, 2005b). Recently, parts of this model have experimentally

been verified. The analysis of *gi* loss of function mutants has revealed a direct influence of GI on *CCA1* and *LHY* expression (Martin-Tryon *et al.*, 2006). The reduced *CCA1* and *LHY* peak abundance observed in the *gi-200* and *gi-201* lines resembles those visible in *toc1-2* mutant plants. However, the effects of the *gi* and *toc1* mutations are additive, as the circadian phenotype of a *gi-200 toc1-2* double mutant is more severe than that of the single mutant lines. Thus, it can be assumed that GI and TOC1 have independent fuctions in the core clockwork (Martin-Tryon *et al.*, 2006).

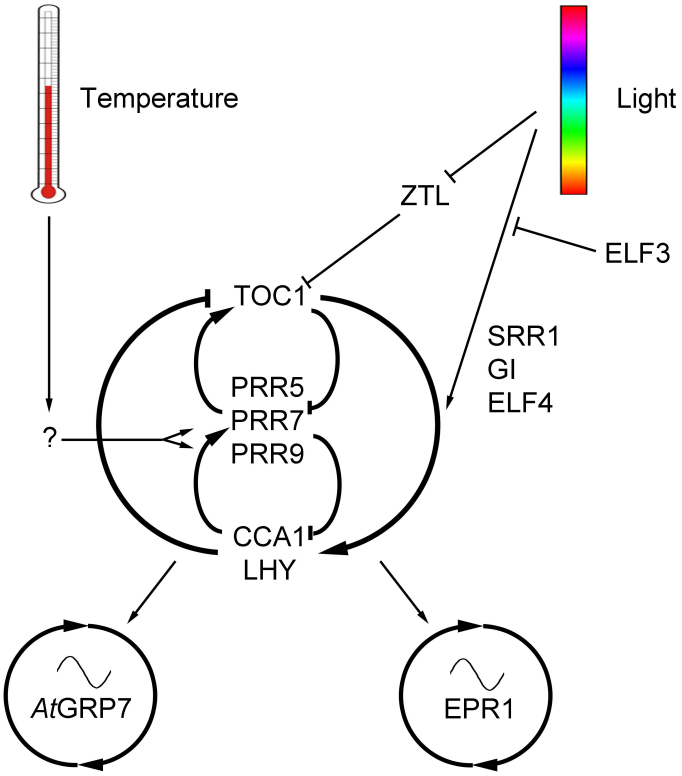

Figure 4: Scheme of the *Arabidopsis thaliana* clock. The central CCA1/LHY – TOC1 oscillator is influenced by many different proteins, has interlocking feedback loops and exhibits secondary oscillators in the output pathways (Schöning *et al.*, 2006). See text for details.

2.1.2.1 Interlocking feedback loops of the *Arabidopsis* clock

Like in *Drosophila* the *Arabidopsis* clock exhibits interlocking feedback loops. In contrast to the fly's system these interlocking loops do not rely on transcription factors but on pseudo-response regulators (PRRs). These PRRs show homology to bacterial response-regulators that act together with sensor histidine kinases in so called two-component systems and exhibit important functions in signal transduction. By a yet unknown

mechanism the *Arabidopsis* PRRs can possibly transmit light and temperature information and thus entrain the core clockwork. Three PRRs (PRR5, PRR7 and PRR9) that oscillate themselves interfere with the activity of TOC1, CCA1 and LHY (Figure 4). Using knockout mutants of these PRRs it could be shown that they repress *CCA1* and *LHY* but activate *TOC1*. In turn they are activated by CCA1 and LHY but repressed by TOC1. This complex feedback structure stabilises and supports the oscillation of the core clockwork (Farré *et al.*, 2005; Nakamichi *et al.*, 2005).

2.1.2.2 Post-translational regulation triggers protein localisation and stability

Post-translational events have also a strong impact on the *Arabidopsis* clock. CASEIN KINASE 2 (CK2) or its regulatory subunit CKB3 influence the period of CCA1 and LHY and other clock proteins (Sugano *et al.*, 1998). The kinase activity of CK2 is directly responsible for these phenotypes since a mutation of the CCA1 phosphorylation sites abolishes CCA1 function (Daniel *et al.*, 2004).

Another post-translational event controls the expression level of TOC1. In the screen for *Arabidopsis* mutants with an altered period length that had identified *toc1* as a short period mutant the long period mutant *toc7* was identified (Millar *et al.*, 1995). The gene affected in this mutant, *ZEITLUPE* (*ZTL*), encoded an F-box protein with an N-terminal LOV (light oxygen voltage) domain and C-terminal kelch repeats (Somers *et al.*, 2000). Later on it was shown that ZTL forms heterodimers with TOC1 via its LOV domain (Más *et al.*, 2003). F-box proteins are important mediators in the ubiquitin proteasome pathway where they connect target proteins with the ubiquitin transferring E3 ligases. Complex formation of ZTL and TOC1 occurs in the dark, afterwards ubiquitinated TOC1 is degraded in a light-dependent process via the proteasome (Más *et al.*, 2003). This light-dependent regulation of TOC1 synchronises the oscillations of the core clockwork with the environmental conditions of the outside world.

Recently another light-dependent post-transcriptional regulation was demonstrated in connection with ZTL (Kim *et al.*, 2007). The ZTL protein levels oscillate with a threefold change in amplitude throughout the day (Kim *et al.*, 2003). Since the ZTL mRNA has a constant steady state abundance, it remained unknown which process drives the circadian regulation of ZTL despite its targeted degradation by the proteasome (Somers *et al.*, 2000; Kim *et al.*, 2003). It could be shown that the interaction of ZTL with GI is the key factor for the regulation of both, GI and ZTL stability (Kim *et al.*, 2007). The interaction of GI

and ZTL occurs via the N-terminal LOV domain of ZTL. Interestingly, the dimerisation process is enhanced and stabilised by blue light, a fact that corresponds well with the implication of LOV domains in blue light signalling. As GI is rhythmically transcribed, the GI expression pattern and thus its availibility for complex formation is directly responsible for the ZTL rhythm (Kim *et al.*, 2007).

2.1.3 Hierachical oscillators in the plant circadian system – the *At*GRP7 feedback loop

Another remarkable feedback mechanism operating the *Arabidopsis* circadian system was discovered in connection with the identification of a novel class of small glycine-rich RNA-binding proteins (van Nocker & Vierstra, 1993; Carpenter *et al.*, 1994; Heintzen *et al.*, 1994). This class of RNA-binding proteins of about 16 kDa comprises a single N-terminal RNA recognition motif (RRM) and a C-terminal glycine-rich stretch with some interspersed serine, tyrosine and arginine residues. Most representatives of this small subset of RNA-binding proteins have been discovered in plants and *Arabidopsis* itself has eight family members (Lorkovic & Barta, 2002). However, related proteins were also found in mammals, amphibians and cyanobacteria. The expression of most of the glycine-rich RBPs is inducible by cold stress (Sachetto-Martins *et al.*, 2000).

For the glycine-rich RNA-binding protein 7 from *Arabidopsis thaliana* (*At*GRP7) it was shown that its RNA and protein are rhythmically expressed (Carpenter *et al.*, 1994; Heintzen *et al.*, 1997). The protein peak was delayed relative to the mRNA peak by about 4 hours suggesting a negative auto-regulation. In transgenic plants overexpressing *At*GRP7, damped oscillations of the endogenous *AtGRP7* mRNA were detected (Heintzen *et al.*, 1997). In addition to the reduced transcript level, it could be shown that the remaining transcript had an intermediate size between pre-mRNA and mature RNA (Staiger *et al.*, 2003). This elongated transcript is generated by the use of a cryptic 5' splice site within the middle of the *AtGRP7* intron (Figure 5). Furthermore, the alternatively spliced transcript has a reduced half-life and a premature termination codon (PTC) preventing further accumulation of functional protein (Figure 5).

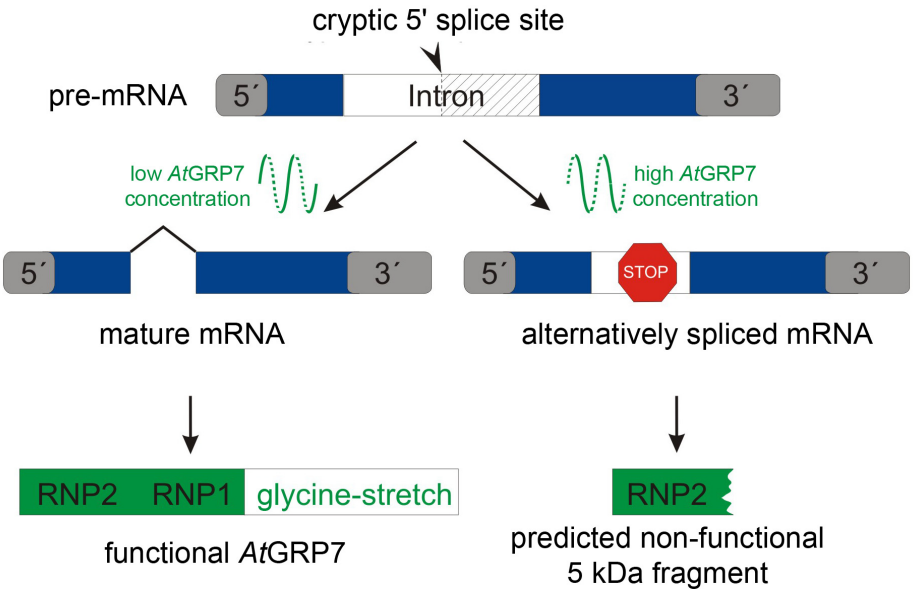

Figure 5: The concentration of *At*GRP7 in the cell influences splice site selection. At low *At*GRP7 levels the *AtGRP7* pre-mRNA is spliced to maturity and functional protein can be produced. Increased *At*GRP7 levels provoke a shift in the splice site selection; the resulting alternatively spliced transcript decays rapidly and does not encode a fuctional protein.

Reporter gene assays with the *AtGRP7* promoter have demonstrated that *At*GRP7 exerts its regulatory activity at the post-transcriptional level (Staiger & Apel, 1999). As it could be shown that *At*GRP7 binds to its own transcript *in vitro* it is likely that *At*GRP7 directly induces the shift in splice site selection (Staiger *et al.*, 2003). The autoregulatory feedback loop of *At*GRP7 can be described as follows. Transcription of *AtGRP7* is activated through binding of CCA1 and LHY to an evening element in the promoter region during the light phase. The *AtGRP7* transcript accumulates with peak abundance in the afternoon and the protein reaches its maximum in the evening. *At*GRP7 binds to its own mRNA, and induces at high levels the shift in splice site selection and the production of the short-lived alternatively spliced transcript prevents further accumulation of the mature mRNA. No further functional protein is produced and the existing *At*GRP7 is proteolytically degraded during the night. Low levels of *At*GRP7 and high levels of CCA1 and LHY at the beginning of the next day start a new cycle. Analysis of other rhythmically expressed genes, such as *CHLOROPHYLL a/b BINDING PROTEIN* (*CAB*) and *CATALASE*, showed that they are not affected by *At*GRP7 overexpression (Heintzen *et al.*, 1997). This implies that *At*GRP7 does not feed back to the central oscillator of *Arabidopsis*. Thus, it was suggested that *At*GRP7 comprises a secondary feedback loop operating downstream of the core clockwork, spreading the signal of the central oscillator to an array of downstream genes in the clock output (Heintzen *et al.*, 1997; Rudolf *et al.*, 2004).

So far, it could be shown that *At*GRP7 also regulates the mRNA abundance of the closely related protein *At*GRP8. Overexpression of *At*GRP7 dampens the oscillations of the *AtGRP8* transcript (Heintzen *et al.*, 1997). The down-regulation of *AtGRP8* provokes the generation of an alternatively spliced transcript, which points to a similar regulatory mechanism as described for the *AtGRP7* auto-regulation (Staiger *et al.*, 2003). Since *At*GRP7 and *At*GRP8 share a 76.9 % identity they probably perform related functions.

2.1.3.1 RNA-binding proteins exert circadian control

Circadian control by RNA-binding proteins has emerged to be a common mechanism across different species. In *Drosophila,* LARK protein but not *lark* mRNA cycles in abundance with highest levels at the end of the light phase and a trough before dawn (McNeil *et al.*, 1998). Physiological analysis revealed that LARK functions as a clock controlled repressor of adult eclosion from pupal cases, a process that is known to be clock controlled and takes place at the transition from dark to light phase. LARK levels and eclosion events cycle in anti-phase and LARK gene dosage experiments yielded a phenotype with earlier or later eclosion for low or high level LARK mutants, respectively. In per^{01} mutant flies LARK and eclosion rhythmicity is completely abolished (Newby & Jackson, 1996; McNeil *et al.*, 1998). Recently, several LARK target transcripts have been identified by a "Ribonomics" approach (Huang *et al.*, 2007). LARK-containing ribonucleoprotein complexes were immunoprecipitated, the bound RNAs were extracted and subsequently analysed by hybridisation to whole-genome microarrays. Several circadianly regulated transcripts were found among the target transcripts. However, no feedback on components of the central oscillator, such as *per*, was detected. Thus, LARK presumably acts downstream of the fly clock (Huang *et al.*, 2007).

A post-transcriptional feedback of mouse LARK (mLARK) on the essential clock component mouse Period 1 (mPER1) could be demonstrated by mLARK knockdown and overexpression experiments (Kojima *et al.*, 2007). Like in *Drosophila* mLARK shows a circadian expression pattern only for the protein. By interaction with the *mper1* 3'UTR mLARK activates translation in a Cap/poly(A) dependent manner. The effect of mLARK on mPER expression is consistent with shortened or lengthened periods in mice with reduced or increased mPER1 levels, respectively. It is discussed whether the post-transcriptional regulation by mLARK contributes to the generation of mPER1 rhythm since mPER1 translation is delayed relative to its transcription (Kojima *et al.*, 2007).

2.1.3.2 Physiological function of *At*GRP7

Beside the autoregulatory mechanism and the regulation of *AtGRP8* only little is known about the physiological role of *At*GRP7. It could be shown that both, *At*GRP7 and *At*GRP8 are induced upon cold stress and are possibly repressed upon treatment with abscisic acid (ABA) (Carpenter *et al.*, 1994; Heintzen *et al.*, 1994; Cao *et al.*, 2006). Thus, a role for *At*GRP7 and *At*GRP8 in abiotic stress response and ABA signaling has been discussed.

Recently a new function for *At*GRP7 has been reported in connection with biotic stress. The plant pathogen *Pseudomonas syringae* that is also capable to infect *Arabidopsis thaliana*, injects type III effector proteins into the plant cell that repress the plant innate immunity (Fu *et al.*, 2007). One of these type III effectors, HopU1, encodes a mono-ADP ribosyltransferase and is able to ADP-ribosylate arginine residues. During the pathogen infection it represses the hypersensitive response, a programmed cell death associated with innate immunity. Interstingly, among the possible targets in *A. thaliana* were three cholorplast RBPs and two glycine-rich RBPs, namely *At*GRP7 and *At*GRP8. Additionally, an *atgrp7-1* knockout line showes higher sensitivity for pathogen infection (Fu *et al.*, 2007). It could be shown that the conserved arginine Arg^{49} of *At*GRP7 is ADP-ribosylated by HopU1 (J.R. Alfano, Plant Science Initiative and Department of Plant Pathology, University of Nebraska, Lincoln, USA, personal communication). Alfano and colleagues concluded that the ADP-ribosylation of this highly important amino acids (see below) may interfere with RNA-binding activity of *At*GRP7 and thus be a key to post-transcriptional regulation of specific mRNAs in response to pathogenic stress (Fu *et al.*, 2007).

Notably, closely related glycine-rich RNA-binding proteins from other organisms are involved in translational control. Mouse neuroblastoma cells overexpressing a myc-tagged version of the mammalian RBM3 showed a stimmulation of the global gene expression and it could be shown that RBM3 interacts with the large subunit of translating ribosomes (Dresios *et al.*, 2005; Smart *et al.*, 2007). This translational enhancement seems to be associated with the reduction a microRNAs (miRNAs) containing fraction (Dresios *et al.*, 2005). Translation regulating activities could also be observed in case of the *Xenopus laevis* cold inducible RNA-binding protein 2 (xCIRP2) (Matsumoto *et al.*, 2000). xCIRP2 is up-regulated upon cold induction like its rhythmically expressed mammalian homologue CIRP and the previously discussed RBM3. Because *At*GRP7 shows a high degree of homology to these proteins it is tempting to speculate that *At*GRP7 may also exert translational control in addition to its described post-transcriptional regulatory activity (cf. 2.1.3).

2.2 The RNA Recognition Motif (RRM)

The post-transcripional negative autoregulatory feedback loop indicates that RNA-binding activity of *At*GRP7 is essential for its regulatory function in the cell (cf. 2.1.3). *At*GRP7 and *At*GRP8 feature an RNA-binding motif called RNA recognition motif (RRM). The RNA recognition motif is an RNA-binding platform that is conserved in all kingdoms of life and can be even found in viruses (Maris *et al.*, 2005). Well characterised representatives of RRM proteins are the spliceosomal protein U1A, the splicing factor Heterogenous Nuclear Ribonucleoprotein A1 (hnRNP A1), the Poly(A) Binding Protein (PABP), the *Drosophila* protein Sex-lethal (SXL) and many other (Maris *et al.*, 2005). The RNA-binding motif consists of four anti-parallel β-strands with two interspersed α-helices in the order β_1-α_1-β_2-β_3-α_2-β_4 (Figure 6). The four β-strands form a stable β-sheet that comprises the RNA-binding interface.

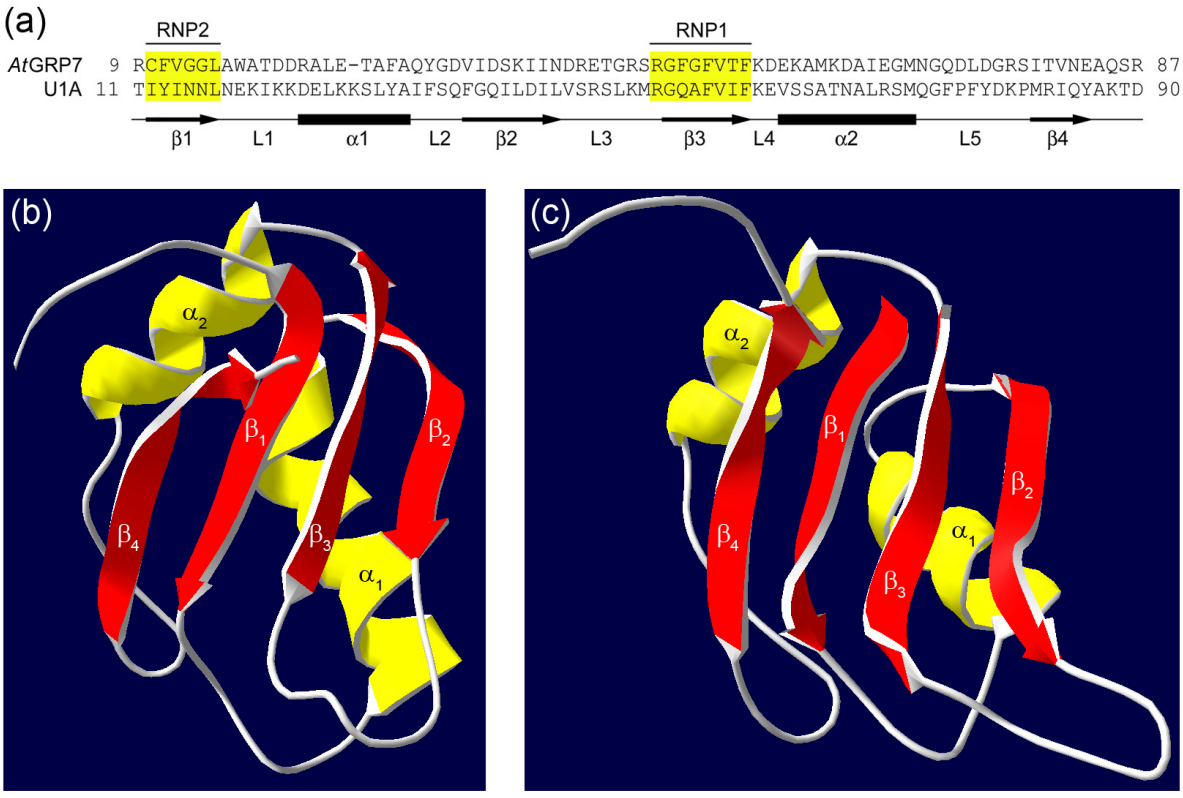

Figure 6: Tertiary structure of the RNA recognition motif. (a) Alignment of the *At*GRP7 RRM amino acid sequence upon the N-terminal RRM of human U1A (Schöning *et al.*, 2007). (b) Structure of the N-terminal RRM of human U1A according to the X-ray crystal structure by Nagai *et al.* (Nagai *et al.*, 1990). (c) Predicted structure of the *At*GRP7 RRM according to homology modeling analysis with CPHmodels 2.0 (Lund *et al.*, 2002). α-helices and β-strands are indicated, L = loop.

Two highly conserved regions have been identified within this structure, the so-called ribonucleoprotein domains (RNPs), the RNP-2 hexapeptide (Ile/Val/Leu-Phe/Tyr-Ile/Val/Leu-X-Asn-Leu) on β_1 and the RNP1 octapeptide (Lys/Arg-Gly-Phe/Tyr-Gly/Ala-Phe/Tyr-Val/Ile/Leu-X-Phe/Tyr) on β_3 (Figure 6). Most of the eukaryotic RRM proteins contain two or more RRMs which allows them to recognise longer RNA sequences or additional RNA-binding domains, such as zinc-finger motifs, for binding of other targets (Maris *et al.*, 2005).

2.2.1 RRM proteins bind to single-stranded nucleic acids

The RRM is known as a classical RNA binding motif. However, some RRM proteins, such as hnRNP A1 or TIAR (TIA-1 Related Protein), can also bind single-stranded DNA (Ding *et al.*, 1999; Suswam *et al.*, 2005). The second RRM of TIAR, a factor involved in splicing, translational control and apoptosis in humans, binds with a very high affinity to uridine-rich sequences within the pre-mRNA of various transcripts. Recently it could be shown that complex formation of TIAR with these targets can be competed with an oligodeoxyribonucleotide derived from the recognised RNA sequence (Suswam *et al.*, 2005). Interestingly, both RNA and DNA are bound by RRM2. Additionally, the DNA oligonucleotide was also bound by the first RRM that did not show a significant binding for RNA molecules of the same sequence. More strikingly, the equilibrium binding constant of TIAR was about six-fold lower for the DNA oligonucleotide in comparison to the homologous RNA oligo (Suswam *et al.*, 2005). This lead to the idea that TIAR has a dual role in the cell. *In vitro* assays showed that the protein can be associated to the single-stranded DNA during the transcription until it is displaced by the polymerase. Afterwards, TIAR binds to the newly sythesised transcript and exerts post-transcriptional control during splicing and translation (Suswam *et al.*, 2005).

2.2.2 Influence of RNA secondary structure on target recognition

Although RNA binding by RRMs requires single-stranded regions in the RNA targets, secondary structures can play an important role in target recognition. The N-terminal RRM of U1A, presumably one of the best characterised RNA-binding domains, specifically interacts with a 21 nucleotides long stem-loop structure within the U1 small nuclear RNA (snRNA) known as U1 hairpin II (U1hpII). The U1 snRNA recruits several specific RNA

binding proteins, such as U1A and U170K, and forms the snRNP particle together with other RNA-binding proteins, so called Sm or core proteins. The U1 snRNP specifically binds to the 5' splice site of the pre-mRNA via direct basepairing of the U1 snRNA. Subsequently, the other subunits of the spliceosome are recruited in a definite order and the intronic sequence is removed in form of the so called lariat, which is rapidly degraded (Will & Lührmann, 2001).

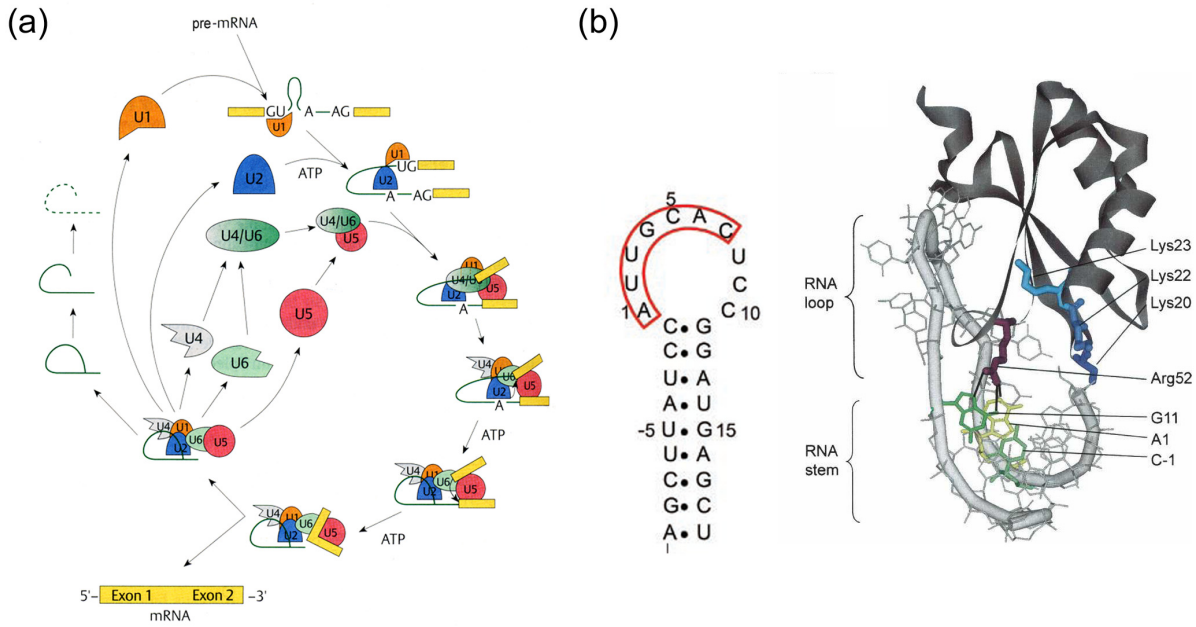

Figure 7: Spliceosome assembly, splicing of pre-mRNAs and the U1A-U1hpII complex. (a) The assembly of the different UsnRNPs within the spliceosome during the removal of intronic sequences from pre-mRNAs (Knippers, 2001). (b) The U1A protein binds to a short hairpin loop, called U1hpII, within the U1 snRNA (left). Critical amino acids and bases for the U1A-U1hpII complex formation are indicated (right) (Law *et al.*, 2006a; Law *et al.*, 2006b).

The consensus sequence recognised by U1A is a 7 nucleotide (nt) single-stranded region at the 5' end of the hairpin loop. However, a closed loop is essential for a stable complex formation (Law *et al.*, 2006b). Although no direct influence of the closing basepair on the binding affinity can be observed, the strong G-C connection prevents an opening of the essential 10 nt loop (Figure 7). Due to an alternative structure that fits less to the binding pocket of the protein a breathing of the loop significantly reduces binding affinity (Law *et al.*, 2006b).

2.2.3 Aromatic amino acids are the heart of the binding motif

Highly conserved aromatic amino acid residues at the positions three and five in RNP1 and at position two in RNP-2 are important players in the contact formation between the RRM and the RNA (Maris *et al.*, 2005). Their strong influence on the stability of RNA-protein complexes could be demonstrated in *in vitro* binding experiments and by analysis of co-crystal structures of several RRM proteins (Oubridge *et al.*, 1994; Price *et al.*, 1998b; Deo *et al.*, 1999; Ding *et al.*, 1999; Handa *et al.*, 1999; Allain *et al.*, 2000; Law *et al.*, 2005). The aromatic rings of these residues are stacked by two bases of the core target sequence resulting in a rearrangement of the DNA or RNA target within the binding site (Maris *et al.*, 2005). Surprisingly, these contacts have no impact on target discrimination. Interactions with all four bases (A, C, G, and U) have been found. Thus, other residues within the RNPs and in between are required for target recognition and the stability of the RNA-protein complex (Law *et al.*, 2006a). The loop1 (between β_1 and α_1) and loop3 (between β_2 and β_3) regions have previously been identified as structures supporting the complex formation (Figure 6). Insertion of additional amino acids or deletion of residues within these loops led to a severe reduction of the binding affinity of the U1A protein (Boelens *et al.*, 1991; Katsamba *et al.*, 2002).

2.2.4 Positively charged amino acids support stable binding

Positively charged amino acids have been assumed to be essential for a stable RNA binding (Law *et al.*, 2006a). Three lysine residues within the first loop of the U1A RRM1 have been analysed by mutational analysis with respect to their importance for complex stability. Each residue by itself did not contribute much to the binding affinity (Figure 7). However, double and triple mutants showed an extreme loss of binding. Supported by the fact that increasing salt concentrations had an equivalent effect, Law and colleagues concluded that positively charged amino acids in close distance to U1hpII stabilise the complex by electrostatic interactions without having direct contact to the nucleic acid (Law *et al.*, 2006a). An influence of U1A loop3, especially the amino acids serine 46 and 48 as well as leucine 49, on the specific recognition of U1hpII has been demonstrated (Allain *et al.*, 1996; Tang & Nilsson, 1999). These residues participate, together with parts of loop1, in the “rigid body” interaction of the RBP and the closing basepairs of the stem-loop structure of U1hpII representing the first step in of complex formation (Allain *et al.*, 1996; Tang & Nilsson, 1999). Subsequently, rearrangements of the hairpin loop and the protein

surface take place. These changes expose the hydrophobic surface of the β-sheet to the RNA bases and allow stacking and hydrophobic interactions with the single-stranded core sequence (Allain *et al.*, 1996). This induced-fit mechanism on the basis of sequence and structure recognition finally yields an extremely tight connection of RNA and protein with an equilibrium dissociation constant of about 3×10^{-11} (Law *et al.*, 2006a).

2.2.5 A conserved basic amino acid residue is essential for binding-initiation

A highly conserved basic amino acid residue at position one of the RNP1 octapeptide emerged to be a key residue in the first steps of target binding (Tang & Nilsson, 1999; Allain *et al.*, 2000; Law *et al.*, 2006a). In crystal structures it can be seen that this residue is placed at the transition of loop 3 to β_3. Both, *At*GRP7 and *At*GRP8 have like U1A, hnRNPA1 and the second RRM of SXL an arginine residue at this position (Nagai *et al.*, 1990; Lee *et al.*, 1997; Ding *et al.*, 1999). For U1A the co-crystal structure and subsequent molecular dynamics simulations predicted a direct contact of Arg^{52} to the first adenine residue of the loop as well as to the guanine of the loop-closing basepair via hydrogen bonds (Oubridge *et al.*, 1994; Tang & Nilsson, 1999). Later on these predictions were verified by Laird-Offringa and co-workers. By mutational analysis of the conserved aromatic amino acid residues within the RNPs they could further show a direct interaction of Arg^{52} with Arg^{47} (Law *et al.*, 2006a). The connection of these two arginines locks the Arg^{52} into a position in which it can subsequently receive the incoming hairpin. This structural arrangement is the prerequisite for the subsequent induced fit process (cf. 2.2.4). After the rearrangement of RNA and protein the flexible loop 3 structure locks the complex by protruding through the RNA loop (Law *et al.*, 2006a). These multiple interactions and functions of $arginine^{52}$ may be an explanation for the observed loss of binding in an Arg^{52}Gln mutation (Nagai *et al.*, 1990). Nagai and co-workers individually mutated all lysine and arginine residues within the first 102 amino acids of the N-terminal U1A RRM since crystallographic studies of DNA-protein complexes had revealed crucial contacts between Lys and Arg residues and the phosphate backbone or bases of the DNA (Nagai *et al.*, 1990; Steitz, 1990). Among all tested U1A variants several showed a reduced binding affinity. However, only in the Arg^{52}Gln mutant the binding was completely abolished (Nagai *et al.*, 1990). This indicates that Arg^{52} in U1A and possibly arginine residues at the same position in other RBPs are essential for stable RNA binding. Nevertheless, a direct relevance of the conserved RNP1 arginine for the physiological function of RNA-binding proteins can only be demonstrated by analysis *in vivo*.

2.3 New methods for nucleic acid – protein interaction analysis: single molecule measurements

During recent years several powerful tools for the analysis of RNA-protein interactions have emerged. Most prominent among them are X-ray crystallisation and nuclear magnetic resonance (NMR), and most of the known features of RBPs presented in section 2.2. are based on results gained by these two methods. Although both techniques provide a good insight into the binding mechanism of the analysed molecules they have a few disadvantages. The production of highly structured crystals is quite difficult and depends on the properties of the protein under investigation. Highly flexible or unstructured regions counteract the crystal formation. This problem occurs even more frequently if co-crystallisation of a protein with a specific ligand is carried out. A second disadvantage concerns the obtained crystal structures. They only represent a static view of the analysed protein. However almost all complexes of proteins and their ligands are highly dynamic. Thus, a lot of information about the mode of action gets lost upon forming fixed structures (Morikis & Lambris, 2004).

In this context the usage of NMR is an improvement as it gains insight into dynamic processes. For this purpose an isotope labelled protein preparation is titrated with a unlabelled ligand. Several NMR spectra are recorded to follow differences due to the ligand binding and intramolecular rearrangements. However, the size of the analysed proteins or protein-complexes is limited to about 30 kDa. Moreover, the interpretation of these spectra is sometimes extremely difficult and ambiguous due to a heterogeneous protein population since NMR spectra are done as ensemble measurements, (Morikis & Lambris, 2004).

As a result alternative tools have been developed for the analysis of nucleic acid-protein interactions at a single molecule level. Atomic force microscopy based force spectroscopy (AFM-FS) and fluorescence correlation spectroscopy (FCS) have successfully been established for the analysis of protein-protein and DNA-protein complexes (Xu *et al.*, 2001; Ros *et al.*, 2004; Neuweiler & Sauer, 2005; Bartels *et al.*, 2007).

2.3.1 Atomic force microscopy based force spectroscopy (AFM-FS)

AFM has been developed as a tool for scanning and displaying surfaces at a nanometer scale (Binnig *et al.*, 1986). The scanning process can be performed in a contact- or non-contact mode. In the contact mode the tip of the AFM is directly pressed on the sample and moved (scanned) over the surface. The movements of the tip are recorded by the reflection of a laser that is spotted on the top of the cantilever. The reflected light is detected by an array of four photodiodes. By this four-field photodetector vertical as well as lateral deflection of the tip and the cantilever can be recorded (Figure 8 a).

In the non-contact mode the cantilever is oscillated by a piezo. Due to varying distances, and thus varying forces, between tip and surface the frequency or amplitude of the oscillating cantilever changes. These changes are again recorded by laser deflection and translated into the resulting image of the surface (Piehler, 2005).

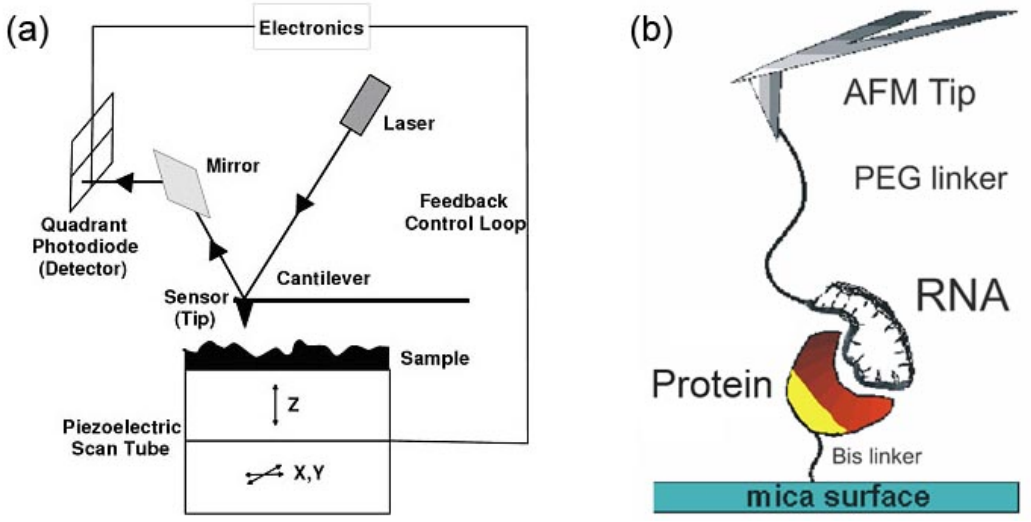

Figure 8: Setup an atomic force microscope. (a) Setup for scanning and displaying surfaces (see text). (b) Setup for AFM based force spectroscopy studies; here the setup is shown in the form as the AFM was used for RNA-protein interaction studies during this thesis (kindly provided by Alexander Fuhrmann).

The same setup as described for the displaying AFM can be used for the analysis of receptor-ligand interactions with a technique called atomic force microscopy based force spectroscopy. For this purpose one of the interaction partners is spotted on the surface, whereas the other is linked to the AFM-tip (Figure 8 b). The cantilever is moved down until it has contact to the surface allowing the two reaction partners to interact and to form stable complexes. Now the cantilever is pulled up leading to a stretching of the complex that is detected by an increased force on the tip. At a certain force, the complex is disrupted

and the cantilever moves back to its starting position allowing a new cycle. During the whole measurement the position of the cantilever as well as the applied force are recorded yielding the characteristic force-distance curves (Figure 9).

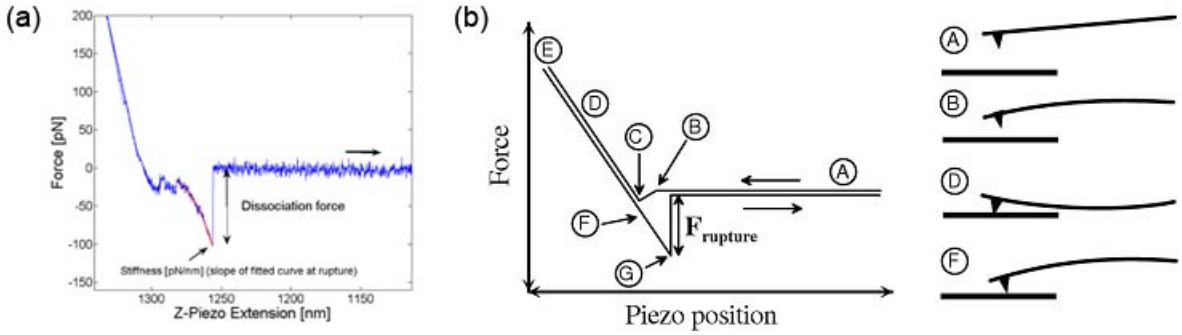

Figure 9: Force-distance curves. (a) Typical force-distance curve obtained by AFM-FS. (b) Scheme of a force-distance curve illustrating approching of the tip (A), electrostatic or van der Waals attraction (B), pressing of the tip on the surface (D) after the first contact (C). During the retraction the cantilever experiences an attractive force (F) causing the tip to remain in contact with the sample until the elastic restoring force exceeds the attractive force (G) and the complex is disrupted (kindly provided by Alexander Fuhrmann).

A difficulty that occurs during analysis of nucleic acid-protein complexes by AFM-FS has been observed on the basis of experiments with DNA-binding proteins. The heterogenity of chemical bonds complicates the interpretation of data obtained from protein-DNA complexes, a fact that is even more problematic in case of RNA-protein complexes due to the more distinct secondary structure of RNA.

2.3.2 Fluorescence correlation spectroscopy (FCS)

Fluorescence correlation spectroscopy as a tool for biophysics was developed by Madge in 1972 and is based on the tracking of fluorescent labelled molecules in very small confocal volume (Madge, 1976). Interactions of the, usually small, labelled receptor molecule with a large, non-fluorescent ligand are detected by monitoring differences in the diffusion time or the fluorescence intensity of the sample (Hess *et al.*, 2002; Piehler, 2005).

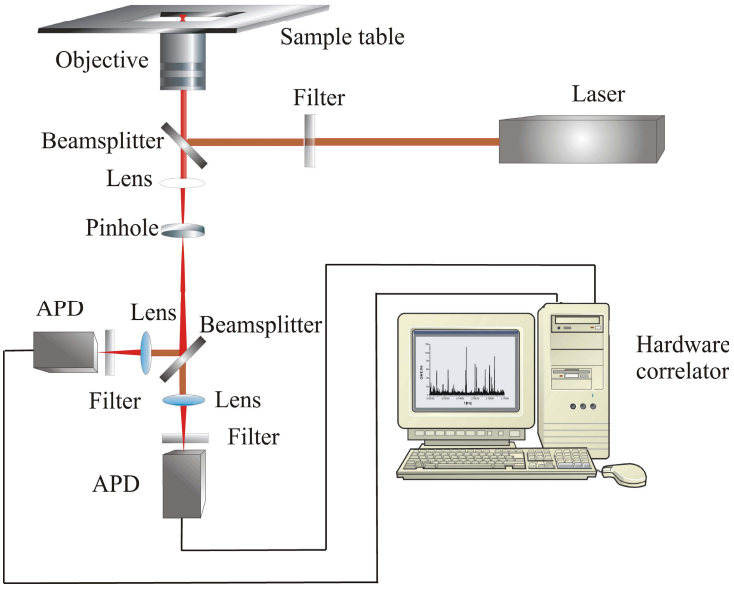

Figure 10: Fluorescence correlation spectroscopy setup consisting of a standard inverted epifluorescence microscope, a Helium-Neon laser, two avalanche photodiodes, and a hardware correlator card (kindly provided by Dr. Mark Schüttpelz).

FCS has been used successfully for the analysis of binding kinetics of DNA molecules, or wide-range ligand-receptor interactions (Kinjo & Rigler, 1995; Schuler *et al.*, 1999; Wohland *et al.*, 1999; Margeat *et al.*, 2001). Moreover, modifications of the principle setup allow the study of protein folding events or the monitoring of conformational dynamics of DNA-hairpin structures by PET-FCS (photoinduced electron transfer-fluorescence correlation spectroscopy) (Neuweiler *et al.*, 2005; Kim *et al.*, 2006). PET-FCS uses the quenching dynamics of the fluorescent dye on a sub millisecond time scale for the prediction of RNA secondary structures. Thus, FCS and PET-FCS are envisaged to be new, powerful tools for the analysis of RNA-protein interactions and conformational dynamics during RNA-protein complex formation.

2.4 Goals of this work

The small glycine-rich RNA-binding protein *At*GRP7 operates downstream of the *Arabidopsis thaliana* central oscillator. Both the transcript and the protein oscillate with a peak in the subjective evening. In transgenic plants ectopically overexpressing *At*GRP7 oscillation of endogenous *AtGRP7* is strongly depressed, indicating that negative feedback contributes to *AtGRP7* rhythmicity. This auto-regulation occurs at the post-transcriptional level, as in *At*GRP7-ox plants the use of a cryptic intronic 5' splice site generates a short-lived splice variant with a premature termination codon (PTC) at the expense of the mRNA.

The main objectives of this work are a detailed characterisation of the RNA-binding properties of *At*GRP7 and its closest homologue *At*GRP8 *in vitro* and the investigation of the molecular mechanism underlying the *At*GRP7 slave oscillator *in vivo*.

The binding process is to be characterised *in vitro* in ensemble measurements and at a single molecule level (in cooperation with the Physics department within the collaborative research centre SFB613). For that purpose, the exact binding sites within the *AtGRP* transcripts have to be mapped to design short synthetic oligoribonucleotides (ORN) covering the identified target sequences. These ORN shall subsequently be used in electrophoretic mobility shift assays (EMSA), fluorescence correlation spectroscopy and atomic force microscopy-based force spectroscopy to obtain specific binding parameters. Mutational analysis of the proteins is to be performed to identify residues that are critical for the RNA binding *in vitro.*

The requirements for a stable binding *in vitro* shall be correlated with *in vivo* function. Towards this end transgenic plants are to be established that constitutively overexpress wild type *At*GRP7 and *At*GRP8 as well as mutated variants that are impaired in RNA binding. The influence of the overexpression of the different protein variants on alternative splicing, mRNA and protein abundance as well as rhythmicity is to be analysed.

3 Materials and Methods

3.1 Plant growth and treatment

3.1.1 Plant growth

Arabidopsis thaliana seeds were surface-sterilised using 6% NaOCl, stratified at 4 °C for two days, germinated and grown on MS medium (Murashige & Skoog, 1962) supplemented with 0.5 % Sucrose and appropriate antibiotics in 16-h light/8-h dark cycles at a constant temperature of 20 °C. After about ten days, seedlings of comparable size were transferred to fresh MS plates without Sucrose and antibiotics. To obtain seeds, plants were transferred to soil and grown to maturation under long day conditions in the greenhouse.

3.1.2 Plant harvest

Aerial parts of plants grown on MS-agar were harvested at defined time points across the day and quickly frozen in liquid nitrogen. The plant material was stored at –80 °C for further analysis.

3.2 Molecular biology methods

3.2.1 RNA preparation

Harvested plants were mortar grinded in liquid nitrogen. The equivalent of 300 µL of frozen plant powder were homogenised in 1 mL of Tri-reagent (0.4 M Ammonium Thiocyanate, 0.8 M Guanidinium Thiocyanate, 4.35 % Glycerol, 0.1 M Sodium Acetate pH 5.2, and 38 % acidic Phenol) with a mini pestle. After centrifugation for 10 minutes at 12,000 × g and 4 °C the supernatant was transferred to a new tube. The lysate was extracted twice with 200 µL of Chloroform/Isoamyl Alcohol (24:1). Subsequently the RNA was precipitated from the supernatant with 600 µL 2-Propanol for 10 min at room temperature. The RNA was pelleted by centrifugation at 12,000 × g and 4 °C for 15 minutes and washed twice with 1 mL of 70 % Ethanol. The pellet was air dried and dissolved in an appropriate amount of RNase free water.

3.2.2 Generation of hybridisation probes

Hybridisation probes were made with a random prime labelling kit (Fermentas, St. Leon-Rot, Germany). 50 ng of template (either a purified PCR product or a linearised plasmid containing the cDNA sequence) were incubated with 2 µL 10 × Klenow reaction buffer and 2 µL of the appropriate primer (Table 1) for 10 minutes at 95 °C. Subsequently, 2 µl of 10 × labelling buffer –dATP, 2 µl of α-[^{32}P]-dATP (110 TBq/mmol), and 1 µL of Klenow Exo$^-$ were added and the sample was incubated at 37 °C for 1 hour. Free nucleotides were removed by gel filtration via Illustra MicroSpin S-200 HR columns (GE Healthcare, Freiburg, Germany). Quantification was done by measuring Čerenkov radiation in a 1900CA Tri-Carb Liquid scintillation analyser (Packard/Perkin Elmer, Waltham, MA, USA).

3.2.3 Northern blot analysis

8 – 12 µg of total RNA were separated on a denaturing 1.5 % Agarose-Formaldehyde gel and transferred onto a GeneScreen® nylon membrane (Perkin Elmer, Waltham, MA, USA) in 10 × SSC buffer (0.15 M Sodium Citrate, 1.5 M NaCl). The RNA was crosslinked to the membrane by UV-radiation (2.4×10^6 J cm^{-1}) in a Stratalinker (Stratagene, La Jolla, CA, USA) followed by baking at 80 °C for 1 hour. Hybridisation was performed over night in HYBSOL (1.5 × SSPE, 7 % SDS, 10 % PEG 8000, 100 µg/ml Salmon Sperm DNA, and 250 µg/ml Heparin) with 4×10^6 cpm α-[^{32}P]-dATP labelled probes and at hybridisation temperatures as listed below (Table 1).

Table 1: Probes and conditions used for hybridisation of northern blots.

Target	AGI	Primer	T_{Hy} [°C]	T_W [°C]	Washing buffer
endogenous *AtGRP7*	At2g21660	AGRP19	58	42	1 × SSC, 0.1 % SDS
endogenous *AtGRP8*	At4g39260	AGRP120	52	42	1 × SSC, 0.1 % SDS
total *AtGRP7*	At2g21660	$p(dN)_6$	65	50	0.2 × SSC, 0.1 % SDS
total *AtGRP8*	At4g39260	$p(dN)_6$	65	50	0.2 × SSC, 0.1 % SDS
ACTIN2	At3g18780	$p(dN)_6$	65	50	0.2 × SSC, 0.1 % SDS
AtTLL1	At1g45201	$p(dN)_6$	65	50	0.2 × SSC, 0.1 % SDS
AtAILP1	At5g19140	$p(dN)_6$	65	50	0.2 × SSC, 0.1 % SDS

T_{Hy}, Hybridisation temperature; T_W, Washing temperature; AGI, *Arabidopsis* gene identifier. Primers see Table 2; $p(dN)_6$ random hexamer primers were purchased from Invitrogen (Karlsruhe, Germany).

The membranes were washed two times for 15 minutes with 0.2 or 1 × SSC, 0.1 % SDS at 42 or 50 °C (Table 1). The blots were developed by exposure to FUJI SuperRX X-ray films (Hartenstein, Würzburg, Germany) or PhosphorImaging (PI) screens (MolecularDynmics, Freiburg, Germany) for 1 to 7 days. PI screens were scanned on a Typhoon 8000 PhosphorImager and analysed by using ImageQuant software (Amersham Pharmacia Biotech, Freiburg, Germany).

3.2.4 cDNA synthesis

2 µg of total RNA were treated with RNase free DNase (Promega, Mannheim, Germany) for 45 minutes at 37 °C. The reaction was stopped by addition of 1µL EGTA stop-solution (Promega, Mannheim, Germany) and heating to 65 °C for 10 minutes. Reverse transcription was performed using the SuperscriptII kit (Invitrogen, Karlsruhe, Germany) and 250 ng of Oligo(dT)$_{12\text{-}18}$ primers according to the manufacturer's instructions.

3.2.5 Polymerase chain reaction

Polymerase chain reaction (PCR) was performed on plasmid DNA, genomic DNA or cDNA as templates. 30 µL reactions contained 1-5 µL template DNA, 3 µL 10 × Biotherm buffer (Genecraft, Münster, Germany), 5 mM dNTPs, 10 pmol primers and 1-2 U Biotherm Taq Polymerase (Genecraft, Münster, Germany). PCRs were operated in an Eppendorf Gradient S thermocycler with primers and annealing temperatures as listed below (Table 2).

Amplification products were separated on 1 – 2 % Agarose-TAE gels and stained with ethidium-bromide. The size of PCR products was determined by comparison to appropriate size standards (Genecraft, Münster, Germany).

Table 2: Primers used for PCR and RT-PCR.

Name	Sequence (5' → 3')	Template	T_A [°C]	Remarks
Act2_667	gttgactacgagcaggagatgg	At3g18780	55 °C	sense
Act2_841	aggttgtctcgtggattccag	At3g18780	55 °C	anti-sense
AGRP6	tctcgactgagcctcgttc	At4g39260	59 °C	anti-sense
AGRP19	gaaatttgaaaagaagatctaag	At5g21660	55 °C	anti-sense
AGRP22	gggatccccatcctccaccaccaccgc	At5g21660	65 °C	anti-sense
AGRP31	ggcctatggctgaagttgagt	At4g39260	59 °C	sense
AGRP63	agaacattcattggtaatccc	At5g21660	56 °C	anti-sense
AGRP100	ctgtaatcccttagatcttc	At5g21660	55 °C	sense
AGRP120	tttggggaaaagaagagaaattaggg	At4g39260	55 °C	anti-sense
AGRP125	cttgatcttccagtctcacg	At5g21660	57 °C	anti-sense
AGRP128	tgtattttcccaaatcgatc	At5g21660	56 °C	sense
AGRP129	gagatcttgtccgttcattc	At5g21660	56 °C	anti-sense
AGRP130	caagatctcgatggccgtag	At5g21660	59 °C	sense
CK2+	ctcggaactgatgaattgaatg	At3g50000	55 °C	sense
CK2-	cattctgctgctttctgctg	At3g50000	55 °C	anti-sense
CuChap+	gctcgcttaattggacaagg	At1g12520	55 °C	sense
CuChap-	tcgttgatacaccagctgtg	At1g12520	55 °C	anti-sense
CuZnSOD+	acaggaccacatttcaaccc	At1g08830	55 °C	sense
CuZnSOD-	cagaattaggaccagtcagagg	At1g08830	55 °C	anti-sense
eIF4a+	caatgaagtacttgagggac	At3g13920	55 °C	sense
eIF4a-	catggacaccagcttggagg	At3g13920	55 °C	anti-sense
FAD2+	gaaaccgacaccacaaagcg	At3g12120	55 °C	sense
FAD2-	tggtggcgacgtagtagaagc	At3g12120	55 °C	anti-sense
GRP7E44K+	tcattaacgatcgtaagaccggtagatcaaggggattc	At5g21660	65 °C	EK mutagenesis *AtGRP7*
GRP7E44K-	gaatccccttgatctaccggtcttacgatcgttaatga	At5g21660	65 °C	
GRP7W17R+	gttggaggtctagcccgggccactgatgac	At5g21660	70 °C	WR mutagenesis *AtGRP7*
GRP7W17R-	gtcatcagtggcccgggctagacctccaac	At5g21660	70 °C	
KS	tcgaggtcgacggtatcg	pBSK-	59 °C	sense
PPR+	aagacagtgaaggtgcaaccttact	At5g55840	55 °C	sense
PPR-	agtttttgagttgtatttgtcagagaaag	At5g55840	55 °C	anti-sense
RQ8for	cgagagtggaagatcccaaggattcggattcgtca	At4g39260	68 °C	RQ mutagenesis *AtGRP8*
RQ8rev	tgacgaatccgaatccttgggatcttccactctcg	At4g39260	68 °C	
SDM1	actggaagatccccaaggattcggattcgtcacctt	At5g21660	67 °C	RQ mutagenesis *AtGRP7*
SDM2	aatccgaatccttgggatcttccagtctcacgatc	At5g21660	67 °C	

The template is given using AGI as TAIR representative gene model for plant templates (Rhee *et al.*, 2003). pBSK- is a cloning vector from Stratagene (La Jolla, CA, USA). Diagnostic restriction sites in mutagenesis primers are underlined.

3.2.6 Southern blot of PCR products

Amplification products obtained by PCR (cf. 3.2.5) were separated on 2 % Agarose gels. Subsequently the DNA was transferred onto a Pall Biodyne® nylon membrane (VWR, Darmstadt, Germany) over night in a denaturing buffer containing 0.5 M NaCl and 0.5 M NaOH. The membrane was shortly neutralised in 0.5 M Tris-HCl, pH 7.0, 0.5 M NaCl and crosslinked by UV radiation and baking (cf. 3.2.3). Hybridisation was performed over night in HYBSOL with 1×10^6 cpm α-[^{32}P]-dATP labelled probes and at hybridisation temperatures as listed above (Table 1). The membranes were washed two times for 15 minutes with 0.2 × SSC, 0.1 % SDS at 50 – 56 °C. The blots were developed by exposure to FUJI SuperRX X-ray films (Hartenstein, Würzburg, Germany) or PI screens (Molecular Dynamics, Freiburg, Germany) for 1 to 7 days. PI screens were scanned on a Typhoon 8000 PhosphorImager and analysed using ImageQuant software (Amersham Pharmacia Biotech, Freiburg, Germany).

3.2.7 Real time PCR

Duplicate samples were analysed in a MJ research opticon cycler. DNAseI-treated RNA was reverse-transcribed (cf. 3.2.4) and 20 ng of cDNA were amplified with the Eppendorf Real MasterMix kit (Eppendorf, Hamburg, Germany) using 2 min at 94 °C , followed by 45 cycles of 20 sec at 94 °C, 30 sec at 60 C and 40 sec at 68 °C. Data were normalised to transcripts encoding eIF-4A-1 (At3g13920) or a PPR protein (At5g55840) (Czechowski *et al.*, 2005). Expression levels in transgenic plants were normalised to those in the wild type (WT) for each experiment with respect to the reference genes. Primers are listed in Table 2. The absence of amplification products from genomic DNA was confirmed in a non-retrotranscribed control.

3.3 Cloning and transformation

3.3.1 Oligonucleotide directed mutagenesis of the *AtGRP7* and *AtGRP8* RNA Recognition Motif

Conserved residues in the RNP1 or the loop regions 1 and 3 of *At*GRP7 and *At*GRP8 were exchanged by oligonucleotide directed mutagenesis PCR with Pfu Turbo polymerase (Stratagene, La Jolla, CA, USA) or Phusion® polymerase (Finnzymes, Espoo, Finnland) using overlapping primers (Table 2). Silent mutations were introduced into the codons of neighbouring amino acids creating diagnostic restriction sites (underlined in Table 2). The inserted mutations were verified by sequencing.

3.3.2 Construction of *Escherichia coli* and plant expression vectors

Constructs for recombinant expression in *E. coli* or *Arabidopsis thaliana* were either derived by direct cloning from cDNA constructs with appropriate restriction enzymes or by amplification with specific primers in a PCR (Table 2). Isolation of plasmids from *E. coli* was done with the Invisorb® Spin Plasmid Mini Two kit (Invitek, Berlin, Germany). Purification of DNA-fragments from agarose gels was accomplished with the NucleoSpin® Extract kit (Macherey-Nagel, Düren, Germany). Ligation products were transformed into *E. coli* Top10 (cf. 3.3.3). Accuracy of the constructs was confirmed by sequencing.

Table 3: Expression and transfection vectors constructed and used for this thesis.

Name	Characteristics / Cloning Strategy
GST-*At*GRP7	*AtGRP7* cDNA (*Eco*RI/*Not*I) in pGEX-6P-1 (GE Healthcare, Freiburg, Germany).
GST-*At*GRP7-RQ	*AtGRP7-RQ* cDNA in pGEX-5X-1, derived by site directed mutagenesis of GST-*At*GRP7 with the SDM primers (Table 2).
pJS13	*AtGRP7-RQ* cDNA (*Ksp*AI/*Sac*I) from GST-*At*GRP7-RQ under control of the CaMV promoter with duplicated enhancer element, the 3' untranslated region and an Ω element in pRT103 (Töpfer *et al.*, 1987)
pJS17	*Hind*III fragment from pJS13 cloned into the binary plant transformation vector pRD400.
JM11Δ*Pst*I	2.9 kb long genomic DNA fragment from *A. thaliana*., containing the *AtGRP7* open reading frame including all regulatory elements, in pBluescript II SK- (Stratagene, La Jolla, USA).
pHPT_GRP7-FL	Cloning of the genomic *AtGRP7* fragment (*Hind*III/*Sca*I) from JM11Δ*Pst*I into the binary plant transformation vector pHPT1 (*Hind*III/*Sma*I).
GRP7RQ-FL	Genomic 2.7 kb *AtGRP7* fragment carrying the $R^{49}Q$ mutation in pBSK-, derived by site directed mutagenesis of JM11Δ*Pst*I with the SDM primers (Table 2).
pHPT_GRP7RQ-FL	Cloning of the 2.7 kb *AtGRP7-RQ* encoding fragment (*Hind*III/*Sma*I) from JM11Δ*Pst*I into the binary plant transformation vector pHPT1 (*Hind*III/*Sca*I).
GST-*At*GRP7-$W^{17}R$	*AtGRP7-*$W^{17}R$ cDNA in pGEX-6P-1, derived by site directed mutagenesis of GST-*At*GRP7 with the GRP7W17R primers (Table 2).
GST-*At*GRP7-$E^{44}K$	*AtGRP7-*$E^{44}K$ cDNA in pGEX-6P-1, derived by site directed mutagenesis of GST-*At*GRP7 with the GRP7E44K primers (Table 2).
pRT-*At*GRP8	*AtGRP8* cDNA under control of the CaMV promoter with duplicated enhancer element, the 3' untranslated region and an Ω element in pRT103.
pHPT6	*Hind*III fragment from pRT-*At*GRP8 cloned into the binary plant transformation vector pHPT1.
pJS27	*AtGRP8-RQ* cDNA under control of the CaMV promoter with duplicated enhancer element, the 3' untranslated region and an Ω element in pRT103, derived by site directed mutagenesis of pRT-*At*GRP8 with the 8RQ primers (Table 2).
pJS28	*Hind*III fragment from pJS27 cloned into the binary plant transformation vector pHPT1.
GST-*At*GRP8	*AtGRP8* cDNA (*Eco*RI/*Not*I) in pGEX-6P-1.
GST-*At*GRP8-RQ	*AtGRP8-RQ* cDNA (*Sac*I/*Bgl*II) from pJS27 in GST-*At*GRP8.
*At*GRP7-GFP	Fusion of the GFP coding sequence to the 3' end of *AtGRP7* (*Bgl*II/*Bam*HI) in pHPT_GRP7-FL
GFP	GFP coding sequence fused to the *AtGRP7* promoter between the *AtGRP7* 5'UTR and 3'UTR (*Bgl*II/*Bam*HI).

The expression constructs are schematically shown in the Results part or the Appendix (cf. 4 & 8.1).

3.3.3 Transformation of *Escherichia coli*

Transformation competent *E. coli* Top10 cells (Invitrogen, Karlsruhe, Germany) were prepared by $CaCl_2$ treatment (Sambrook & Russel, 2001). The competent cells were aliquoted, shock-frozen in liquid nitrogen and stored at –80 °C.

For each transformation 1-10 µg of plasmid DNA or 5 µL of a ligation reaction were added to 50 µL of freshly thawed competent *E. coli* cells. The suspension was carefully mixed by tapping and afterwards incubated on ice for 20 minutes. The cells were heat-shocked for 50 seconds in a water bath of exactly 42 °C and immediately returned on ice for another 2 minutes. Subsequently 900 µL SOC (20 g/L Tryptone/Peptone from Casein, 5 g/L Yeast Extract, 10 mM NaCl, 10 mM $MgSO_4$, 2.5 mM KCl, 2 mM Glucose) medium were added and the transformation was incubated for 1 hour at 37 °C with moderate shaking.

Afterwards 100 µL of the transformation reaction were plated on LB-agar (10 g/L Tryptone/Peptone from Casein, 5 g/L Yeast Extract, 10 g/L NaCl, 14 g/L Agar-Agar) supplemented with the appropriate antibiotics for selection.

3.3.4 Transformation of *Agrobacterium tumefaciens*

Transformation competent cells of *Agrobacterium tumefaciens* C58 were prepared as follows: An *Agrobacterium tumefaciens* C58 culture was grown at 28 °C until an OD_{600} of 0.8 was reached. The cells were harvested by centrifugation at 5,000 × g, 4 °C for 15 minutes, washed in 100 mL ice cold LB medium supplemented with 0.5 mg/L $MgSO_4$, and centrifuged again. The supernatant was discarded and the pellet was resuspended in 10 mL ice cold 25 mM $CaCl_2$. The competent cells were aliquoted, shock-frozen in liquid nitrogen and stored at –80 °C.

1 µg of the binary vector containing the transgene of interest (Table 3) were added to 50 µL of competent *Agrobacterium tumefaciens* culture. The suspension was mixed by tapping and subsequently incubated on ice for 5 minutes. The suspension was frozen in liquid nitrogen for 5 minutes and thawed afterwards by incubation at 37 °C for 5 minutes. 1 mL of LB medium with 0.5 mg/L $MgSO_4$ was added and the transformation reaction was incubated for 1.5 hours at 28 °C under moderate shaking. After that 50-750 µL of the suspension were plated on LB plates containing the appropriate type of antibiotics for selection. Clones were obtained after incubation at 28 °C for 2 days.

3.3.5 *In planta* transformation of *Arabidopsis thaliana*

For stable expression of transgenes, plants were transformed by *Agrobacterium tumefaciens* vacuum infiltration (Ye *et al.*, 1999). Transgenic *Agrobacteria* were cultivated in $MgSO_4$ containing LB medium on a rotary shaker at 28 °C in until an OD_{600} of 0.8 was reached. Cells were harvested by 15 minutes centrifugation at 5,000 × g and resuspended in infiltration medium (2.2 g/L MS medium, 50 g/L Sucrose, 0.044 µM Benzylaminopurine, 0.02 % Silwet L-77). *Arabidopsis* inflorescences were immersed in the suspension and vacuum was applied for 5 minutes. The plants were returned to greenhouse, allowed to grow to maturity and seeds were harvested. Transgenic lines (T1) were identified by selection on Kanamycin (50 µg/mL) or Hygromycin (30 µg/mL) containing MS-Agar and verified by molecular analysis. Homozygous lines were selected via their segregation pattern in the third generation after transformation (T3). Transgenic lines established during this work are listed in Table 4.

Table 4: Transgenic *Arabidopsis thaliana* lines created and used for this thesis.

Name	Ecotype / Line	Transfected with
GRP7-RQ-ox	C24, Col-2	pJS17
GRP7-FL	*grp7-1*	pHPT_GRP7-FL
GRP7-RQ-FL	*grp7-1*	pHPT_GRP7RQ-FL
GRP8-ox	Col-2, Col-0	pHPT6
GRP8-RQ-ox	C24, Col-2, Col-0	pJS28
7RQ+8RQ	C24	pJS17 + pJS28
*At*GRP7-GFP	Col-2	*At*GRP7-GFP
GFP	Col-2	GFP

For detailed information about the used transfection vectors see Table 3.

3.4 Biochemical methods

3.4.1 Protein extraction from plant

20-30 mg of mortar grinded plant powder was homogenised in eight volumes denaturing protein extraction buffer (62.5 mM Tris-HCl, pH 6.8, 20 % (w/v) Glycerol, 2 % (w/v) SDS, 1 % (v/v) β-Mercaptoethanol). The suspension was boiled for 10 minutes at 95 °C and centrifuged for 10 minutes at 16,000 × g. The supernatant contained the soluble protein fraction. The concentration of proteins was determined using the Esen assay (Esen, 1978).

3.4.2 Western blot analysis

Extracted proteins were separated on 15 % SDS-polyacrylamide gels (Laemmli, 1970). The proteins were transferred onto a PVDF membrane by electroblotting in transfer buffer (25 mM Tris, 192 mM Glycine, 0.05 % (w/v) SDS, 20 % (v/v) Methanol) at 30 V (const.) over night. Subsequently, the membrane was blocked in TBST (Tris-buffered saline, 0.1 % Tween) + 2 % (w/v) low-fat milk powder for one hour at 4 °C and subsequently incubated with the specific primary antibody (Table 5) for another hour at room temperature. After three washing steps of 10 minutes with TBST the blot was incubated with the Horse Radish Peroxidase (HRP) conjugated secondary antibody for 30 minutes. The blot was washed four times for 15 minutes with TBST and developed using enhanced luminol chemiluminescence (Haan, 2007) and exposed to FUJI SuperRX X-ray films (Hartenstein, Würzburg, Germany).

Table 5: Antibodies used for western blot analysis.

Antibody	Dilution	Organism	Remarks
α-*At*GRP7	1:5000	Rabbit	directed against synthetic peptide: CRALETAFAQY
α-*At*GRP8	1:5000	Rabbit	directed against synthetic peptide: CEDLQRTFSQF
α-LHCP	1:25000	Rabbit	poly-clonal antibody against LHCP
α-Rabbit-HRP	1:5000	goat	Sigma-Aldrich (Seelze, Germany)

As a loading control the blots were either developed with an antibody against the light-harvesting chlorophyll a/b binding protein (LHCP) or stained with coomassie brilliant blue.

3.4.3 Expression and purification of recombinant GST-fusion proteins

All *At*GRP7 and *At*GRP8 wild type and mutant protein variants (Table 6) were recombinantly expressed as GST-fusion proteins in *E. coli* BL21 DE3. Induction was performed using 0.5 mM IPTG for 24 hrs at 18 °C. The fusion proteins were purified by chromatography on Glutathione Sepharose according to the supplier's instructions (GE Healthcare, Freiburg, Germany). Removal of Glutathione and concentration of the protein solution were done by centrifugation through Centricon® 30 filter devices (Millipore, Billerica, MA, USA). Protein concentration was determined by Bradford assay (Biorad, Munich, Germany).

Table 6: Recombinantly expressed GST-fusion proteins.

Protein	Molecular weight	pI	Buffer	Concentration
GST-*At*GRP7	44.1 kDa	5.65	20 mM HEPES-KOH, pH 7.5, 1 mM DTT	3.7 mg/mL
GST-*At*GRP7-RQ	44.1 kDa	5.54	20 mM HEPES-KOH, pH 7.5, 1 mM DTT	14.8 mg/mL
GST-*At*GRP7-$E^{44}K$	44.1 kDa	5.90	50 mM Tris-HCl, pH 8, 10 mM Glutathione	0.5 mg/mL
GST-*At*GRP7-$W^{17}R$	44.1 kDa	5.77	50 mM Tris-HCl, pH 8, 10 mM Glutathione	0.36 mg/mL
GST-*At*GRP8	43.8 kDa	5.58	20 mM HEPES-KOH, pH 7.5, 1 mM DTT	6.7 mg/mL
GST-*At*GRP8-RQ	43.8 kDa	5.48	20 mM HEPES-KOH, pH 7.5, 1 mM DTT	149.8 mg/mL

3.4.4 RNP-immunoprecipitation

To isolate RNAs that are directly associated to *At*GRP7 *in vivo*, ribonucleoprotein (RNP) immunoprecipitation was performed according to a modified protocol from Niranjanakumari and colleagues (Niranjanakumari *et al.*, 2002). For this purpose, RNP complexes containing *At*GRP7 were cross-linked *in planta* and subsequently precipitated via a specific antibody. To exclude as much unspecific co-precipitation as possible, transgenic plants were used that express a GFP tagged *At*GRP7 in combination with a monoclonal α-GFP antibody. As a control transgenic GFP plants with the same regulatory regions were used (Table 3; Figure 19). Col GFP and Col *At*GRP7-GFP plants were grown under long day conditions for about three weeks (cf. 3.1.1). Plants of comparable size were harvested at ZT10 (zeitgeber time, hours after light on). RNP complexes in the cells were cross-linked by vacuum infiltration of X-link buffer (phosphate-bufferd saline (PBS), pH 7.0 containing 1 % Formaldehyde) for 5 minutes and a subsequent incubation in X-link buffer on a rotary shaker for 20 minutes. The cross-linking reaction was stopped by addition of Glycine (0.25 M final concentration) and a final incubation for 5 minutes.

Harvested plants were shock-frozen and mortar grinded in liquid nitrogen. 300 µL of frozen plant powder were homogenised in 1 mL of RIPA buffer (50 mM Tris-HCl, pH 7.5, 150 mM NaCl, 1 mM EDTA, 1 % NP-40, 0.5 % Na-deoxycholate, 0.05 % SDS, 40 µL/ml Complete® protease inhibitor, 20 µL/mL Ribonucleoside Vanadyl Complex (RVC), 2µL/mL RiboLock® RNase inhibitor) with a mini pestle. After centrifugation for 10 minutes at 16,000 × g and 4 °C the supernatant was transferred to a new tube. The lysate was pre-cleared with 50 µL MagnaBind™ Protein G beads (Pierce, Rockford, IL, USA) along with unspecific competitor tRNA from yeast (100 µg/mL final concentration) by rotation at 4 °C for 1 hour. The beads were sedimented and the supernatant was transferred to a new tube containing 4 µg of monoclonal α-GFP antibody (Roche, Basel, Switzerland) or BSA (Sigma-Aldrich, Seelze, Germany), respectively. The samples were rotated at 20 °C for 1 hour. Subsequently 50 µL of fresh MagnaBind™ Protein G beads were added and the samples were rotated for another 30 minutes. The beads were sedimented and washed six times for ten minutes with Washing buffer (50 mM Tris-HCl, pH 7.5, 1 M NaCl, 2 - 4 M Urea, 1 mM EDTA, 1 % NP-40, 1 % Na-deoxycholate, 0.1 % SDS, 20 µL/ml Complete® protease inhibitor). The RNA was eluted from the RNP complexes by addition of 100 µL of Elution buffer (50 mM Tris-HCl, pH 7.5, 5 mM EDTA, 10 mM DTE, 1 % SDS) and incubation at 65 °C with moderate shaking for 30 minutes. The eluted RNAs were isolated by Phenol/Chloroform extraction and subsequent 2-Propanol precipitation. After final washing with 400 µL 70 % (v/v) Ethanol, the pellet was air-dried and dissolved in 20 µL of RNase free water. cDNA from the precipitated RNAs was generated as described (3.2.4).

3.5 Electrophoretic Mobility Shift Assays (EMSA)

3.5.1 ^{32}P-labelling of synthetic oligoribonucleotides

Synthetic oligoribonucleotides were purchased from Biomers (Ulm, Germany; Table 7). 250 pmol oligoribonucleotide (ORN) were denatured in a buffer containing 25 mM Tris-HCl, pH 9.5, 2.5 mM Spermidine and 0.6 mM EDTA at 70 °C for 5 minutes. Afterwards, the samples were chilled immediately on ice. 50 pmol of the denatured ORN were labelled with γ-[^{32}P]ATP using T4 polynucleotide kinase (Fermentas, St. Leon-Rot, Germany) for 60 minutes at 37 °C. The reaction was stopped by incubation at 70 °C for 10 minutes. 30 µL of RNase free water were added and the labelled oligos were purified on microQuick RNA columns (Roche, Mannheim, Germany). Quantification was done by measuring Čerenkov radiation in a 1900CA Tri-Carb Liquid scintillation analyser (Packard/Perkin Elmer, Waltham, MA, USA).

3.5.2 Determination of RNA-protein complex formation *in vitro*

For *in vitro* analysis of RNA-protein complexes electrophoretic mobility shift assays were used. Standard complex formation of 5 nM ^{32}P-labelled ORN (Table 7) with 0.5 µg GST-fusion protein (Table 6) was performed in 1 × binding buffer (20 mM HEPES-KOH, pH 7.5, 1 mM $MgCl_2$, 100 mM NaCl, 0.01 % NP40) for 20 minutes in presence of 0.1-10 µg yeast tRNA (Sigma-Aldrich, Seelze, Germany). As a control, water was added instead of protein.

The samples were separated on native 6 % Polyacrylamide TAE gels, gels were dried on a vacuum drier and exposed to PI screens (MolecularDynamics, Freiburg, Germany) over night.

Table 7: Synthetic oligoribonucleotides.

Name	Sequence	Source	Modification
7-UTR_WT	AUUUUGUUCUGGUUCUGCUUUAGAUUUGAUCU	*At*GRP7	none
7-UTR_G_4mut	AUUUU**A**UUCU**AA**UUCUGCUUUAGAUUU**A**AUCU	*AtGRP7*	none
7-UTR_U_7mut	AU**AC**UG**A**UCUGC**A**UCUGCU**C**UAGAU**AC**GAUCU	*AtGRP7*	none
7-intron_WT	GUUCAGUUUUGUUGGAUUGUUUUGCUGAUCUG	*AtGRP7*	none
7-intron_G_6mut	GUUCA**A**UUUU**A**UU**AA**AUU**A**UUUU**A**CUGAUCUG	*AtGRP7*	none
7-intron_U_5mut	GUUCAGU**AC**UG**AC**GGAU**A**GU**AC**UGCUGAUCUG	*AtGRP7*	none
8-intron_WT	CUUCCACGAUUGUUUUUGCUGAUGUGU	*AtGRP8*	none
8-intron_G_2U_2mut	CUUCCACGAUU**A**U**CC**UU**A**CUGAUGUGU	*AtGRP8*	none
8-UTR_WT	GUUUUUGGUUUAGAUUUGGUUUUGUGU	*AtGRP8*	none
8-UTR_938	CGUUUGGUUUACUUUUUUGAUGAAACA	*AtGRP8*	none
8-UTR_G_6mut	GUUUUU**AA**UUUA**A**AUUU**AA**UUUU**A**UGU	*AtGRP8*	none
8-UTR_Permut	UUGUAUCUGUGUAUUCUGUAUCUUGUU	artificial	none
8-UTR_UG	UUUGUUUUGCUUUGUUUUGCUUUGUUU	artificial	none
Poly_A	AAAAAAAAAAAAAAAAAAAAAAAAAA	artificial	3' C_3SH
Poly_U	UUUUUUUUUUUUUUUUUUUUUUUUUU	artificial	3' C_3SH
Poly_G	GGGGGGGGGGGGGGGGGGGGGGGGGG	artificial	3' C_3SH
7-UTR_WT-SH	AUUUUGUUCUGGUUCUGCUUUAGAUUU	*AtGRP7*	3' C_3SH
7-UTR_G_4mut-SH	AUUUU**A**UUCU**AA**UUCU**A**CUUUAGAUUU	*AtGRP7*	3' C_3SH
8-UTR_WT-SH	GUUUUUGGUUUAGAUUUGGUUUUGUGU	*AtGRP8*	3' C_3SH
8-UTR_G_6mut-SH	GUUUUU**AA**UUUA**A**AUUU**AA**UUUU**A**UGU	*AtGRP8*	3' C_3SH
8-UTR_938-SH	CGUUUGGUUUACUUUUUUGAUGAAACA	*AtGRP8*	3' C_3SH
8-UTR_938-G_4mut	CGUUU**AA**UUUACUUUUUU**A**AU**A**AAACA	*AtGRP8*	3' C_3SH
7-UTR_WT-NH_2	AUUUUGUUCUGGUUCUGCUUUAGAUUUGAUCU	*AtGRP7*	3' C_3NH_2
7-UTR_DNA-NH_2	ATTTTGTTCTGGTTCTGCTTTAGATTTGATCT	*AtGRP7*	3' C_3NH_2
7-UTR_SL	**G**U**G**GUUCUGG**C**A**C**	*AtGRP7*	3' C_3NH_2
7-UTR_O	UUUGUUCUGGUUC	*AtGRP7*	3' C_3NH_2
7-UTR_UA	**G**UU**G**GUUCUGG**CAA**C	*AtGRP7*	3' C_3NH_2
7-UTR_GC	**GG**U**G**GUUCUGG**CA**C**C**	*AtGRP7*	3' C_3NH_2
7-UTR_$(GC)_2$	**GGG**U**G**GUUCUGG**CA**C**CC**	*AtGRP7*	3' C_3NH_2
DNA_1	CTATTTTGTTCT	*AtGRP7*	3' C_3NH_2
DNA_2	ATTTTGTTCTGG	*AtGRP7*	3' C_3NH_2
DNA_3	TTTGTTCTGGTT	*AtGRP7*	3' C_3NH_2
DNA_4	TGTTCTGGTTCT	*AtGRP7*	3' C_3NH_2
DNA_5	TTCTGGTTCTGC	*AtGRP7*	3' C_3NH_2
DNA_6	CTGGTTCTGCTT	*AtGRP7*	3' C_3NH_2
DNA_7	GGTTCTGCTTTA	*AtGRP7*	3' C_3NH_2
DNA_8	TTCTGCTTTAGA’	*AtGRP7*	3' C_3NH_2

Mutated bases are highlighted in boldface.

3.5.3 Competitive specificity assay

Specificity of the detected RNA-protein complexes was demonstrated in competition assays. Complex formation was performed as described above (cf. 3.5.2), but tRNA concentration was kept constant at 1 µg per reaction. Homologous or heterologous, non-labelled competitor ORNs were added in concentrations of 0 – 500 pmol. The heterologous ORNs were of the same size, but different point mutations were introduced into the sequence (Table 7). Competition and thus efficient binding of the non-labelled ORNs is visible as a reduced amount of RNA-protein complex in the autoradiogramm. The amount of labelled RNA-protein complex is inversely proportional to the binding affinity of the competitor ORN.

3.5.4 Determination of equilibrium dissociation constants (K_d)

Binding affinities of the *At*GRP7 and *At*GRP8 protein variants were determined by K_d measurements. Important for the determination of K_d values is the precondition that the concentration of the labelled probe is much smaller than the K_d. The concentration of the labelled probe [A] is kept constant and the concentration of binding partner [B] is varied and the amount of complex [AB] is measured. In this case the complex formation kinetic follows Equation 1.

$$\frac{[AB]}{[A]_{total}} = \frac{[B]}{[B] + K_d} \qquad \textbf{(Equation 1)}$$

The fact that [B] is much higher than [A] and [AB] allows to consider $[B] = [B]_{total}$. Thus, the bound fraction $[AB]/[A]_{total}$ can be plotted against $[B]_{total}$ yielding the $K_d = [B]$ if $[AB]/[A]_{total}$ is equal to 0.5 (Figure 11).

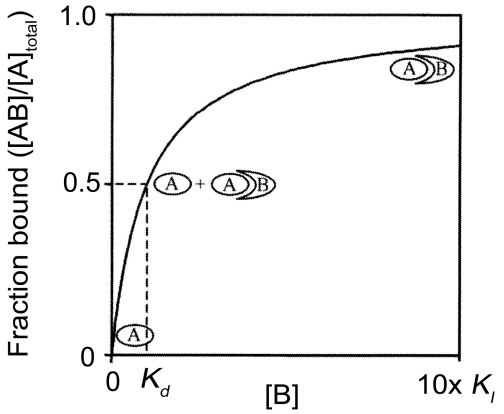

Figure 11: Hyperbolic curve defined by Equation 1. The dashed lines indicate that K_d is the concentration at which the fraction bound is 50 % (Goodrich & Kugel, 2007).

For the K_d determination of several *At*GRP7 and *At*GRP8 protein variants (Table 6) 5 nM ^{32}P-labelled ORN (Table 7) were incubated with increasing amounts of GST-fusion protein. For the direct calculation of K_d values log (complexed/free probe) was plotted against the log (protein concentration) and lines were obtained by linear regression according to Equation 2. The plot yields the log (K_d) = log ([B]) as x-intercept.

$$\log\left(\frac{[AB]}{[A]}\right) = a \cdot \log([B]) + c \qquad \textbf{(Equation 2)}$$

3.6 Sample preparation for single molecule measurements

3.6.1 Atomic force microscopy based force spectroscopy (AFM-FS)

Fusion proteins were expressed in *E. coli* and purified as described (3.4.3). For immobilisation of the protein on a mica surface (Provac, Florida, USA), a BS3 (bis(sulfosuccinimidyl)suberate) cross-linker (Sigma-Aldrich, Seelze, Germany) was used. The thiol-linked oligoribonucleotides (Table 7) were denatured for 3 minutes at 70 °C and a PEG linker (N-hydroxysuccinimid-poly(ethylenglycol)-maleimid (NHS-PEG-MAL, MW 3.4 kD); Nektar, Huntsville, Alabama, USA) was added in a 1:1 molar ratio. 0.5 pmol/µL RNA and PEG linker solution was subsequently incubated with activated Si_3N_4 cantilevers (Microlevers, Veeco Intruments) for 90 minutes at 4 °C. The AFM force spectroscopy experiments were performed in 20 mM HEPES-KOH, pH7.5, 100 mM NaCl, 1 mM $MgCl_2$, 0.01 % NP40 in the presence of 1 mg/mL yeast tRNA and 0.4 U/mL RiboLock (Fermentas, St. Leon-Rot, Germany). The AFM-FS measurements were carried out by Alexander Fuhrmann (Applied Biophysics and NanoSciences, Faculty of Physics, Bielefeld University, Bielefeld, Germany).

3.6.2 Fluorescence correlation spectroscopy (FCS)

Fusion proteins were purified as described above (3.4.3). The synthetic, amino-linked DNA or RNA oligonucleotides (Table 7) were end-labelled with the fluorescent oxazine dye MR121 and subsequently purified by HPLC. FCS measurements were carried out at nanomolar concentration of the labelled nucleic acids in connection with varying protein concentrations in a total volume of 100 µL PBS, pH 7.5 supplemented with 0.05 % Tween20, 0.3 mg/mL BSA and 0.5 U/mL RiboLock RNase-inhibitor. Measurements were performed by Dr. Mark Schüttpelz (Applied Laser Physics and Laser Spectroscopy, Faculty of Physics, Bielefeld University, Bielefeld, Germany).

3.7 Bioinformatic analysis

For the determination of *At*GRP7 binding sites within the *AtGRP8* transcript a bioinformatic approach was used. Homology analysis was done by pairwise alignment of the *AtGRP8* transcript to the known binding sites within *AtGRP7* using ClustalW and Diaglin (Thompson *et al.*, 1994; Morgenstern, 2004). The identified regions were further analysed for possible secondary structures by *in silico* folding with the programs mfold and RNAshapes (Zuker, 2003; Steffen *et al.*, 2006) since the existence of single-stranded regions is essential for the binding process (cf. 2.2.1).

A general approach to identify conserved secondary structures in the *AtGRP7* and *AtGRP8* transcripts was done in cooperation with Prof. Dr. Irmtraud Meyer (Bioinformatics Center, University of British Columbia, Vancouver, Canada). Amino acid sequences of homologous proteins were aligned with *AtGRP7*. Subsequently, this alignment was transferred to the nucleotide sequences of the transcripts. The aligned and annotated sequences were further analysed with the program RNA-Decoder (Pedersen *et al.*, 2004) for evolutionary conserved secondary structures.

4 Results

The circadian clock-regulated RNA-binding protein *At*GRP7 feeds back on the oscillations of its own transcript (Heintzen *et al.*, 1997). By this negative auto-regulation *At*GRP7 forms a secondary oscillator downstream of the *Arabidopsis* clock transmitting time signals within the cell. An direct interaction of *AtGRP7* RNA and *At*GRP7 protein has been demostrated *in vitro* (Staiger *et al.*, 2003). A deletion analysis of the *AtGRP7* transcript has revealed two binding sites for *At*GRP7 within the 3'UTR and the second half of the intron of its own transcript (Staiger *et al.*, 2003).

The molecular charcterisation of this novel type of slave oscillator is of fundamental interest. The present work aimed at the identification of definite binding sites within the transcript, the characterisation of crucial amino acids within the *At*GRP7 RRM and the determination of specific binding parameters to obtain a more detailed insight into the regulatory mechanisms of *At*GRP7. Moreover, the homologous *At*GRP8 protein was analysed *in vitro* and *in vivo* to yield insights into the regulatory feedback loop: Do *At*GRP7 and *At*GRP8 show a reciprocal regulation and do they have different or overlapping functions in the plant cell.

4.1 *At*GRP7 binds to its own transcript *in vitro*

For a detailed analysis of the *At*GRP7 protein-RNA interaction, synthetic oligoribonucleotides (ORNs) covering the presumed *At*GRP7 target sequences were designed on the basis of previous deletion experiments (Staiger *et al.*, 2003). These two 32 nucleotides long ORNs, derived from the 3' UTR and the second half of the intron (7-UTR_WT and 7-intron_WT, respectively), were used as templates in gel shift experiments (Figure 12 a). GST-*At*GRP7 forms stable complexes with both ORNs even at high concentrations of unspecific competitor tRNA (Figure 12 b). In order to demonstrate sequence specificity of the *At*GRP7-RNA binding process, point mutations were introduced into the ORNs. A preliminary experiment had demonstrated a preference for guanine-rich sequences (Staiger *et al.*, 2003). Thus, several guanines were exchanged for adenines (Figure 12 a). Subsequently, it was tested whether the mutated ORNs can compete for the binding of the wild type sequences by GST-*At*GRP7. The addition of 500 pmol heterologous 7-UTR_G_4mut ORN, with four guanines exchanged for adenines, competed only weakly for the binding of GST-*At*GRP7 (Figure 12 c). In contrast, the wild

type ORN competed efficiently with the radioactively labelled probe for the binding site at the GST-*At*GRP7 protein. This resulted in an almost complete loss of labelled complex if 250 pmol of cold competitor RNA were added (Figure 12 c).

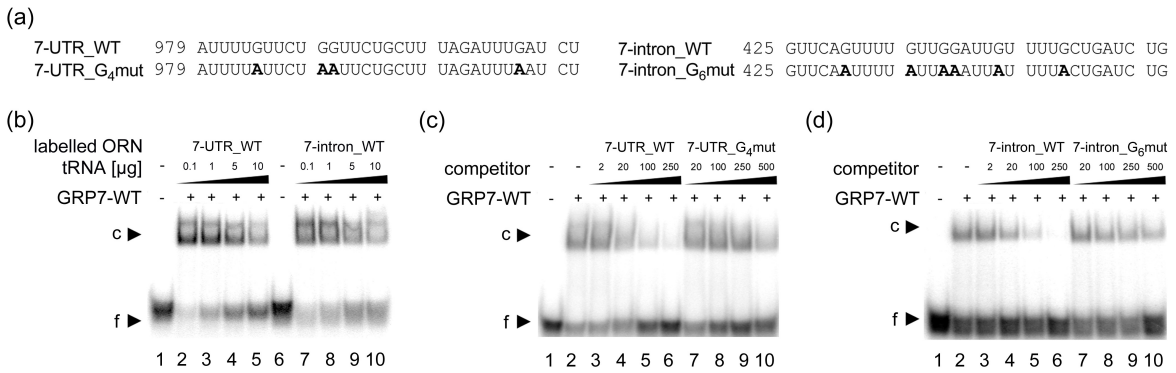

Figure 12: *At*GRP7 binds to synthetic ORNs derived from the *AtGRP7* transcript in a sequence specific way. (a) Sequence of the ORN 7-UTR_WT containing the *At*GRP7 binding site within the 3´ UTR, mutated 7-UTR_G_4mut with four G residues exchanged for A (in bold), 7-intron_WT and mutated ORN 7-intron_G_6mut with six G residues exchanged for A (in bold). Numbering is relative to the transcription start site (Staiger & Apel, 1999). (b) GST-*At*GRP7 WT protein was incubated with labelled 7-UTR_WT ORN (lanes 2-5) and 7-intron_WT ORN (lanes 7-10) in the presence of 1 to 10 µg of tRNA. Lanes 1 and 6, free ORN. (c) GST-*At*GRP7 WT protein was incubated with labelled 7-UTR_WT ORN in the presence of 5 µg of tRNA (lanes 2-10) and 2, 20, 100 and 250 pmoles of unlabelled 7-UTR_WT ORN (lanes 3-6) or 20, 100, 250 and 500 pmoles of unlabelled 7-UTR_G_4mut (lanes 7-10), respectively. Lane 1, free ORN. (d) GST-*At*GRP7 protein was incubated with labelled 7-intron_WT ORN in the presence of 5 µg of tRNA (lanes 2-10) and 2, 20, 100 and 250 pmoles of unlabelled 7-intron_WT ORN (lanes 3-6) or 20, 100, 250 and 500 pmoles of unlabelled 7-intron_G_6mut ORN (lanes 7-10), respectively. Lane 1, free ORN.

Likewise, six guanines within the intronic binding site were exchanged for adenines (7-intron_G_6mut; Figure 12 a). Again, the mutated ORN competed less for the GST-*At*GRP7 binding, whereas GST-*At*GRP7 and the wild type ORN formed stable complexes, visible in the efficient competition by addition of 250 pmol cold 7-intron_WT ORN (Figure 12 d).

These data clearly demonstrate a sequence-specific binding of GST-*At*GRP7 to the two identified target sequences within the *AtGRP7* transcript.

4.1.1 Exchange of arginine[49] to glutamine reduces *At*GRP7 binding *in vitro*

To identify amino acids that make direct contacts to the RNA substrate single point mutations were introduced into the RNA binding domain. In a first approach the highly conserved regions of the RRM were mutagenised. Based on the co-crystal structure of the U1A RRM with U1hpII, the highly conserved arginine[49] of the *At*GRP7 RNP1 octapeptide was chosen as target for the mutagenesis. This very arginine was predicted to contribute to stable RNA binding of U1A by the formation of salt bridges with the RNA target (Nagai *et al.*, 1990; Oubridge *et al.*, 1994; Tang & Nilsson, 1999).

The *At*GRP7 Arg[49] was exchanged for glutamine by oligonucleotide directed mutagenesis with the SDM primers (Figure 13 a; Table 2). The PCR product was cloned into pGEX-6P-1 to produce recombinant GST-fusion protein in *E. coli.* Subsequently, the GST-*At*GRP7-RQ fusion protein was purified by affinity chromatography.

Both, wild type GST-*At*GRP7 and GST-*At*GRP7-RQ were subjected to electrophoretic mobility shift assays (EMSA) with the radioactively labelled 7-UTR_WT and 7-intron_WT ORNs (cf. 4.1). The wild type *At*GRP7 showed stable complex formation with the ORNs derived from the 3'UTR (7-UTR_WT) and the intron (7-intron_WT), whereas only little shifted complex was observed when the same ORNs were incubated with the mutated protein (Figure 13 c). To quantify the impact of the *At*GRP7-RQ mutation on the binding affinity of the protein, equilibrium dissociation constants were determined. Increasing amounts of fusion protein were added to 50 fmol of radioactively labelled 7-UTR_WT ORN. The percentage of RNA incorporated into RNA-protein complexes was recorded. The calculated K_d values revealed an about seven times higher affinity of the wild type protein towards the 3' UTR ORN in comparison to the *At*GRP7-RQ mutant (Figure 13 d).

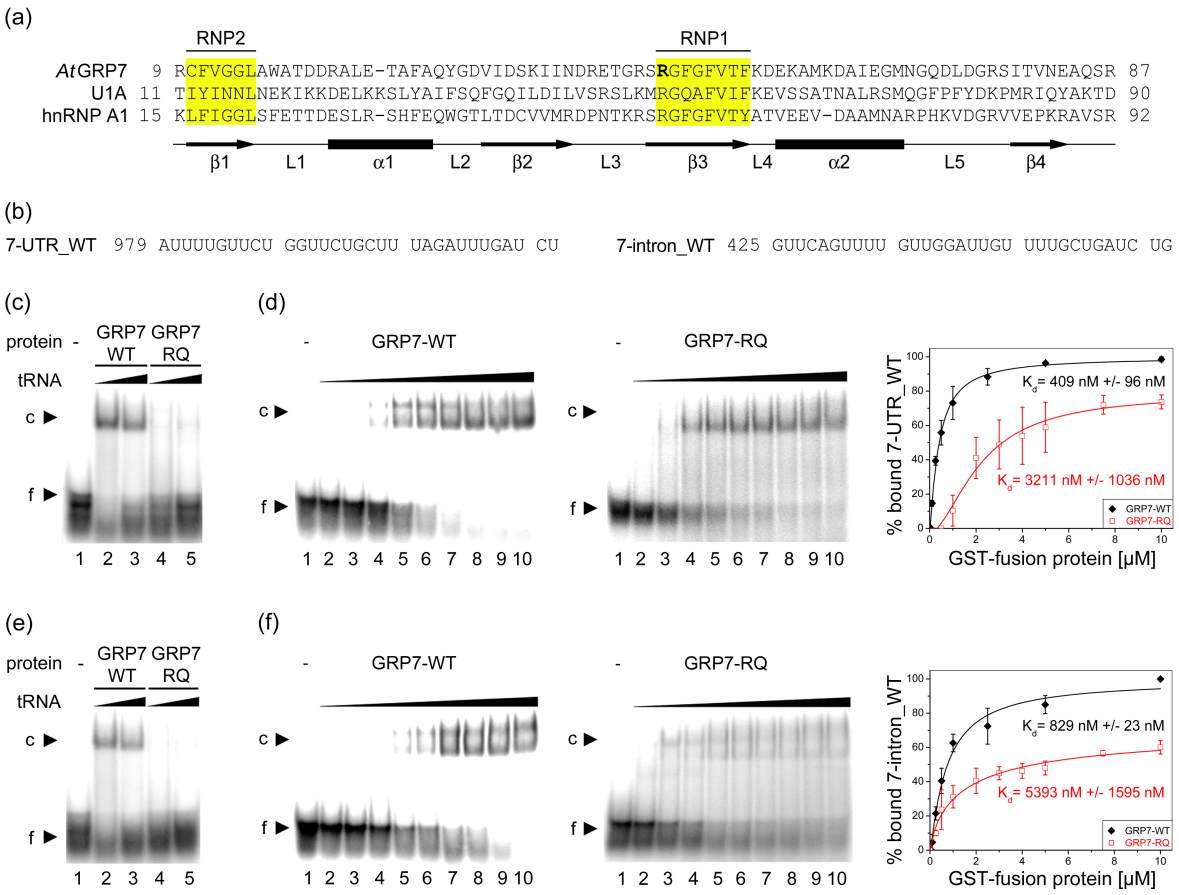

Figure 13: **Influence of the *At*GRP7 RNP1 RQ mutation on *At*GRP7 binding activity.** (a) *At*GRP7 RRM aligned upon the N-terminal RRM of U1A and hnRNP A1 (Maris *et al.*, 2005). The conserved RNP1 and RNP2 and predicted secondary structure elements are indicated. R^{49} mutated to Q is highlighted in boldface. L, loop. (b) Sequence of the ORN 7-UTR_WT containing the *At*GRP7 binding site within the 3´ UTR and the sequence of the ORN 7-intron_WT. Numbering is relative to the transcription start site (Staiger & Apel, 1999). (c) Labelled 7-UTR_WT was incubated with GST-*At*GRP7 (lanes 2, 3) or GST-*At*GRP7-RQ (lanes 4, 5) and 1 µg (lanes 2, 4) or 10 µg (lanes 3, 5) of tRNA, respectively. Lane 1, free ORN (f). c, RNA-protein complex. (d) To compare binding affinities of WT and mutant protein, 50 fmoles of labelled 7-UTR_WT were incubated with 0.01, 0.05, 0.1, 0.25, 0.5, 1, 2.5, 5 and 10 µM of GST-*AtT*GRP7 (lanes 2-10) or 0.5, 1, 2, 3, 4, 5, 7.5, 10 and 20 µM of GST-*At*GRP7-RQ (lanes 2-10), respectively, in the presence of 1 µg tRNA. Bound and free RNA were quantified and K_d values calculated based on three independent experiments as described in Materials and Methods. (e) Labelled 7-intron_WT was incubated with GST-*At*GRP7 (lanes 2, 3) or GST-*At*GRP7-RQ (lanes 4, 5) and 1 µg (lanes 2, 4) or 10 µg (lanes 3, 5) of tRNA, respectively. Lane 1, free ORN. (f) To compare binding affinities of WT and mutant protein, 50 fmoles of labelled 7-intron_WT were incubated with 0.01, 0.05, 0.1, 0.25, 0.5, 1, 2.5, 5 and 10 µM of GST-*At*GRP7 (lanes 2-10) or 0.25, 0.5, 1, 2, 3, 4, 5, 7.5 and 10 µM of GST-*At*GRP7-RQ (lanes 2-10), respectively, in the presence of 1 µg tRNA. K_d values were determined as in (d).

Corresponding results were obtained with the ORN derived from the second half of the *AtGRP7* intron (7-intron_WT). The GST-*At*GRP7 wild type protein bound to this sequence with an affinity comparable to that determined for the 3'UTR ORN (Figure 13 f). In contrast, the GST-*At*GRP7-RQ mutant protein formed only little shifted complex and had an sixfold increased equilibrium dissociation constant (Figure 13 f).

Although a complex formation was still observed at high GST-*At*GRP7-RQ concentrations, an apparent smearing suggested a dissociation of the RNA-protein complex during the gel run (Figure 13 d & f, middle).

To exclude that the exchange of arginine[49] to glutamine interferes with a correct folding of the RRM, circular dichroism spectra of the wild type *At*GRP7 and *At*GRP7-RQ were recorded in cooperation with Sven Hennig and Dr. Eva Wolf (Max Planck Institute of Molecular Physiology, Dortmund, Germany). The minimum of the curves at 208 nm and a trough at 222 nm indicated the presence of separate α-helical and β-sheet regions (Figure 14).

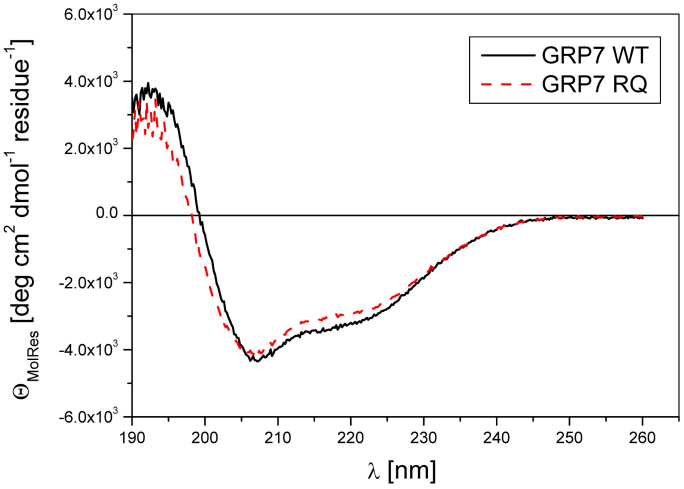

Figure 14: Secondary structures of *At*GRP7 and *At*GRP7-RQ are almost identical. Circular dichroism spectra of both proteins were recorded at a 10 µM concentration.

The curves of wild type and mutant protein resembled the typical structure of RRM proteins and were almost indistinguishable. This suggested that the reduced binding affinity of *At*GRP7-RQ was not caused by an unfavourable secondary structure.

To examine an influence of the *At*GRP7-RQ muation on binding specificity, competition assays were carried out. In analogy to the competition assays performed with the wild type protein, G-mutated ORNs were used as heterologous competitors (cf. 4.1). Both, the 7_UTR-G_4mut and the 7_intron-G_6mut oligonucleotides competed less efficiently for the GST-*At*GRP7-RQ binding than the corresponding wild type sequences (Figure 15).

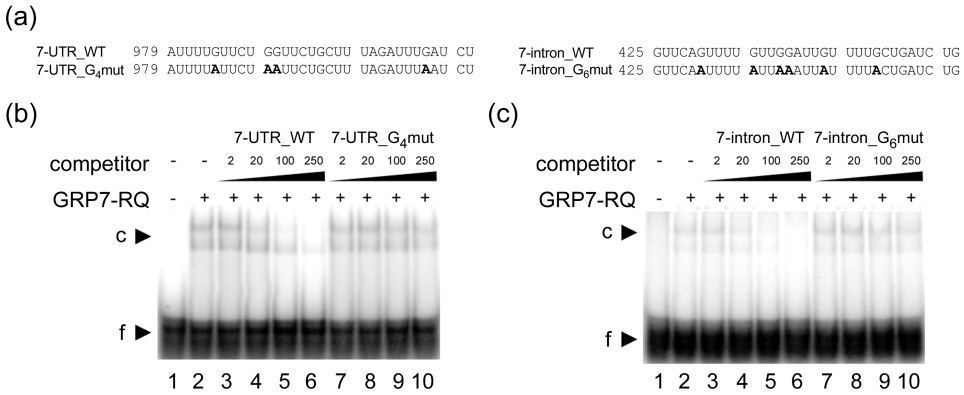

Figure 15: The *At*GRP7-RQ mutation does not alter the sequence specificity. (a) Sequence of the ORN 7-UTR_WT containing the *At*GRP7 binding site within the 3´ UTR, mutated 7-UTR_G_4mut with four G residues exchanged for A (in bold), 7-intron_WT and mutated ORN 7-intron_G_6mut with six G residues exchanged for A (in bold). Numbering is relative to the transcription start site (Staiger & Apel, 1999). (b) GST-*At*GRP7-RQ protein was incubated with labelled 7-UTR_WT ORN in the presence of 5 µg of tRNA (lanes 2-10) and 2, 20, 100 and 250 pmoles of unlabelled 7-UTR_WT ORN (lanes 3-6) or 7-UTR_G_4mut (lanes 7-10), respectively. Lane 1, free ORN. Note that this gel was exposed about three times longer than the gel shown in Figure 13 c. Occasionally the labelled ORN showed apparent heterogeneity, presumably representing different conformations separated in the non-denaturing PAGE. This resulted in two retarded bands. (c) GST-*At*GRP7-RQ protein was incubated with labelled 7-intron_WT ORN in the presence of 5 µg of tRNA (lanes 2-10) and 2, 20, 100 and 250 pmoles of unlabelled 7-intron_WT ORN (lanes 3-6) or unlabelled 7-intron_G_6mut ORN (lanes 7-10) as indicated. Lane 1, free ORN. Note that this gel was exposed about three times longer than the gel shown in Figure 13 e.

Thus, the GST-*At*GRP7-RQ mutant protein showed the same sequence specificity as previously demonstrated for the wild type protein (cf. 4.1). Accordingly, the Arg^{49} of *At*GRP7 is essential for the stability of the ribonucleoprotein complex but not for the target discrimination.

4.1.2 Influence of mutations within the loop regions of the *At*GRP7 RRM on binding affinity and specificity

In addition to the analysis of an RNP1 residue for its importance in the RNA binding process, two other residues of the *At*GRP7 RRM were tested for their impact on complex formation. To identify residues that do not only contribute to the RNA-binding affinity of *At*GRP7 but also to the specificity in target selection, amino acids in the less conserved loop regions of the *At*GRP7 RRM were mutated. The loop regions of other RRM proteins like U1A have been postulated to be crucial for the discrimination of different RNAs during the complex formation (Scherly *et al.*, 1990; Katsamba *et al.*, 2002). In *At*GRP7 a tryptophan at position 11 within the first loop region between β_1 and β_2 was exchanged for arginine and a glutamic acid residue at position 44 in loop 3 was replaced by lysine (Figure 16 a). Oligonucleotide directed mutagenesis was carried out with the primer pairs

GRP7W17R and GRP7E44K, respectively (Table 2). The mutated *AtGRP7* sequences were cloned into pGEX-6P-1 for the production of GST fusion proteins in *E. coli*. The loop mutant proteins were subsequently purified by affinity chromatography.

To test the mutants for an altered binding affinity in comparison to the wild type GST-*At*GRP7, EMSAs were performed with 0.5 µg fusion protein and two different tRNA concentrations (1 and 10 µg). A radioactively labelled ORN (7-UTR_WT-SH), corresponding to the 7-UTR_WT ORN from the *AtGRP7* 3'UTR, with a C_3-thiol linker at the 3' end served as binding template. The thiol tag that was attached for single-molecule analysis by AFM did not influence the binding affinity (cf. 4.5.2) but stabilised secondary structures of the free ORN. The different secondary structures are visible as additional bands of the free ORN in the native gels (Figure 16 b, c). Complex formation of both *At*GRP7 protein variants, GST-*At*GRP7-E^{44}K and GST-*At*GRP7-W^{17}R, with 7-UTR_WT-SH was only marginally reduced compared to the wild type protein (Figure 16 b), indicating an almost similar binding affinity.

To check for a reduced binding specificity of the loop mutant proteins three mutated versions of the target site or artificial RNA sequences were synthesised. The recognition of the 7-UTR_G_4mut-SH ORN (the SH indicates the introduction of a C3-thiol linker as described for the 7-UTR_WT-SH ORN, see above) by GST-*At*GRP7-E^{44}K was also slightly reduced in comparison to GST-*At*GRP7 (Figure 16 c). Moreover, for an artificial sequence that was constructed by permutation of the 7-UTR_WT-SH ORN (7-UTR_Permut) only a minimally reduced complex was observed between the wild type protein and the GST-*At*GRP7-E^{44}K loop mutant (Figure 16 d). Interestingly, a potential minimal binding element must have been retained in the mutated sequence since a relatively robust binding of all fusion proteins, wild type and mutants, was visible (Figure 16 d). In contrast, a completely artificial sequence nearly exclusively comprised of guanines and adenines (7-UTR_UG) did not show a strong complex formation with GST-*At*GRP7-E^{44}K and GST-*At*GRP7 and only little shifted complexes were visible with both proteins (Figure 16 e). Thus, *At*GRP7 Glu^{44} has no significant influence on target selection and discrimination.

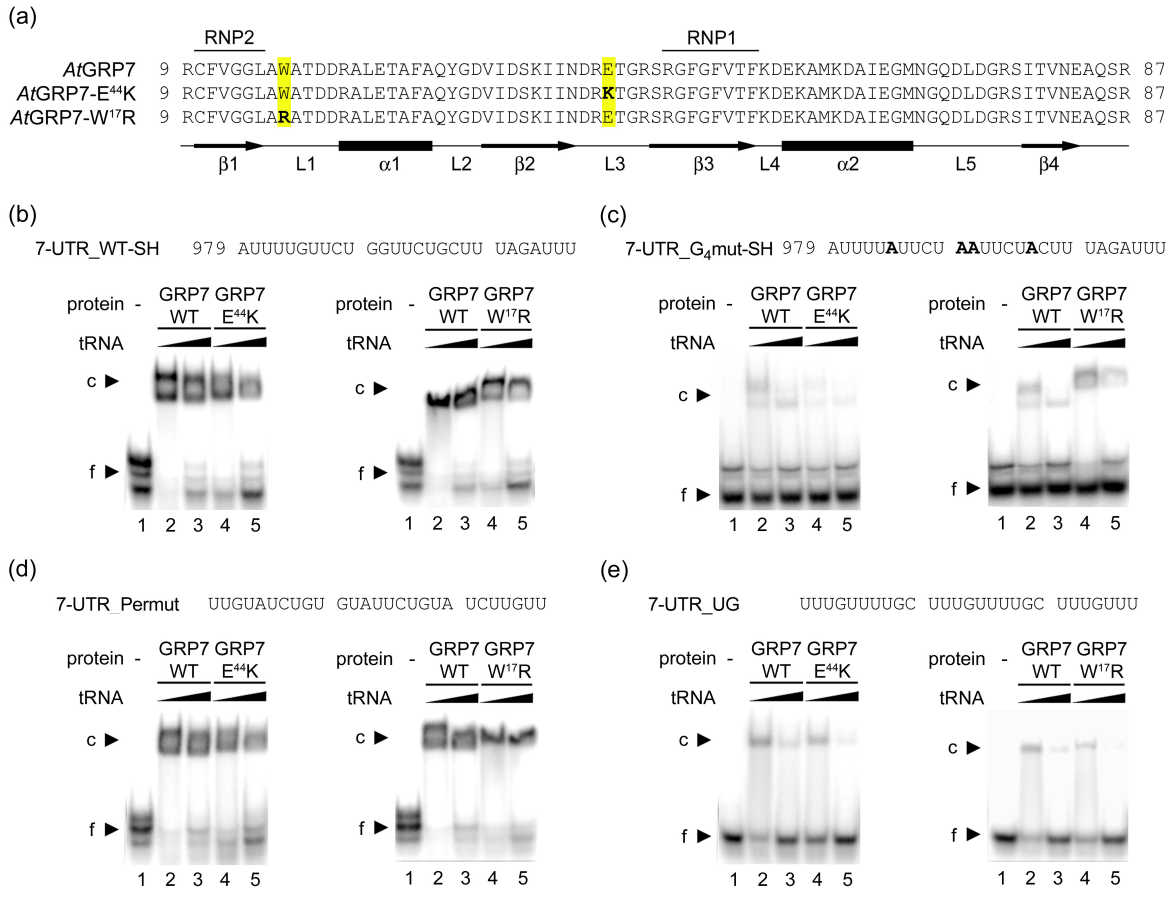

Figure 16: Influence of two *At*GRP7 loop mutations on *At*GRP7 binding activity. (a) Amino acid sequence of the RRMs of wild type *At*GRP7 and the two loop mutant protein variants. The conserved RNP1 and RNP2 and predicted secondary structure elements are indicated. The mutated sites are indicated in yellow and the exchanges of W^{17} for R and E^{44} for K are highlighted in boldface. L, loop. (b-e, left gel) GST-*At*GRP7 (lanes 2, 3) or GST-*At*GRP7-E^{44}K (lanes 4, 5) were incubated with 7-UTR_WT (b), 7-UTR_G_4mut-SH (c), 7-UTR_Permut (d) or 7-UTR_UG (e). Varying amounts of tRNA were added: 1 µg (lanes 2, 4) or 10 µg (lanes 3, 5), respectively. Lane 1, free ORN. (b-e, right gel) GST-*At*GRP7 (lanes 2, 3) or GST-*At*GRP7-W^{17}R (lanes 4, 5) were incubated with 7-UTR_WT (b), 7-UTR_G_4mut-SH (c), 7-UTR_Permut (d) or 7-UTR_UG (e). 1 µg (lanes 2, 4) or 10 µg (lanes 3, 5) of tRNA were added. Lane 1, free ORN. (b, c) The 7-UTR_WT-SH and the 7-UTR_G_4mut-SH ORNs are tagged with a C_3-thiol linker. The thiol linker that was initially introduced for parallel analysis by AFM-FS (cf. 4.5.2) had no influence on the *At*GRP7 binding affinity but is responsible for the multiple bands of the free ORN. Numbering is relative to the transcription start site (Staiger & Apel, 1999).

Likewise, the *At*GRP7-W^{17}R protein variant was tested for binding to the three mutated ORNs. Also for GST-*At*GRP7-W^{17}R a marginally reduced binding was detected towards 7-UTR-Permut and 7-UTR_UG (Figure 16 d, e). However, a slightly enhanced binding was determined in case of the 7-UTR_G_4mut-SH ORN in comparison to the wild type protein (Figure 16 c). The reduced binding of GST-*At*GRP7-W^{17}R to the 7-UTR_WT-SH ORN and the increased binding to the 7-UTR_G_4mut-SH ORN indicates a somewhat reduced target sensitivity of the *At*GRP7-W^{17}R protein variant and thus a potential role for the Trp^{17} residue in target recognition.

4.2 The *At*GRP7-R^{49}Q mutation impairs negative auto-regulation *in vivo*

Electrophoretic mobility shift assays have shown that the RNP1 arginine is essential for binding of *At*GRP7 to its target sequences *in vitro*. To check whether the reduced binding affinity of the *At*GRP7-RQ mutant (cf. 4.1.1) has direct influence on the regulatory activity of *At*GRP7 *in vivo*, the mutated protein was overexpressed in transgenic *Arabidopsis thaliana* lines. An expression vector carrying the *AtGRP7-RQ* cDNA sequence under control of the constitutive CaMV promoter was constructed (Figure 17 a; cf. Table 3) analogous to the constructs for overexpression of the wild type protein (Heintzen *et al.*, 1997). The plasmid was transformed into C24 and Columbia (Col) ecotypes by *Agrobacterium tumefaciens* vacuum infiltration. The transgenic offspring were screened for Kanamycin resistance and tested for the overexpression of the recombinant protein by western blot analysis (Figure 17 b).

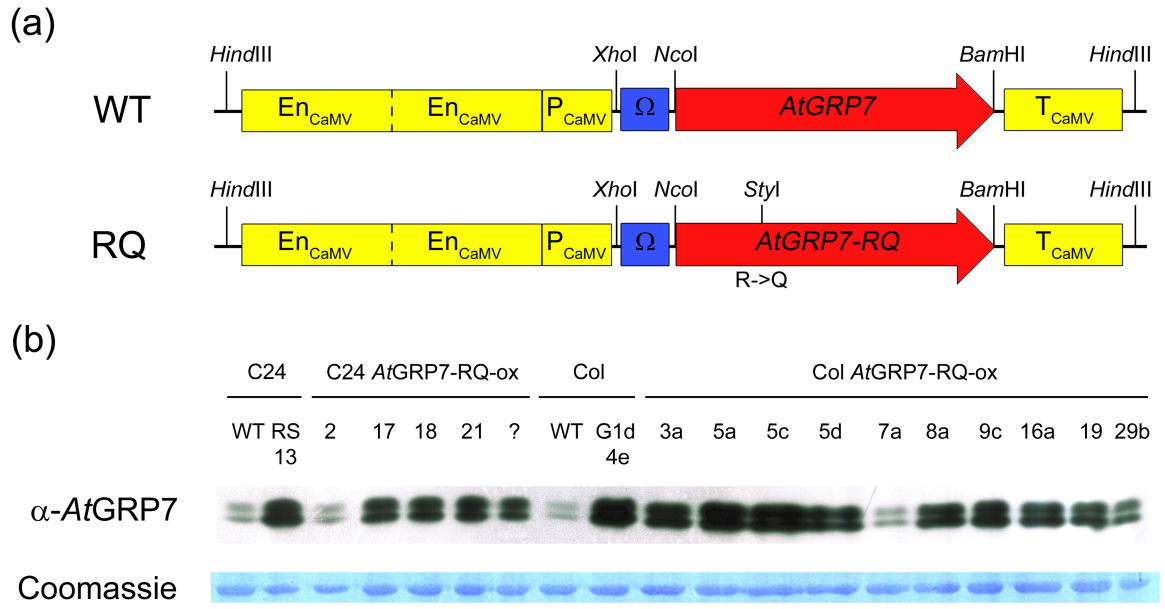

Figure 17: Western blot analysis of *Arabidopsis* *At*GRP7-RQ-ox lines. (a) Illustration of the *At*GRP7 (top) and *At*GRP7-RQ (bottom) overexpression constructs. A diagnostic *Sty*I site has been created by the mutation of Arg^{49} to Gln. Regulatory elements of the CaMV promoter (En = enhancer, P = promoter), and T = terminator are displayed in yellow, the *At*GRP7 coding sequence is displayed in red. The TMV omega element is a translational enhancer (Ω, blue). (b) The *At*GRP7 expression level in the transgenic plants was compared to wild type and *At*GRP7-ox lines. 5 µg total protein per lane have been blotted. Coomassie staining of the membrane served as a loading control.

For further characterisation transgenic lines were selected that overexpress the *At*GRP7-RQ mutant protein (*At*GRP7-RQ-ox) at levels comparable to the overexpression of the wild type potein (*At*GRP7-ox) in C24 RS13 and Col G1d (Figure 18 b). To test the

influence of the introduced Arg^{49}Gln mutation on the down-regulation of the endogenous transcript, northern blot analysis was carried out using a gene-specific probe against the 5' UTR of the endogenous *AtGRP7* transcript. Since the overexpression construct harbours recombinant CaMV (Cauliflower Mosaic Virus) promoter and the TMV omega element (Gallie *et al.*, 1987) instead of the *AtGRP7* promoter and 5' UTR, this probe is capable to discriminate between the endogenous and the transgenic transcript (Figure 17 a). In *At*GRP7-ox lines a severe down-regulation of the mature *AtGRP7* mRNA can be obsereved. In contrast, the level of endogenous *At*GRP7 in *At*GRP7-RQ-ox lines is almost indistinguishable from that in wild type plants.

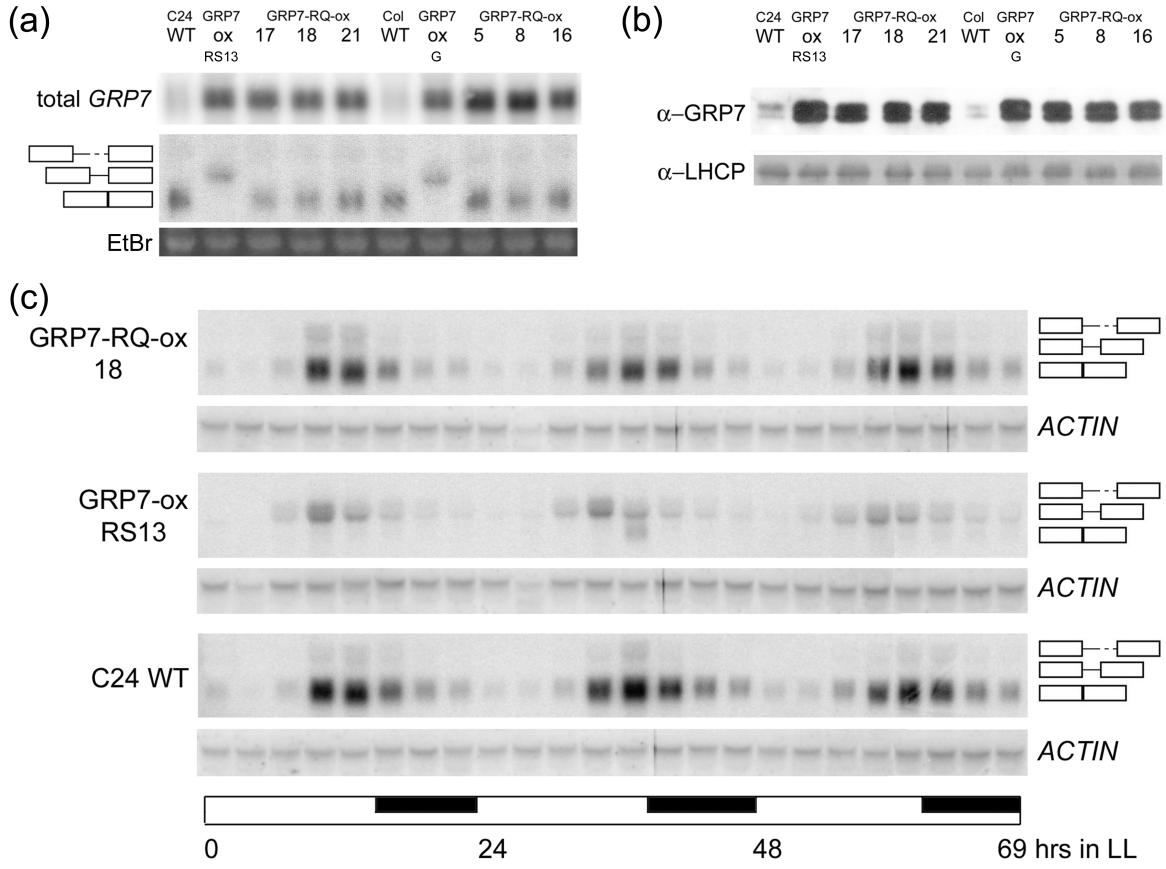

Figure 18: Overexpression of the *At*GRP7-RQ mutant protein does not feed back on endogenous *AtGRP7*. (a) *At*GRP7-RQ-ox plants in the C24 and Col background as well as the corresponding *At*GRP7-ox and WT plants were harvested at ZT12. The RNA gel blot was hybridised with the *AtGRP7* cDNA to determine the total transcript level (top) and with a gene-specific probe to detect the level of the endogenous *AtGRP7* transcript (middle). The positions of the pre-mRNA, *as_AtGRP7* retaining the first half of the intron and the mRNA are indicated. Boxes represent exons, the solid and broken lines represent the first and second halves of the intron, respectively. The ethidium-bromide stained gel shows equal loading (bottom). (b) The immunoblot of the same samples as in (a) was incubated with an antibody against *At*GRP7 (top). The double band may reflect proteolytic degradation or post-translational modification. Subsequently, the blot was probed with an antibody against LHCP as a loading control (bottom). (c) C24 WT, *At*GRP7-ox (RS13) and *At*GRP7-RQ-ox plants 18 were harvested at 3 h intervals after transfer to LL. The endogenous *AtGRP7* transcript was detected with a gene-specific probe (top). Hybridisation with *ACTIN* served as constitutive control (bottom).

Also the emergence of the alternatively spliced *AtGRP7* transcript (*as_AtGRP7*) at the expense of the mature mRNA can only be seen in *At*GRP7-ox but not in *At*GRP7-RQ-ox lines (Figure 18 a). This revealed a severe difference in the regulatory activity between the wild type *At*GRP7 and *At*GRP7-RQ.

In *At*GRP7-ox plants the oscillations of the endogenous transcript are damped. To investigate a similar influence of the *At*GRP7-RQ overexpression on the *AtGRP7* transcript oscillation, *AtGRP7* expression was monitored under constant conditions. Wild type, *At*GRP7-ox and *At*GRP7-RQ-ox plants were grown under long day conditions (LD; 16 h light, 8 h darkness). At an age of about two weeks the seedlings were transferred to constant light conditions (LL) and were harvested at three hour intervals for 72 hours.

The northern blot showed the expected alternative splicing of *AtGRP7* pre-mRNA at the expense of the mature RNA and, as a result, a reduced transcript level in the *At*GRP7-ox line (Figure 18 c). In contrast, splicing pattern, amplitude, period and phase of the endogenous transcript in *At*GRP7-RQ-ox plants remained more or less identical to those in wild type plants (Figure 18 c).

Thus, the reduced binding affinity of *At*GRP7-RQ obviously prevents efficient negative auto-regulation and alternative splicing of the *AtGRP7* mRNA. Consequently, no influence of the *At*GRP7-RQ overexpression on circadian rhythmicity is detectable.

4.2.1 Evidence for direct binding of *At*GRP7 to its own transcript *in vivo*

The alternative splicing of the *AtGRP7* transcript in *At*GRP7-ox plants and concomitant down-regulation of the *At*GRP7 protein as well as the loss of this negative auto-regulation in *At*GRP7-RQ-ox plants indicate a requirement of *At*GRP7 binding activity for its function *in vivo*. It can be assumed that a direct binding of *At*GRP7 to its own transcript initiates this process. To demonstrate an RNA binding *in vivo*, *At*GRP7 containing mRNPs (messenger ribonucleoprotein particles) were isolated from plant extracts by RNP-immunoprecipitation in order to exctract the mRNAs contained in the precipitate. To exclude as much co-precipitation of unspecific RNA and protein as possible, an experimental setup was designed that allowed the use of a monoclonal antibody instead of the polyclonal α-*At*GRP7 serum that was used for immunoblotting. Thus, Col *At*GRP7-GFP and Col GFP plants were used in combination with a monoclonal α-GFP antibody. The construct for the *At*GRP7-GFP fusion protein harboured all regulatory *AtGRP7* regions, such as promoter, intron and UTRs, and the *GFP* tag sequence was fused in frame

to the 3' end of the second *AtGRP7* exon. The *GFP* construct contains the same regulating regions as the *AtGRP7-GFP* fusion construct (Figure 19 a). The Col GFP plants were used as a negative control. An additional control was an *At*GRP7-GFP sample in which the antibody was omitted. The RNA-protein complexes in the plants were first cross-linked by infiltration of formaldehyde. Subsequently, the mRNPs were precipitated via the specific α-GFP antibody and the RNA was extracted from the complexes by denaturation of the proteins.

The precipitated RNA was reverse-transcribed and analysed by RT-PCR. For a first analysis a primer combination binding within the second exon of *AtGRP7* was chosen (AGRP100/AGRP125; cf. Table 2). The hybridisation of the Southern blotted amplification products revealed an 8-fold increased level of the *AtGRP7* transcript in the *At*GRP7-GFP precipitate in comparison to the GFP control sample. The blank sample without α-GFP antibody showed almost no precipitation of *AtGRP7* (Figure 19 b).

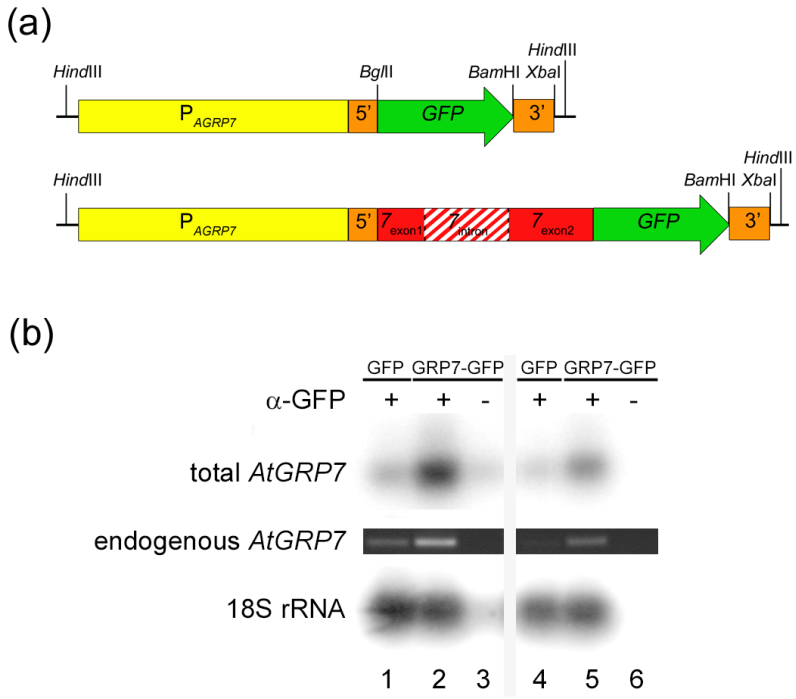

Figure 19: *At*GRP7-RNA-immunoprecipitation. (a) Scheme of the GFP (top) and *At*GRP7-GFP (bottom) expression constructs. The *AtGRP7* coding sequence is displayed in red, the intron is indicated by a hatched red box. *AtGRP7* promoter (yellow) and regulatory elements of *AtGRP7* (orange) are indicated. The GFP coding sequence is presented in green. (b) Two independent RNP-immunoprecipitation experiments were performed with different washing conditions (2M (lanes 1-3) and 4M (lanes 4-6) urea) to remove as much unspecific background as possible. Precipitated RNAs were reverse-transcribed with oligo(dT)$_{12\text{-}18}$ primers. PCR amplification of total *AtGRP7* was performed using primers within the second exon and 24 cycles. The gel with the PCR products was blotted and hybridised with the *AtGRP7* cDNA (top). Amplification with 18S rRNA primers served as control (bottom). The PCR for *At*GRP7 was repeated with primers excluding the amplification of the *At*GRP7-GFP transgene (middle), see text.

18S rRNA served as a control template to document the amount of unspecifically precipitated RNA. Both samples treated with the α-GFP antibody showed comparable levels of *18S* rRNA, whereas in the blank sample almost no 18S rRNA was detectable (Figure 19 b). To further exclude that the enrichment of the *AtGRP7* RNA is due to the additional expression of the *AtGRP7-GFP* transgene the RT-PCR was repeated with primers specific for the endogenous *AtGRP7* transcript (AGRP63/AGRP130). Again, a strong enrichment of the *AtGRP7* transcript could be detected in the eluates from the *At*GRP7-GFP samples in comparison to the GFP control samples (Figure 19 b).

The enrichment of *AtGRP7* mRNA by RNP-immunoprecipitation points to direct *At*GRP7 binding to its own mRNA *in vivo*.

4.3 Regulation of downstream targets by *At*GRP7

Since *At*GRP7 binding is essential for its negative auto-regulation (cf. 4.2) it was examined whether *At*GRP7 binding is also necessary for the regulation of downstream targets. The transcript of the closely related *At*GRP8 protein is severely down-regulated upon *At*GRP7 overexpression (Heintzen *et al.*, 1997; Staiger *et al.*, 2003). *At*GRP7 protein represses *AtGRP8* accumulation by the same mechanism that it uses for the auto-regulation. High *At*GRP7 levels induce alternative splicing. The alternatively spliced product that occurs at the expense of the mature RNA comprises a premature termination codon that prevents the accumulation of functional protein (Staiger *et al.*, 2003). To analyse whether the regulation of *AtGRP8* by *At*GRP7 requires a functional RRM, an influence of the $Arg^{49}Gln$ on target regulation was investigated in *At*GRP7-RQ-ox plants.

4.3.1 *At*GRP7-R^{49}Q interferes with target regulation

To identify an influence of *At*GRP7-RQ overexpression on the regulation of *AtGRP8*, the levels of the three different *AtGRP8* splice variants in *At*GRP7-RQ-ox plants was compared to those in wild type plants and *At*GRP7-ox lines. In *At*GRP7-ox lines only a single band corresponding to *as_AtGRP8* was visible (Figure 20 a). In contrast, in *At*GRP7-RQ-ox plants the pre-mRNA and the mature mRNA were detectable at wild type levels, and only little alternatively spliced *AtGRP8* transcript (*as_AtGRP8*) was observed (Figure 20 a).

An extended time course assay in continous light, for which plants were harvested over 3 days in 3 h intervals, showed similar oscillation patterns for *At*GRP7-RQ-ox and wild type plants. In *At*GRP7-ox the *as_AtGRP8* still oscillated, however, at a reduced level (Figure 20 c). Coherent with these results, the abundance of the *At*GRP8 protein was significantly reduced in *At*GRP7-ox plants, whereas it was indistinguishable from wild type in *At*GRP7-RQ-ox lines (Figure 20 b).

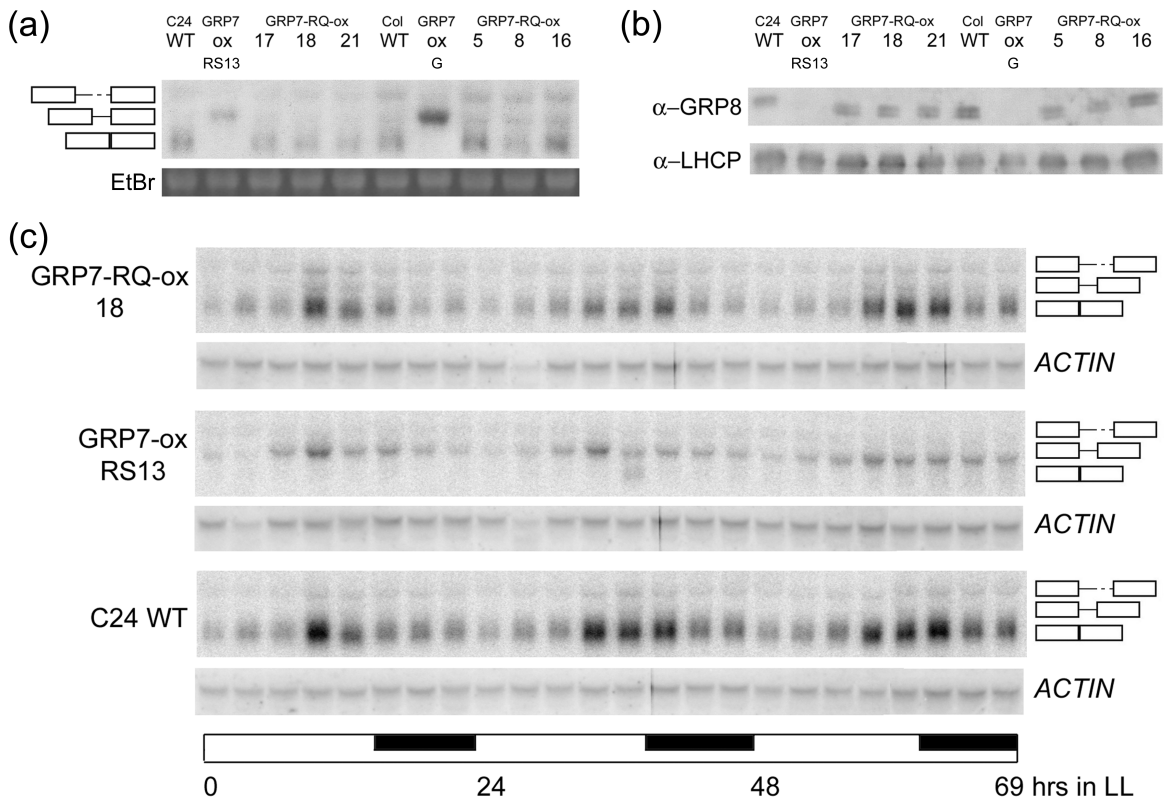

Figure 20: The *At*GRP7-RQ mutation interferes with regulation of *AtGRP8*. (a) *At*GRP7-RQ-ox plants in the C24 and Col background as well as the corresponding *At*GRP7-ox and WT plants were harvested at ZT12. The RNA gel blot was hybridised with the gene-specific *AtGRP8* probe (top). The positions of the pre-mRNA, the alternatively spliced transcript *as_AtGRP8* retaining the first half of the intron and the mRNA are indicated. Boxes represent the exons, the solid and broken lines represent the first and second halves of the intron, respectively. The ethidium-bromide stained gel shows equal loading (bottom). (b) The immunoblot of the same samples as in (a) was incubated with an antibody against *At*GRP8. (c) WT C24, *At*GRP7-ox (RS13) and *At*GRP7-RQ-ox (18) plants entrained in LD were harvested at 3 h intervals after transfer to LL. The *AtGRP8* transcript was detected with a gene-specific probe (top) on the blot previously hybridised with *AtGRP7* (see Figure 18c). Hybridisation with *ACTIN* served as constitutive control (bottom).

Thus, the reduced binding affinity of *At*GRP7-RQ also interferes with the regulation of the downstream target *AtGRP8*.

4.3.2 *At*GRP7 binds to sequences within the *AtGRP8* transcript

Because *AtGRP8* is severely reduced in *At*GRP7-ox plants but not in *At*GRP7-RQ-ox plants, it was conceivable that *At*GRP7 is also capable to directly bind to the *AtGRP8* transcript. For the determination of putative binding sites a combined approach of bioinformatic analysis and *in vitro* binding assays was used.

4.3.2.1 Prediction of *At*GRP7 binding sites within the *AtGRP8* transcript by bioinformatic analysis

Since the binding sites within the *AtGRP7* transcript had been narrowed down perviously to 32 nucleotides (cf. 4.1), these sequences were used to uncover the target sites within *AtGRP8*. The pre-mRNAs of *AtGRP7* and *AtGRP8* exhibit 64 % identity. Thus, in a first, simple approach the *AtGRP8* pre-mRNA was analysed for sequence homologies to the known *AtGRP7* 7-UTR_WT and 7-intron_WT ORN sequences (cf. 4.1) using ClustalW and Dialign (Thompson *et al.*, 1994; Morgenstern, 2004). In addition to a score for homology, two further parameters were set to reduce the number of potential binding sites. First, the regions for possible target sequences were restricted to the 3' UTR and the second half of the intron. Second, the position of guanines in the sequences was weighted stronger than that of other bases. This parameter aimed at the efficient reduction of binding upon exchange of these guanines in case of the *AtGRP7* binding sites (cf. 4.1) and the competition of poly(G) sequences for the binding of *At*GRP7 to both, 3' UTR and intron (Staiger *et al.*, 2003).

Using these criteria three regions were identified within the *AtGRP8* transcript, one in the second half of the intron and two in the 3'UTR (Figure 21 a).

In a second step the identified sequences were analysed for the occurrence of stable secondary structures, to omit sequences that form long double-stranded regions and are thus not accessible for RRM proteins (cf. 2.2.1). For the analysis of the secondary structure mfold and RNAshapes were used (Zuker, 2003; Steffen *et al.*, 2006). Both programs predicted for 8-intron_WT and 8-UTR_WT a hairpin structure with a long loop and a short stem that should not interfere with *At*GRP7 binding and looks similar to the structures predicted for the *AtGRP7* 7-UTR_WT and 7-intron_WT ORNs (Figure 21 b). The 8-UTR_938 ORN was assumed to form a longer, more stable stem that could probably reduce the accessibility of the sequence (Figure 21 b).

(a)

```
353 ...CUCGGAG AUCGAUCGAU UUUUGCUUUA UAUUCAUCGC UUUGUUUUAU

400 AUUCCUUCCA CGAUUGUUUU UGCUGAUGUG UAUGAUUUUG UUUGUUUACA
                  8-intron_WT

450 GAUCAUUAAC GACCGCGAGA GUGGAAGAUC AAGGGGAUUC GGAUUCG...


833 ...GCGGUGG UGGCGGCUGG UAAUCAAAGA UAGAGUUGUU UGCGUGCUGC

880 UGCUCUGUUU UUGGUUUAGA UUUGGUUUUG UGUCACCACU UCUGGUUUGG
                  8-UTR_WT

930 UUAUCGUUCG UUUGGUUUAC UUUUUUGAUG AAACAGUUUC GUUUAAG...
                  8-UTR_938
```

(b)

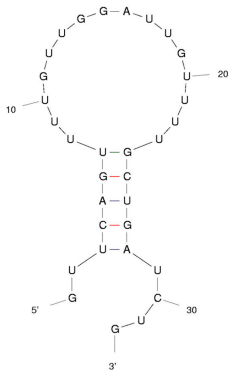

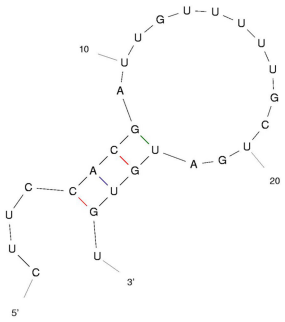

(c)

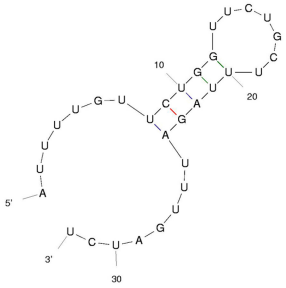

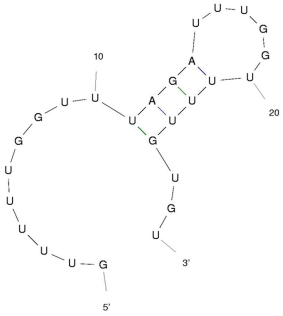

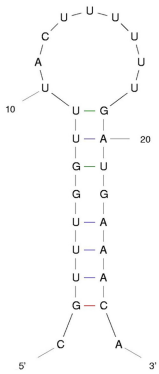

Figure 21: Bioinformatic prediction of *At*GRP7 binding sites within the *AtGRP8* transcript. (a) The sequences of the oligoribonucleotides identified as target sites in *AtGRP7* were aligned with ClustalW to the *AtGRP8* pre-mRNA yielding three potential binding sequences in *AtGRP8*. The potential target sequences are highlighed in red. 3' splice site (green) and stop codon (blue) are indicated. (b) The predicted secondary structures for 7-intron_WT (left) and 8-intron_WT (right). (c) The predicted secondary structures for 7-UTR_WT (left), 8-UTR_WT (middle) and 8-UTR_938 (right).

Since the secondary structure prediction for short sequences does not mirror the folding *in vivo*, a third test was performed to predict the secondary structure of the binding regions in an entire pre-mRNA context. In co-operation with Prof. Dr. Irmtraud Meyer (Bioinformatics Center, University of British Columbia, Vancouver, Canada), the pre-mRNAs of *AtGRP7* and *AtGRP8* were analysed for evolutionary conserved secondary structures. Eight sequences, homologous to *At*GRP7, from other plant species (Table 8) were used as templates for the structure conservation search with the RNAdecoder tool (Pedersen *et al.*, 2004).

Table 8: Transcripts used for the prediction of evolutionary conserved secondary structures in pre-mRNAs and mRNAs of glycine-rich RNA-binding proteins.

Name	Species	Accession number (AGI)
AtGRP7	*Arabidopsis thaliana*	NM120087 (At2g21660)
AtGRP8	*Arabidopsis thaliana*	NM127738 (At4g39260)
BnGRP10	*Brassica napus*	Z14143
NsRGP-1a	*Nicotiana sylvestris*	D16204
OsGRP	*Oryza sativa*	AK289192
PhGRP2	*Pelargonium hortorum*	AF009004
SaGRP1c	*Sinapis alba*	L31376
SaGRP2c	*Sinapis alba*	L31378
ZmGRP	*Zea mays*	X12564

Three larger regions with a high degree of secondary structure conservation could be uncovered. Two are located in the intron, the other in the 3' UTR (Figure 22; cf. 8.2). Interestingly, both binding sequences defined for *AtGRP7* located to regions with a high degree of structural conservation. Moreover, the predicted folding of the binding sequences within these regions comprised extended single-stranded regions that allow RRM binding (Figure 22, left panel).

The analysis for the predicted *AtGRP8* sequences showed that all three sequences were also located in conserved regions. However, the 8-intron_WT and the 8-UTR_WT sequences were predicted to be easily accessible, whereas the 8-UTR_938 sequence was predicted to be located in a region with a less favourable secondary structure (Figure 22, right panel).

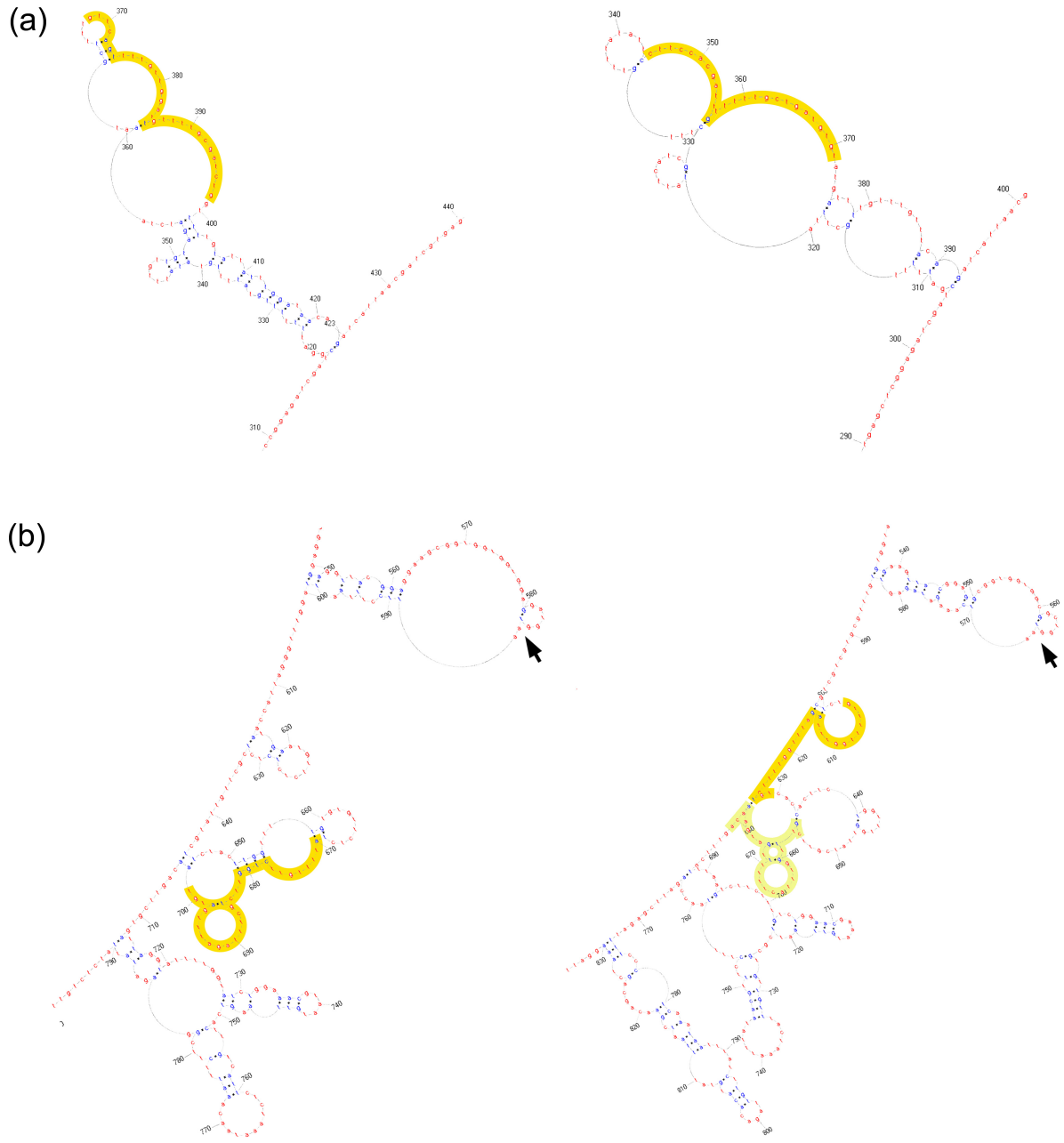

Figure 22: The identified *At*GRP7 target sites in the *AtGRP7* pre-mRNA and the predicted binding sites in *AtGRP8* are located in regions with evolutionary conserved secondary structures. (a) The introns of *AtGRP7* (left) and *AtGRP8* (right) have conserved secondary structure elements. The assumed target sites for *At*GRP7 binding are highlighted. The numbering is relative to the start codon. (b) The 3' untranslated regions of *AtGRP7* (left) and *AtGRP8* (right) exhibit an extensive secondary structure. The sequences of 7-UTR_WT and 8_UTR-WT are highlighted in yellow, the sequence of 8-UTR_938 is highlighted in beige (see text). The stop codon is indicated by an arrow.

Although a conservation of secondary structures implicates a high importance for regulation, the lack of such a conservation or a reduced accessibility is no final criterion for the exclusion of a potential target sequence. Nevertheless, the bioinformatic analysis revealed a preference for 8-intron_WT and 8-UTR_WT as target regions.

4.3.2.2 Identification of *AtGRP8* target sites by *in vitro* binding assays

The bioinformatic analysis had predicted three sequences from the *AtGRP8* pre-mRNA as potential target sites for *At*GRP7 binding. Since *AtGRP7* harbours only two identified target sites electrophoretic mobility shift assays were used to uncover differences in binding affinity.

Oligoribonucleotides of the three sequences were synthesised and radioactively labelled at the 5' end (Figure 23 a). First binding assays showed a complex formation of all three ORNs with GST-*At*GRP7 (data not shown). Thus, equilibrium dissociation constants were determined to identify distinctions in binding affinity. 8-intron_WT (Figure 23 b) and 8-UTR_WT (Figure 23 c) showed K_d values comparable to those calculated for the *At*GRP7 binding sites in the *AtGRP7* pre-mRNA (Figure 23 e, cf. 4.1.1). In contrast, the 8-UTR_938 ORN (Figure 23 d) showed a 15-fold reduced binding affinity compared to the 8-UTR_WT sequence and a 2-fold higher K_d value than 8-intron_WT (Figure 23 e).

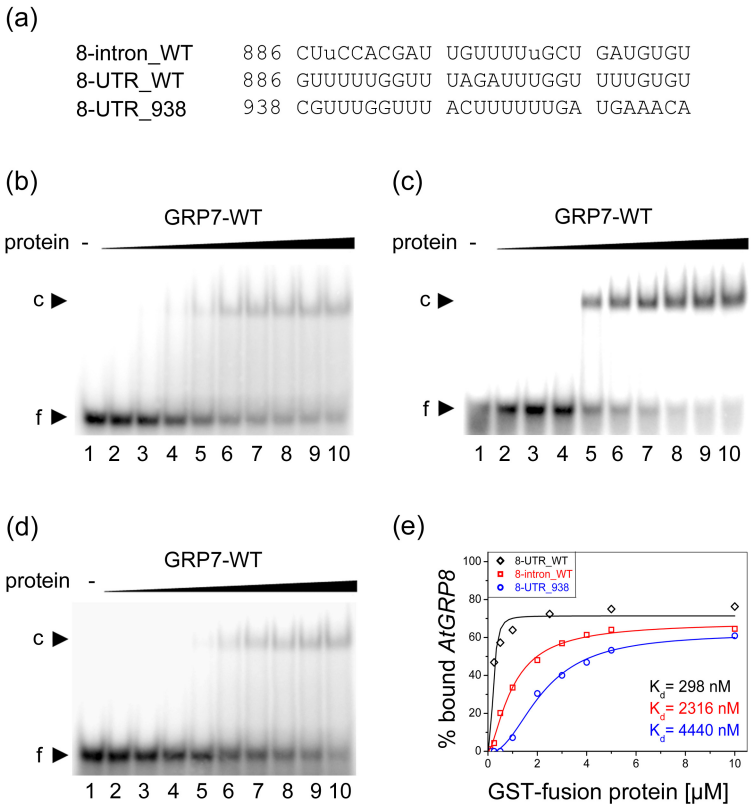

Figure 23: *At*GRP7 shows different affinities to the predicted binding sites in *AtGRP8*. (a) Sequences of the ORNs containing the predicted binding sites within the second half of the *AtGRP8* intron and the *AtGRP8* 3´ UTR, respectively. Numbering is relative to the transcription start site (Staiger, unpublished). (b-d) Determination of the K_d vaules for the interaction of the *AtGRP8* ORNs (8-intron_WT, 8-UTR-WT and 8 UTR_938, respectively) with GST-*At*GRP7. (e) Comparison of the binding affinities of the three ORNs derived from the *AtGRP8* pre-mRNA (see text).

In parallel, competition experiments showed that an exess of unlabelled 8-UTR_WT competed stronger for *At*GRP7 binding than the 8-UTR_938 ORN did. 100 pmol 8-UTR_WT ORN were sufficient to abrogate the binding of GST-*At*GRP7 to 8-UTR_938, whereas 250 pmol of homologous ORN were not able to completely repress complex formation (Figure 24).

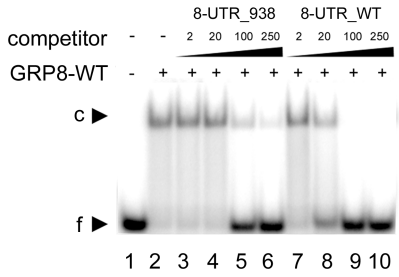

Figure 24: *At*GRP7 binds tighter to 8-UTR_WT than to 8-UTR_938. GST-*At*GRP7 protein was incubated with labelled 8-UTR_938 ORN in the presence of 5 µg of tRNA (lanes 2-10) and 2, 20, 100 and 250 pmoles of unlabelled 8-UTR_938 ORN (lanes 3-6) or 20, 100, 250 and 500 pmoles of unlabelled 8-UTR_WT (lanes 7-10), respectively. Lane 1, free ORN.

Together with the bioinformatic analysis that had revealed some preference for the 8-UTR_WT sequence (cf. 4.3.2.1), the binding assays suggest 8-UTR_WT and 8-intron_WT as most probable *At*GRP7 target sites within the *AtGRP8* pre-mRNA.

To strengthen this result, both sequences (8-intron_WT and 8-UTR_WT) were analysed more closely for binding of the GST-*At*GRP7 wild type and GST-*At*GRP7-RQ mutant protein.

The K_d values for GST-*At*GRP7-RQ were determined to be nine-fold higher for 8-UTR_WT and five-fold elevated for the intronic sequence (Figure 25 c and e, respectively). The reduction of the *At*GRP7-RQ binding affinity towards the *AtGRP8* ORNs is comparable to that observed in case of the *AtGRP7* binding sequences (cf. 4.1.1). In contrast to GST-*At*GRP7, GST-*At*GRP7-RQ did not show a high affinity to the binding sequences within the *AtGRP8* pre-mRNA (Figure 25 b, d). Thus the $Arg^{49}Gln$ mutation also reduces the binding affinity of the *At*GRP7 protein towards the target sequences in the *AtGRP8* pre-mRNA.

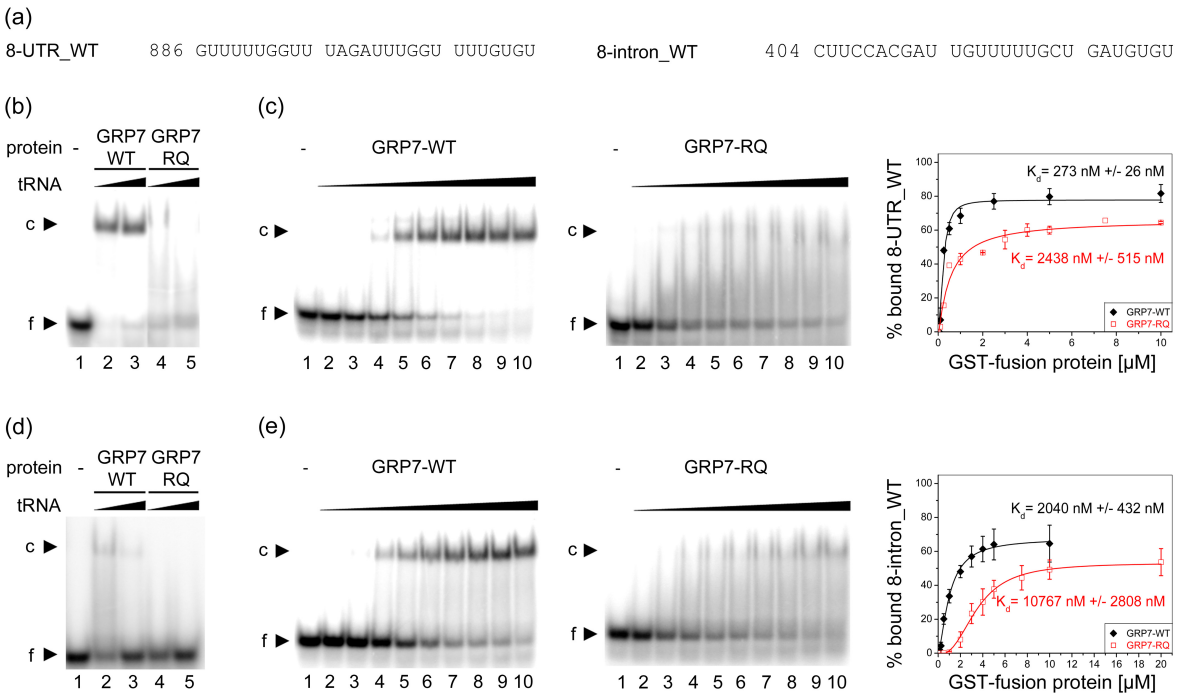

Figure 25: Influence of the RNP1 RQ mutation on *At*GRP7 binding to the *AtGRP8* intron and 3' UTR. (a) Sequence of the 8-UTR_WT and the 8-intron_WT ORN, respectively. Numbering is relative to the start site of transcription (Staiger, unpublished). (b, d) The labelled 8-UTR_WT (b) and 8-intron_WT (d) ORN were incubated with GST-*At*GRP7 (lanes 2, 3) or GST-*At*GRP7-RQ (lanes 4, 5) and 1 µg (lanes 2, 4) or 10 µg (lanes 3, 5) of tRNA, respectively. Lane 1, free ORN. (c) To compare binding affinities of WT and mutant protein, 50 fmoles of labelled 8-UTR_WT ORN were incubated with 0.01, 0.05, 0.1, 0.25, 0.5, 1, 2.5, 5 and 10 µM of GST-*At*GRP7 (left, lanes 2-10) or GST-*At*GRP7-RQ (middle, lanes 2-10), respectively. (e) 50 fmoles of labelled 8-intron_WT ORN were incubated with 0.1, 0.25, 0.5, 1, 2, 3, 4, 5 and 10 µM of GST-*At*GRP7 (left, lanes 2-10) or 1, 2, 3, 4, 5, 7.5, 10, 20 and µM of GST-*At*GRP7-RQ (middle, lanes 2-10), respectively. All reactions contain 1 µg tRNA. Bound and free RNA were quantified and K_d values calculated based on the mean of three independent experiments as described in Materials and Methods (cf. 3.5.4).

Competition assays were performed to investigate sequence specificity of the *At*GRP7-*AtGRP8* complex formation. In analogy to the competition assays with *At*GRP7 binding to its own transcript (cf. 4.1), ORNs were designed carrying several point mutations (Figure 26 a). Both, the 8-UTR_G_6mut and the 8-intron_G_2U_2mut competed less for the *At*GRP7 binding than the corresponding wild type sequences from the 3' UTR (Figure 26 b, d) and the intron (Figure 26 c, e).

250 pmol of the 8-UTR_WT ORN nearly completely abolished complex formation with wild type GST-*At*GRP7, whereas the same concentration of 8-UTR_G_6mut did not show any competition (Figure 26 b). Similar results were obtained for the intronic ORN (Figure 26 c). However, the amount for a strong competition of the wild type sequence was reduced to 100 pmol which is consistent with the slightly higher K_d value for this sequence.

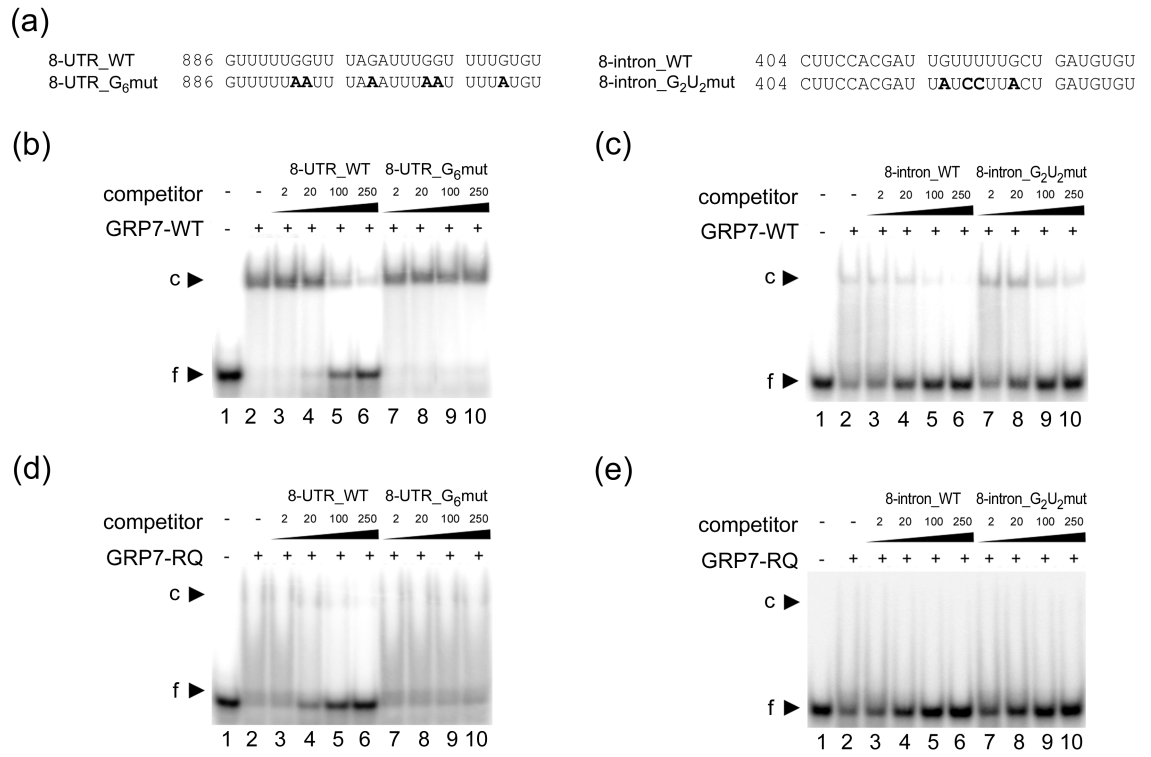

Figure 26: *AtGRP8* point mutations interfere with binding. (a) Sequence of the 8-UTR_WT and the 8-intron_WT ORN and the corresponding mutated 8-UTR_G_6mut and 8-intron_G_2U_2mut with six G residues exchanged for A or two G and two U residues exchanged for A or C (in bold), respectively. Numbering is relative to the start site of transcription (Staiger, unpublished). (b) GST-*At*GRP7 protein was incubated with labelled 8-UTR_WT ORN in the presence of 5 µg of tRNA (lanes 2-10) and 2, 20, 100 and 250 pmoles of unlabelled 8-UTR_WT ORN (lanes 3-6) or 8-UTR_G_6mut (lanes 7-10), respectively. Lane 1, free ORN. (c) GST-*At*GRP7 protein was incubated with labelled 8-intron_WT ORN in the presence of 5 µg of tRNA (lanes 2-10) and 2, 100 and 250 pmoles of unlabelled 8-intron_WT ORN (lanes 3-6) or 8-intron_G_2U_2mut (lanes 7-10), respectively. Lane 1, free ORN. (d) GST-*At*GRP7-RQ protein was incubated with labelled 8-UTR_WT ORN in the presence of 5 µg of tRNA (lanes 2-10) and 2, 20, 100 and 250 pmoles of unlabelled 8-UTR_WT ORN (lanes 3-6) or 8-UTR_G_6mut (lanes 7-10), respectively. Lane 1, free ORN. (e) GST-*At*GRP7-RQ protein was incubated with labelled 8-intron_WT ORN in the presence of 5 µg of tRNA (lanes 2-10) and 2, 100 and 250 pmoles of unlabelled 8-intron_WT ORN (lanes 3-6) or 8-intron_G_2U_2mut (lanes 7-10), respectively. Lane 1, free ORN.

Likewise, the competition assays showed that GST-*At*GRP7-RQ retained sequence specificity for the *AtGRP8* binding sites. Although the binding is much weaker, the wild type sequences still compete better for the GST-*At*GRP7-RQ binding than their mutated counterparts (Figure 26 d, e). Again, a smearing of the AtGRP7-RQ containing complexes appears during the gel run, pointing to a reduced stability of the RNA-*At*GRP7-RQ interaction (Figure 26 d, e).

Thus, the binding sequences for the *AtGRP8* transcript predicted by bioinformatic analysis could be verified *in vitro*. The identified sequences resemble their homologues in *AtGRP7* concerning binding affinity and sequence specificity. Thus, 8-UTR_WT and 8-intron_WT can be annotated as *bona fide* target sequences of *At*GRP7.

4.4 Molecular analysis of *At*GRP8 function *in vitro* and *in vivo*

Because of the high degree of homology between *At*GRP7 and *At*GRP8 at the amino acid level (82 % identity) it was examined whether both proteins exhibit similar or identical functions within the plant. First, a detailed molecular analysis of the RNA-binding properties of wild type *At*GRP8 and a mutated protein variant was done *in vitro*. Second, the *At*GRP8 protein was constitutively and ectopically overexpressed in *Arabidopsis* to investigate a potential influence of *At*GRP8 on transcript maturation and circadian rhythmicity. Third, transgenic *Arabidopsis* lines overexpressing an *At*GRP8-RQ mutant protein were generated to show a direct requirement of RNA-binding activity for *in vivo* function.

4.4.1 Binding of *At*GRP8 to its own transcript

As *At*GRP7 binds to its own transcript to induce alternative splicing and negative auto-regulation it was analysed whether *At*GRP8 shows an identical behaviour. For this purpose gel shift experiments were performed using synthetic oligoribonucleotides comprising the binding sites for *At*GRP7 in *AtGRP8* and recombinantly expressed GST-*At*GRP8 fusion protein. Stable complex formation was observed for both sequences (Figure 27 c, e). Equilibrium dissociation constants were determined for binding of GST-*At*GRP8 to 8-UTR_WT and 8-intron_WT (Figure 27 d, f). The obtained K_d values were comparable to those calculated for binding of GST-*At*GRP7 to the same sequences (cf. 4.3.2.2).

In analogy to the experiments performed with *At*GRP7-RQ an *At*GRP8 mutant protein was engineered. Again the conserved arginine of RNP1 (Arg^{47}) was mutated (Figure 27 a). A site directed mutagenesis PCR using the 8RQ primer pair (Table 2) was performed on a plasmid containing the *AtGRP8* cDNA to exchange Arg^{47} for glutamine. The sequence encoding the *At*GRP8-RQ mutant protein was subcloned into the pGEX-6P-1 vector for recombinant expression as GST-fusion protein in *E. coli*. The purified GST-*At*GRP8-RQ protein was tested in EMSA experiments and showed a severely reduced binding to the *AtGRP8* ORNs (Figure 27 c, e).

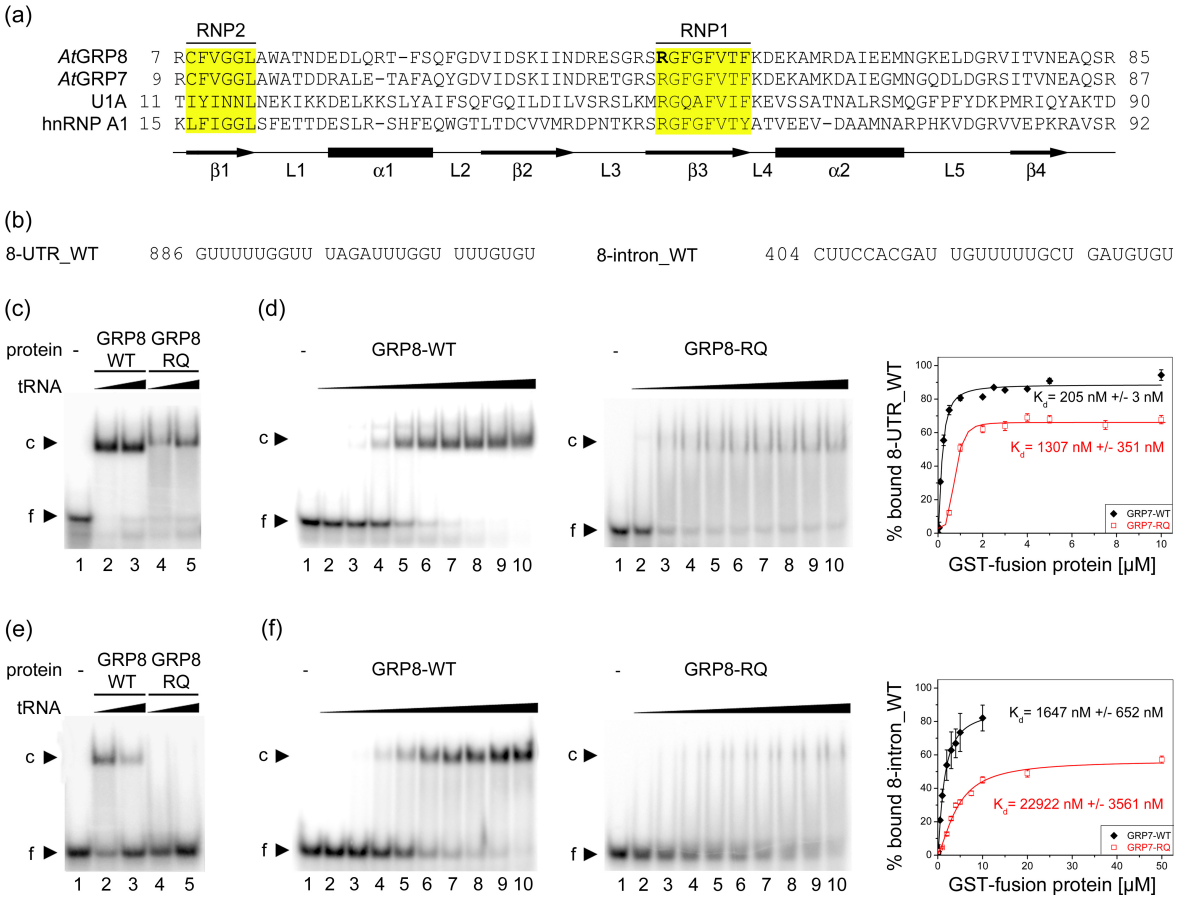

Figure 27: Binding of *At*GRP8 and *At*GRP8-RQ to its own transcript. (a) *At*GRP8 RRM aligned upon the *At*GRP7 RRM and the N-terminal RRM of U1A and hnRNP A1 (Maris *et al.*, 2005). The conserved RNP1 and RNP2 and predicted secondary structure elements are indicated. R^{47} mutated to Q is highlighted in boldface. L, loop. (b) Sequence of the *AtGRP8* 3' UTR (8-UTR_WT) and intron (8-intron_WT) ORN. Numbering is relative to the start site of transcription (Staiger, unpublished). (c, e) The labelled 8-UTR_WT (c) and 8-intron_WT (e) ORN were incubated with GST-*At*GRP8 (lanes 2, 3) or GST-*At*GRP8-RQ (lanes 4, 5) and 1 µg (lanes 2, 4) or 10 µg (lanes 3, 5) of tRNA, respectively. Lane 1, free ORN. (d) To compare binding affinities of WT and mutant protein, 50 fmoles of labelled 8-UTR_WT ORN were incubated with 0.01, 0.05, 0.1, 0.25, 0.5, 1, 2.5, 5 and 10 µM of GST-*At*GRP8 (left, lanes 2-10) or GST-*At*GRP8-RQ (middle, lanes 2-10), respectively. (f) 50 fmoles of labelled 8-intron_WT ORN were incubated with 0.1, 0.25, 0.5, 1, 2, 3, 4, 5 and 10 µM of GST-*At*GRP8 (left, lanes 2-10) or 1, 2, 3, 4, 5, 7.5, 10, 20 and 50 µM of GST-*At*GRP8-RQ (middle, lanes 2-10), respectively. All reactions contained 1 µg tRNA. Bound and free RNA were quantified and K_d values calculated based on the mean of three independent experiments as described in Materials and Methods (cf. 3.5.4).

K_d values were determined for the binding of GST-*At*GRP8-RQ to the *AtGRP8* binding sites (Figure 27 d, f). The exchange of Arg^{47} for Gln yields an about 6-fold higher K_d value in case of the 8UTR_WT ORN and 14-fold higher K_d value for 8-intron_WT in comparison to the wild type protein (Figure 27 d, f). Although a complex formation was still observed at high GST-*At*GRP8-RQ concentrations, an apparent smearing suggested a dissociation of the RNA-protein complex during the gel run, as it was already observed for the *At*GRP7-RQ mutant (Figure 27 d, f, middle; cf. 4.1.1).

Furthermore, competition assays showed that the wild type ORNs 8-UTR_WT and 8-intron_WT competed more efficiently for the GST-*At*GRP8 and GST-*At*GRP8-RQ complex formation than their mutated counterparts 8- UTR_G_6mut and 8-intron_G_2U_2mut (Figure 28).

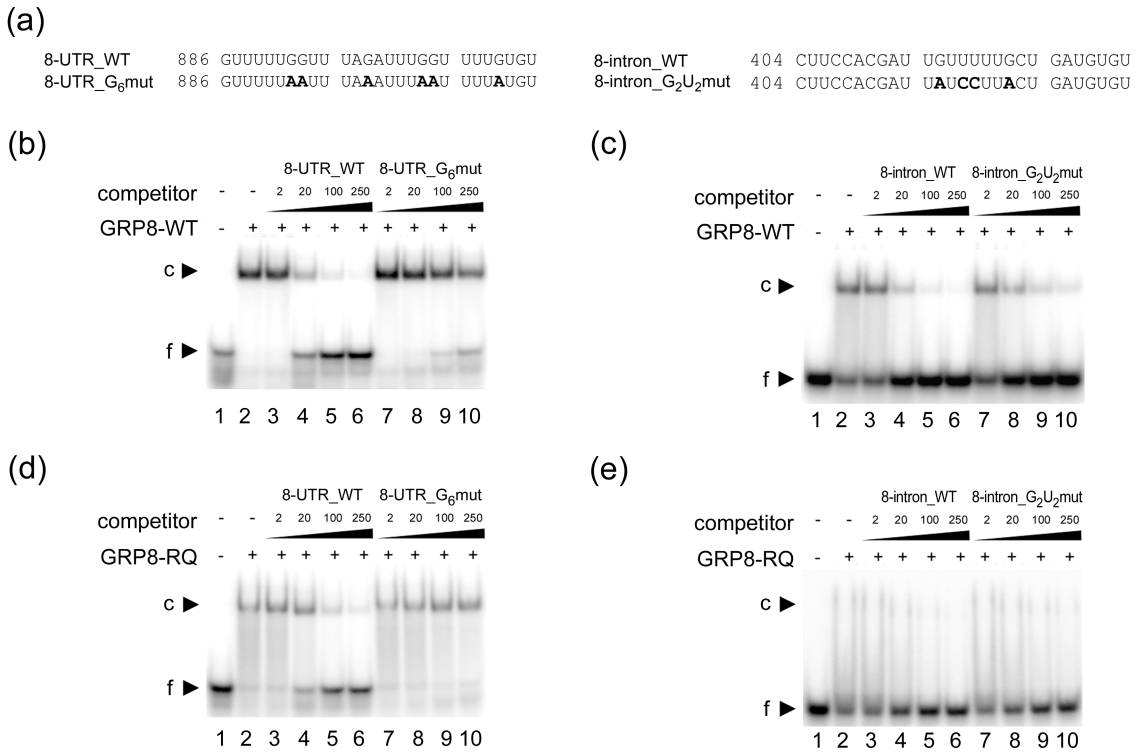

Figure 28: Point mutations interfere with the binding of *At*GRP8 and *At*GRP8-RQ to ORNs from the *AtGRP8* transcript. (a) Sequence of the 8-UTR_WT and the 8-intron_WT ORN and the corresponding mutated 8-UTR_G_6mut and 8-intron_G_2U_2mut with six G residues exchanged for A or two G and two U residues exchanged for A or C (in bold), respectively. Numbering is relative to the start site of transcription (Staiger, unpublished). (b) GST-*At*GRP8 protein was incubated with labelled 8-UTR_WT ORN in the presence of 5 µg of tRNA (lanes 2-10) and 2, 20, 100 and 250 pmoles of unlabelled 8-UTR_WT ORN (lanes 3-6) or 8-UTR_G_6mut (lanes 7-10), respectively. Lane 1, free ORN. (c) GST-*At*GRP8 protein was incubated with labelled 8-intron_WT ORN in the presence of 5 µg of tRNA (lanes 2-10) and 2, 100 and 250 pmoles of unlabelled 8-intron_WT ORN (lanes 3-6) or 8-intron_G_2U_2mut (lanes 7-10), respectively. Lane 1, free ORN. (d) GST-*At*GRP8-RQ protein was incubated with labelled 8-UTR_WT ORN in the presence of 5 µg of tRNA (lanes 2-10) and 2, 20, 100 and 250 pmoles of unlabelled 8-UTR_WT ORN (lanes 3-6) or 8-UTR_G_6mut (lanes 7-10), respectively. Lane 1, free ORN. (e) GST-*At*GRP8-RQ protein was incubated with labelled 8-intron_WT ORN in the presence of 5 µg of tRNA (lanes 2-10) and 2, 100 and 250 pmoles of unlabelled 8-intron_WT ORN (lanes 3-6) or 8-intron_G_2U_2mut (lanes 7-10), respectively. Lane 1, free ORN.

Thus, *At*GRP8 shows the same binding properties as *At*GRP7 *in vitro*: *At*GRP8 binds specifically to sequences within its own pre-mRNA, and a mutation of the conserved RNP1 arginine reduces this binding activity but does not influence the sequence specificity.

4.4.2 *At*GRP8 overexpression induces negative auto-regulation

The regulatory activity of *At*GRP8 was analysed *in vivo*. *Arabidopsis* plants were transformed with a construct for the constitutive overexpression of *At*GRP8. The *Agrobacterium tumefaciens* C58 pHPT6 strain (provided by D. Staiger) used for the transformation carried a binary vector system encoding an *AtGRP8* cDNA construct under control of a CaMV promoter with duplicated enhancer region and an TMV Ω element as well as a Hygromycin resistance gene (Figure 29 a). The offspring were selected via Hygromycin resistance and tested for the level of *At*GRP8 protein overexpression in western blot experiments with a specfic anti-peptide antibody (Diploma thesis Yahong Gao). Positive lines with highest *At*GRP8 overexpression were selected for further characterisation (Figure 29 b).

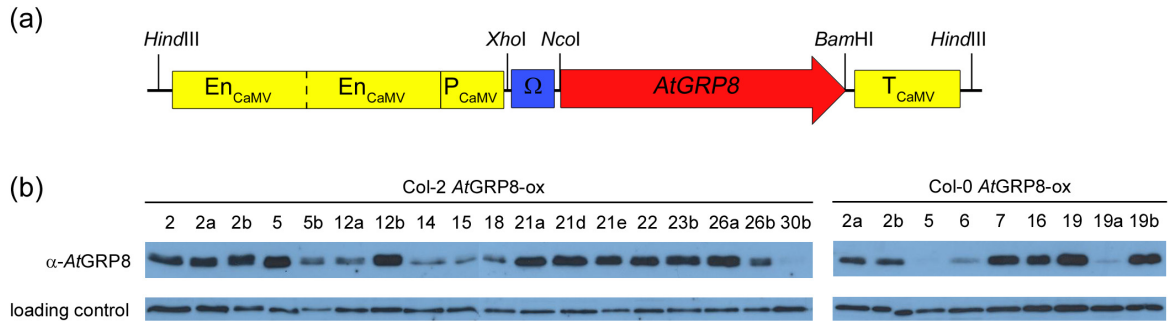

Figure 29: Identification of transgenic *Arabidopsis* lines with high expression levels of the *At*GRP8 transgene by western blot analysis. (a) Illustration of the *At*GRP8 overexpression construct. Regulatory elements of the CaMV promoter (En = enhancer, P = promoter) and T = terminator are displayed in yellow; the coding sequence is displayed in red. The omega element is a translational enhancer (Ω, blue). (b) Different *At*GRP8-ox lines in the Col-2 and Col-0 background, respectively, were compared for their *At*GRP8 expression level. 10 µg protein per lane have been blotted. An unspecific band at about 60 kDa crossreacting with the α-*At*GRP8 antibody served as a loading control.

Two representative *At*GRP8-ox lines as well as Columbia wild type plants were grown under long day conditions and harvested at timepoints of maximal and minimal *AtGRP8* expression (ZT3 and ZT11). Northern blot hybridisation with the *AtGRP8* cDNA confirmed constitutive high-level expression of *AtGRP8* as, in contrast to the wild type, no differences in *AtGRP8* level are visible between the time points ZT3 and ZT11 (Figure 30 a, top).

Hybridisation of the same northern blot with a probe against the endogenous *AtGRP8* transcript showed a strong repression of the mature *AtGRP8* RNA and an enhanced level of the alternatively spliced transcript in the *At*GRP8-ox lines (Figure 30 a, bottom). Protein extraction from the ZT11 samples and subsequent westen blot analysis confirmed the overexpression (Figure 30 b).

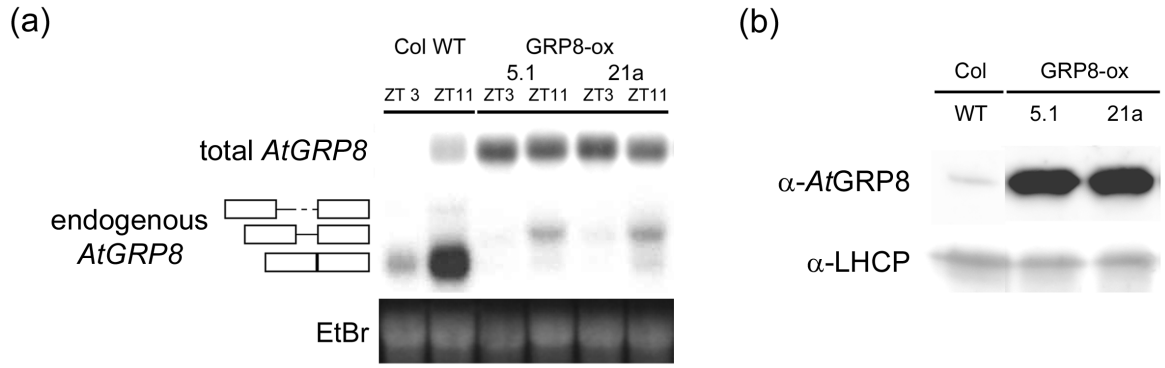

Figure 30: *At*GRP8 induces alternative splicing and negative auto-regulation at high protein concentrations. *At*GRP8-ox plants in Col-2 background and WT plants were harvested at ZT3 and ZT11. (a) The RNA gel blot was hybridised with the *AtGRP8* cDNA probe to confirm the constitutive overxpression (top). The same blot was hybridised with a gene-specific probe for *AtGRP8* (middle). The positions of the pre-mRNA, the alternatively spliced transcript *as_AtGRP8* retaining the first half of the intron and the mRNA are indicated. Boxes represent the exons, the solid and broken lines represent the first and second halves of the intron, respectively. The ethidium-bromide stained gel shows equal loading (bottom). (b) The immunoblot of samples harvested at ZT11 was incubated with an antibody against *At*GRP8 (top). Subsequently, the blot was probed with an antibody against LHCP as a loading control (bottom).

Thus, *At*GRP8 negatively regulates its own expression by the induction of alternative splicing at high protein levels.

4.4.3 The *At*GRP8-R^{47}Q mutation interferes with negative auto-regulation

In addition to the *At*GRP8-ox plants, transgenic *Arabidopsis* lines overexpressing the *At*GRP8-RQ construct were established to investigate the influence of a reduced *At*GRP8 binding on the negative auto-regulation. The *AtGRP8-RQ* sequence was cloned into the pHPT1 vector, yielding a construct homologous to the pHPT6 plasmid (Figure 31 a, cf. 4.4.2), and transformed into wild type plants. The offspring was screened for overexpression of the transgene by western blot analysis.

Three *At*GRP8-RQ-ox lines in the Col-2 background and a single C24 *At*GRP8-RQ-ox line with high expression levels were selected for further characterisation. The plants were grown under long day conditions and harvested at ZT3 and ZT11. Subsequently, the

overexpression of the mutated *At*GRP8 at ZT11 was confirmed by western blot experiments in comparison to *At*GRP8-ox and wild type plants (Figure 31 b).

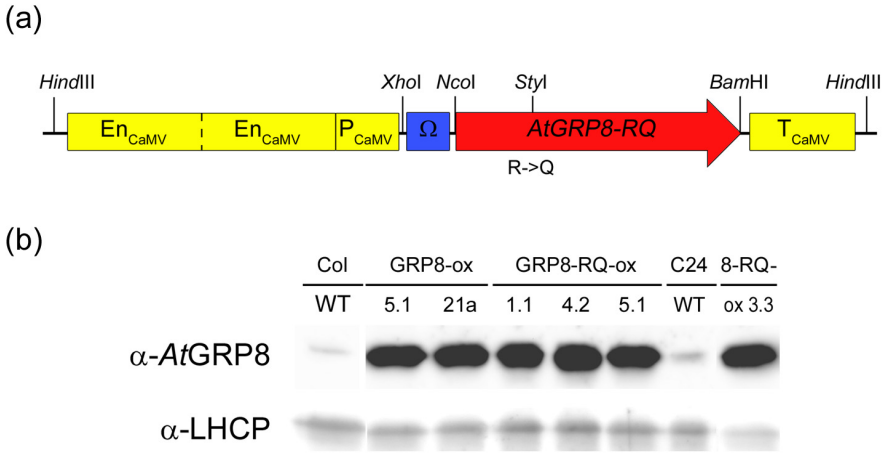

Figure 31: *At*GRP8-ox and *At*GRP8-RQ-ox lines express the transgene at comparable levels. (a) Scheme of the *At*GRP8-RQ overexpression construct. Regulatory elements of the CaMV promoter (En = enhancer, P = promoter) and T = terminator are displayed in yellow; the coding sequence is displayed in red. The TMV omega element is a translational enhancer (Ω, blue). The $R^{47}Q$ mutation yields a diagnostic *Sty*I site. (b) *At*GRP8-ox, *At*GRP8-RQ-ox and wild type plants in Col-2 background and WT plants were harvested at ZT11. 10 µg protein per lane have been blotted. The blot was developed with an α-*At*GRP8 antibody (top). Development of the same blot with an α-LHCP antibody served as a loading control (bottom).

Afterwards, the overexpression of *AtGRP8-RQ* was analysed at the transcript level by northern blotting. The *At*GRP8-RQ-ox lines showed a constitutive overexpression of the transgene, even stronger than in *At*GRP8-ox lines (Figure 32, top).

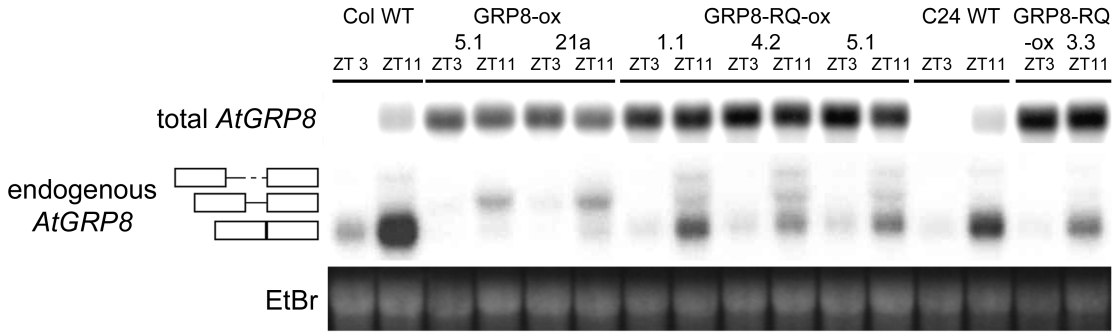

Figure 32: The *At*GRP8-RQ mutation interferes with negative auto-regulation. *At*GRP8-RQ-ox plants in Col-2 and C24 background as well as the corresponding *At*GRP8-ox plants in the Col-2 background and WT plants were harvested at ZT3 and ZT11. The RNA gel blot was hybridised with the *AtGRP8* cDNA probe to confirm the constitutive ovrexpression (top). The same blot was hybridised with a gene-specific probe for *AtGRP8* (middle). The positions of the pre-mRNA, the alternatively spliced transcript *as_AtGRP8* retaining the first half of the intron and the mRNA are indicated. Boxes represent the exons, the solid and broken lines represent the first and second halves of the intron, respectively. The ethidium-bromide stained gel demonstrates equal loading (bottom).

Hybridisation of the same northern blot with a gene-specific *AtGRP8* probe showed a severe down regulation of the endogenous transcript in *At*GRP8-ox. In contrast, in *At*GRP8-RQ-ox lines almost no alternativ splicing could be detected (Figure 32, bottom). However, the level of mature *AtGRP8* was somewhat reduced in comparison to wild type but higher than in *At*GRP8-ox. This repression of the endogenpous transcript is stronger in the Columbia ecotype than in C24 (Figure 32, bottom).

Thus, only little negative auto-regulation could be induced by the overexpression of an *At*GRP8-RQ construct implying the requirement of *At*GRP8 RNA-binding activity for this process. However, the weak residual binding activity of *At*GRP8-RQ is sufficient to achieve some degree of down regulation.

4.4.4 Reciprocal regulation of *At*GRP7 and *At*GRP8

*At*GRP7 has been shown to bind both, its own mRNA and that of *AtGRP8*. Since *At*GRP8 resembled *At*GRP7 in all details analysed so far, it was likely that *At*GRP8 was also able to bind to the *AtGRP7* transcript. The direct binding of *At*GRP8 to sequences of *AtGRP7* would be the basis for a reciprocal regulation of *At*GRP7 and *At*GRP8 within a common feedback loop.

4.4.4.1 Binding of *At*GRP8 to the *AtGRP7* transcript *in vitro*

Binding of recombinantly expressed GST-*At*GRP8 and GST-*At*GRP8-RQ to 7-UTR_WT and 7-intron_WT was tested in band shift experiments. The wild type fusion protein showed a stable complex formation with both ORNs, 7-UTR_WT and 7-intron_WT (Figure 33 b, d). Contrarily, the ability of GST-*At*GRP8-RQ to form complexes with the two *AtGRP7* ORNs was clearly reduced (Figure 33 b, d).

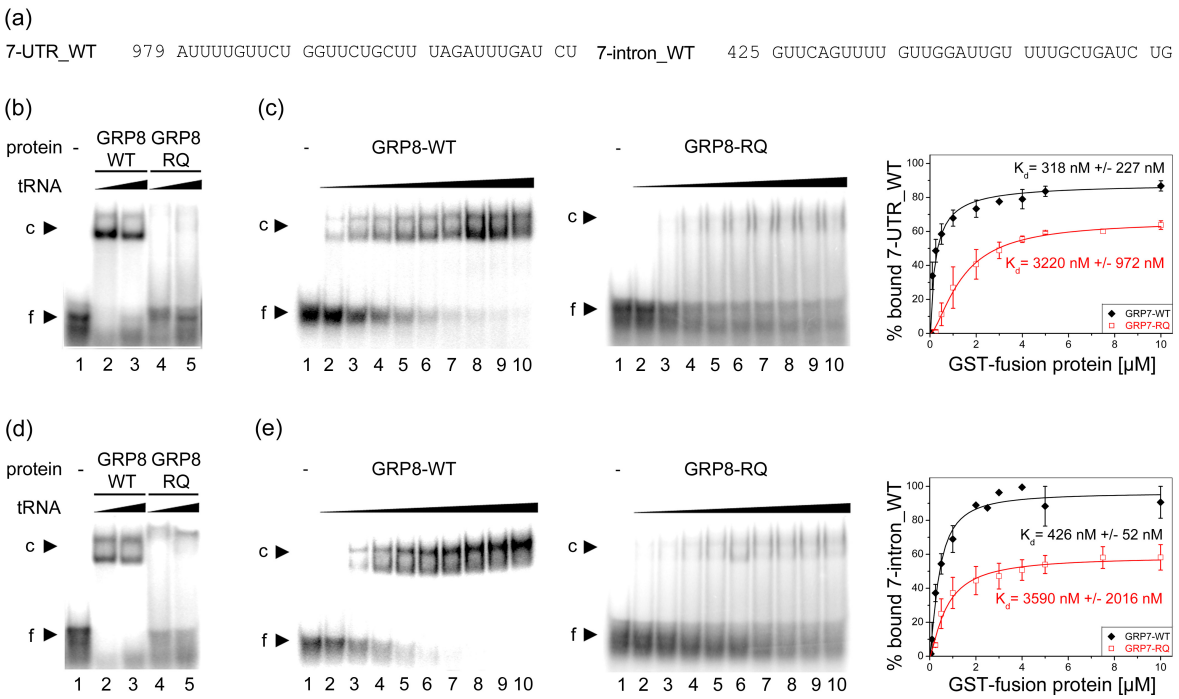

Figure 33: *At*GRP8 binds to sequences within the *AtGRP7* transcript. (a) Sequence of the ORNs 7-UTR_WT and 7-intron_WT containing the binding site within the *AtGRP7* 3´ UTR and intron, respectively. Numbering is relative to the transcription start site (Staiger & Apel, 1999). (b) Labelled 7-UTR_WT was incubated with GST-*At*GRP8 (lanes 2, 3) or GST-*At*GRP8-RQ (lanes 4, 5) and 1 µg (lanes 2, 4) or 10 µg (lanes 3, 5) of tRNA, respectively. Lane 1, free ORN (f). c, RNA-protein complex. (c) To compare binding affinities of WT and mutant protein, 50 fmoles of labelled 7-UTR_WT were incubated with 0.01, 0.05, 0.1, 0.25, 0.5, 1, 2.5, 5 and 10 µM of GST-*AtT*GRP8 (lanes 2-10) or 0.5, 1, 2, 3, 4, 5, 7.5, 10 and 20 µM of GST-*At*GRP8-RQ (lanes 2-10), respectively, in the presence of 1 µg tRNA. Bound and free RNA were quantified and K_d values calculated based on three independent experiments as described in Materials and Methods. (d) Labelled 7-intron_WT was incubated with GST-*At*GRP8 (lanes 2, 3) or GST-*At*GRP8-RQ (lanes 4, 5) and 1 µg (lanes 2, 4) or 10 µg (lanes 3, 5) of tRNA, respectively. Lane 1, free ORN. (e) To compare binding affinities of WT and mutant protein, 50 fmoles of labelled 7-intron_WT were incubated with 0.01, 0.05, 0.1, 0.25, 0.5, 1, 2.5, 5 and 10 µM of GST-*At*GRP8 (lanes 2-10) or 0.25, 0.5, 1, 2, 3, 4, 5, 7.5 and 10 µM of GST-*At*GRP8-RQ (lanes 2-10), respectively, in the presence of 1 µg tRNA. K_d values were determined as in (c).

The K_d values of GST-*At*GRP8 were determined to be 3.2×10^{-7} for the interaction with 7-UTR_WT and 4.3×10^{-7} for the binding to 7-intron_WT (Figure 33 c, e). In contrast, the K_d of the GST-*At*GRP8-RQ mutant protein was calculated to be 10- and 8-fold higher for these sequences, respectively (Figure 33 c, e). Competition assays revealed a sequence specificity for both proteins (Figure 34). The wild type sequence derived from the *AtGRP7* 3'UTR (7-UTR_WT) competed much better for the binding of GST-*At*GRP8 and GST-*At*GRP8-RQ than the corresponding G-mutated sequence did (Figure 34 b, d). Similar results were obtained for the 7-intron_WT and 7-intron_G_6mut ORNs (Figure 34 c, e). A likewise behaviour of *At*GRP7 had been observed in identical experiments with GST-*At*GRP7 (cf. 4.1).

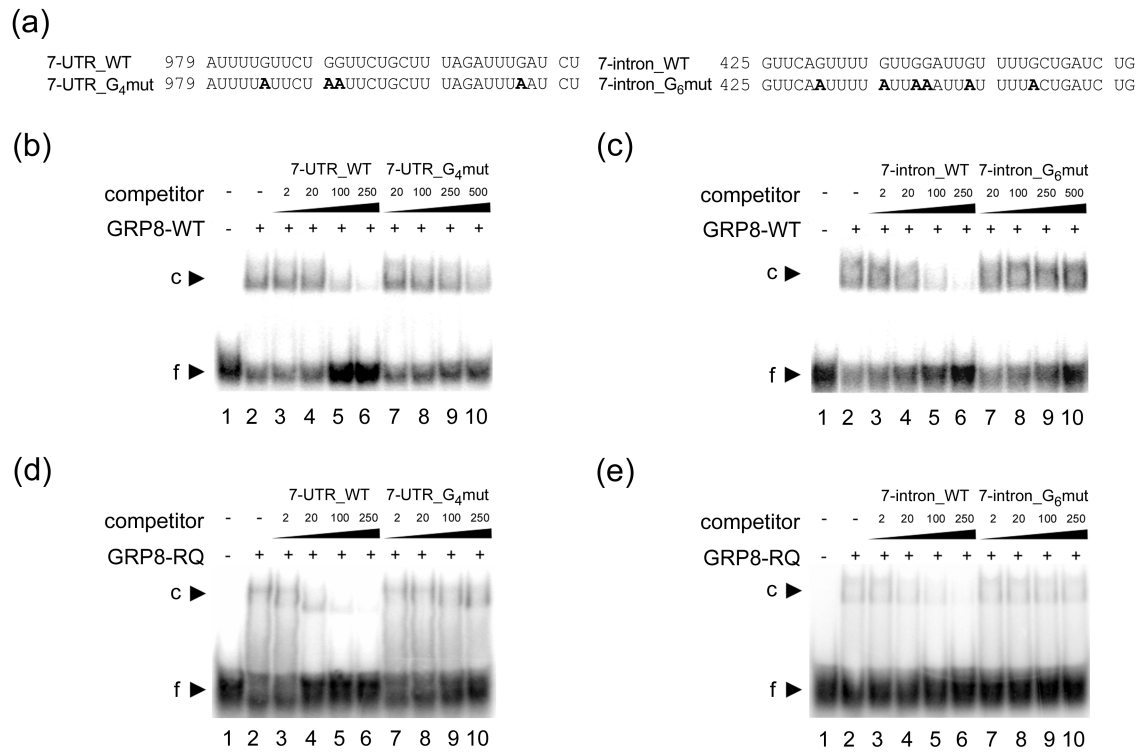

Figure 34: *AtGRP7* point mutations interfere with binding of *At*GRP8 and *At*GRP8-RQ. (a) Sequence of the ORNs 7-UTR_WT, mutated 7-UTR_G_4mut with four G residues exchanged for A (in bold), 7-intron_WT and mutated 7-intron_G_6mut with six G residues exchanged for A (in bold). Numbering is relative to the transcription start site (Staiger & Apel, 1999). (b) GST-*At*GRP8 WT protein was incubated with labelled 7-UTR_WT ORN in the presence of 5 µg of tRNA (lanes 2-10) and 2, 20, 100 and 250 pmoles of unlabelled 7-UTR_WT ORN (lanes 3-6) or 20, 100, 250 and 500 pmoles of unlabelled 7-UTR_G_4mut (lanes 7-10), respectively. Lane 1, free ORN. (c) GST-*At*GRP8 protein was incubated with labelled 7-intron_WT ORN in the presence of 5 µg of tRNA (lanes 2-10) and 2, 20, 100 and 250 pmoles of unlabelled 7-intron_WT ORN (lanes 3-6) or 20, 100, 250 and 500 pmoles of unlabelled 7-intron_G_6mut ORN (lanes 7-10), respectively. Lane 1, free ORN. (d) GST-*At*GRP8-RQ protein was incubated with labelled 7-UTR_WT ORN in the presence of 5 µg of tRNA (lanes 2-10) and 2, 20, 100 and 250 pmoles of unlabelled 7-UTR_WT ORN (lanes 3-6) or 7-UTR_G_4mut (lanes 7-10), respectively. Lane 1, free ORN. Note that this gel was exposed about two times longer than the gel shown in Figure 33 b. (e) GST-*At*GRP8-RQ protein was incubated with labelled 7-intron_WT ORN in the presence of 5 µg of tRNA (lanes 2-10) and 2, 20, 100 and 250 pmoles of unlabelled 7-intron_WT ORN (lanes 3-6) or unlabelled 7-intron_G_6mut ORN (lanes 7-10) as indicated. Lane 1, free ORN. Note that this gel was exposed about three times longer than the gel shown in Figure 33 d.

Therefore, *At*GRP8 binds to the *At*GRP7 target sequences in the *AtGRP7* 3' UTR and the intron in a sequence dependent manner. This binding requires a functional RRM and shows affinities comparable to those determined for the interaction of *At*GRP7 with its own transcript.

4.4.4.2 *At*GRP8 interferes with *AtGRP7* transcript accumulation *in vivo*

The direct and stable binding of *At*GRP8 to sequences within the *AtGRP7* pre-mRNA pointed to a regulation of *AtGRP7* by *At*GRP8 *in vivo*. Thus, the established transgenic *At*GRP8-ox and *At*GRP8-RQ-ox lines (cf. 4.4.2 & 4.4.3) were analysed for the expression of *AtGRP7*. The overexpression of *At*GRP8 (AtGRP8-ox) led to an accumulation of the alternative *AtGRP7* splice form and an almost complete loss of the mature transcript (Figure 35).

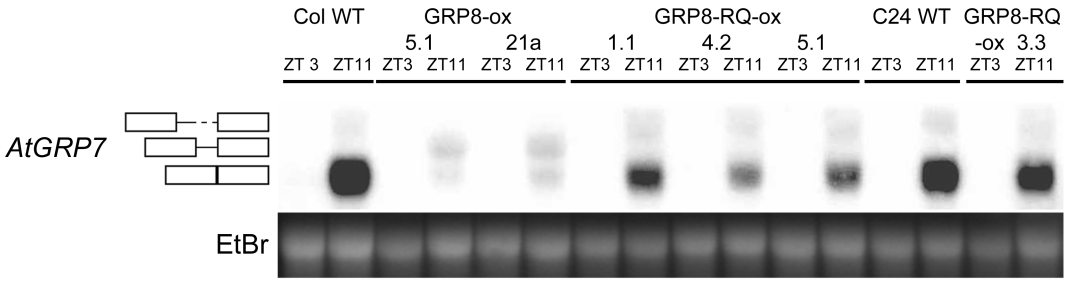

Figure 35: *At*GRP8 overexpression induces alternative splicing of the *AtGRP7* transcript. *At*GRP8-ox plants in Col-2 background as well as the corresponding *At*GRP8-RQ-ox plants in the Col-2 and C24 background and WT plants were harvested at ZT3 and ZT11. The blot was hybridised with a gene-specific probe for *AtGRP7* (top). The positions of the pre-mRNA, the alternatively spliced transcript *as_AtGRP7* retaining the first half of the intron and the mRNA are indicated. Boxes represent the exons, the solid and broken lines represent the first and second halves of the intron, respectively. The ethidium-bromide stained gel shows equal loading (bottom).

In contrast, no alternatively spliced *AtGRP7* transcript was detected in *At*GRP8-RQ-ox plants and the level of mature *AtGRP7* mRNA was only marginally reduced (Figure 35). Thus, the overexpression of *At*GRP8-RQ does not have a significant influence on the splice site selection. Almost no *At*GRP7 protein can be detected in *At*GRP8-ox, whereas protein is still detectable in *At*GRP8-RQ-ox lines, however at reduced levels (Figure 36). The reduction of *At*GRP7 protein in the *At*GRP8-RQ-ox lines corresponds to the slightly reduced *AtGRP7* mRNA level in these lines (Figure 35).

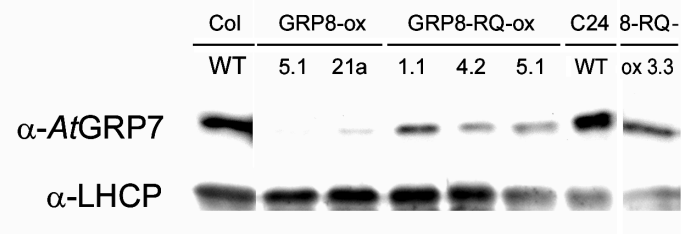

Figure 36: The level of *At*GRP7 is severely reduced in *At*GRP8-ox but not in *At*GRP8-RQ-ox. Columbia wild type plants served as control samples. 10 µg total protein per lane have been blotted. The blot was developed with an α-*At*GRP8 antibody (top). Development of the same blot with an α-LHCP antibody served as a loading control (bottom).

These data show that *At*GRP8 does not only perform negative auto-regulation but also negatively regulates the expression of *At*GRP7. Thus, besides their autoregulatory activity *At*GRP7 and *At*GRP8 regulate each other reciprocally. This indicates that *At*GRP7 and *At*GRP8 form an interlocking secondary feedback loop downstream of the *Arabidopsis* clock.

4.4.5 *At*GRP7 and *At*GRP8 regulate identical target transcripts

Further experiments addressed the question whether *At*GRP8 and *At*GRP7 regulate identical targets *in vivo*. Previously, several transcripts had been identified that are regulated differentially in *At*GRP7-ox and wild type plants using Affymetrix® AG and ATH1 GeneChips (F. Rudolf, C. Streitner, M. Neuenschwander, J.L. Gómez-Porras and D. Staiger, unpublished). Among these target transcripts are *Casein Kinase 2* (*CK2*, At3g50000), a fatty acid desaturase (*FAD2*, At3g12120), a copper-zinc superoxide dismutase (*CuZnSOD2*, At1g08830) and its copper chaperone (*Cu-Chaperone*, At1g12520). It could be shown that upon *At*GRP7 overexpression *FAD2* is down-regulated, whereas *CuZnSOD2*, *Cu-Chaperone* and *CK2* are up-regulated. An influence of *At*GRP8 on the regulation of the *At*GRP7 target transcripts was investigated by means of RT-PCR.

For this purpose RNA samples from wild type and *At*GRP8-ox and *At*GRP7-ox plants were reverse-transcribed. RT-PCR was performed using specific primers (Table 2), the amplification products were either separated on an agarose gel and stained with ethidium-bromide or blotted and hybridised with radioactively labelled cDNA probes. The blots were exposed to PhosphorImager screens and signals were quantified with the ImageQuant program. The newly generated *At*GRP8-ox lines 5, 21a and 26a showed a strong overexpression of the transgene whereas the previously established *At*GRP8-ox line 15 (D. Staiger, unpublished) had an only weakly increased *AtGRP8* level (Figure 37; independent observation by Y. Gao). Accordingly, *AtGRP7* was completely down-regulated in the *At*GRP8-ox lines 5, 21a and 26a, whereas it was less reduced in line 15 (Figure 37). As expected, the expression of *FAD2* and *AtGRP8* was repressed in *At*GRP7-ox, whereas *CuZnSOD2*, *Cu-Chaperone* and *CK2* was up-regulated. The analysis of the same transcripts upon *At*GRP8 overexpression showed a strong down-regulation of *FAD2* in the *At*GRP8-ox lines 5, 21a, 26a (Figure 37). Concomitantly, the expression of *Cu-Chaperone* and *CuZnSOD2* was highly up-regulated in these lines. The abundance of *CK2* was only

modestly increased. Again, the *At*GRP8-ox line 15 did only show a weak influence on target regulation (Figure 37).

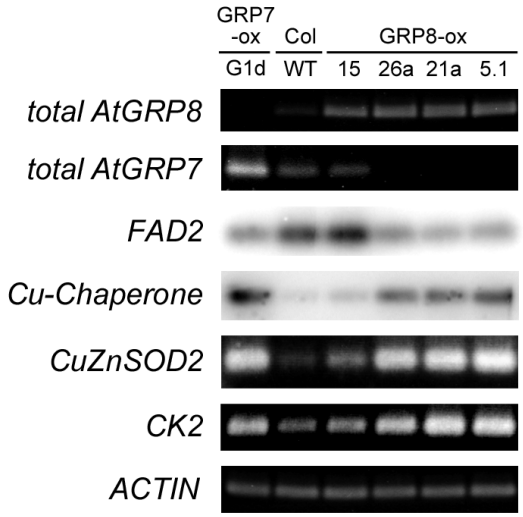

Figure 37: *At*GRP7-ox and *At*GRP8-ox lines have the same effect on the potential target transcripts selected for analysis. The PCR amplification products for *FAD2* and *Cu-Chaperone* were blotted and hybridised with cDNA probes. The amplification products of *AtGRP8*, *AtGRP7, CuZnSOD2*, *CK2* and *ACTIN* were stained with ethidium-bromide (see text).

The RT-PCR demonstrates an identical regulation of selected target transcripts in *At*GRP7-ox and *At*GRP8-ox plants. Moreover, the impact of *At*GRP8 overexpression on the target abundance is dose dependent.

4.5 Analysis of the *At*GRP7 and *At*GRP8 binding activity at the single molecule level

So far, ensemble measurements have been used for the analysis of RNA-protein interactions *in vitro*. To gain a deeper insight into the binding mechanism of *At*GRP7 and *At*GRP8 two new single molecule techniques were established for the analysis of RNA-protein interactions. In cooperation with the Department of Physics within the Collaborative Research Centre SFB613 fluorescence correlation spectroscopy and atomic force microscopy based force spectroscopy experiments were performed yielding more information about the behaviour of RNA and protein during the binding process (cf. 2.3).

4.5.1 Analysis of the *At*GRP7 binding at the single molecule level

For the analysis of *At*GRP7 binding at the single molecule level Dr. Mark Schüttpelz (Department for Applied Laser Physics and Laser Spectroscopy, Bielefeld University) used standard fluorescence correlation spectroscopy and photoinduced electron transfer FCS (PET-FCS). Two main aspects of binding were addressed: What is the minimal binding sequence and does the secondary structure of the RNA influence the target recognition.

4.5.1.1 FCS studies reveal minimal binding sequence

The usability of the FCS technique for the analysis of RNA-protein complexes was first tested with purified *At*GRP7 protein and a fluorescence labelled ORN covering the binding site in the *AtGRP7* 3'UTR (7-UTR_WT-NH_2). The 7-UTR_WT-NH_2 ORN has a C_3-amino linker at the 3' end for the fluorescence labelling. In band shift assays it could be shown that neither the linker nor the fluorescent dye interferes with the *At*GRP7 binding (data not shown). For the complex of *At*GRP7 with 7-UTR_WT-NH_2 a K_d value of 4.9×10^{-7} was determined, demonstarting an affinity that is comparable to that previously calulated on the basis of EMSA experiments (Table 9, cf. 4.1.1). In a second experiment the affinity of *At*GRP7 towards DNA oligonucleotides was tested. The K_d measurements revealed a high affinity of *At*GRP7 to the DNA analogon of the 3'UTR ORN (7-UTR_DNA-NH_2). The K_d value of 1.0×10^{-7} was even slightly lower than that determined for the 7-UTR_WT-NH_2 ORN. This shows that *At*GRP7 formes stable complexes with both, DNA and RNA targets.

Such a dual capacity for the binding of DNA and RNA had previously been reported for the related RBP hnRNP A1 (Buvoli *et al.*, 1990).

Thus, for the determination of a minimal binding sequence single-stranded DNA oligonucleotides were used due to lower costs and a higher stability of the DNA molecules during the labelling process. In a first approach to shorten the sequence it had been shown that the first half of the 7-UTR_WT-NH_2 ORN was bound more tightly by *At*GRP7 than the second half (Mark Schüttpelz, Department for Applied Laser Physics and Laser Spectroscopy, Bielefeld University; personal communication). Accordingly, the first half of 7-UTR_DNA-NH_2 was subdivided into smaller overlapping 12mers (DNA_1-8; Table 9). Each 12mer was shifted against the other by two nucleotides (Table 9).

Table 9: Delineation of the *AtGRP7* binding site by FCS.

Name	RNA / DNA oligonucleotide sequence	K_d [M]
7-UTR_WT-NH_2	5′-AUU UUG UUC UGC UUC UGC UUU AGA UUU GAU GU-3′	4.9×10^{-7}
7-UTR_DNA-NH_2	5′-ATT TTG TTC TGC TTC TGC TTT AGA TTT GAT GT-3′	1.0×10^{-7}
DNA_1	5′-CT ATT TTG TTC T-3′	$> 1.1 \times 10^{-6}$
DNA_2	5′-ATT TTG TTC TGG-3′	2.7×10^{-7}
DNA_3	5′-T TTG TTC TGG TT-3′	2.4×10^{-7}
DNA_4	5′-TG TTC TGG TTC T-3′	3.7×10^{-7}
DNA_5	5′-TTC TGG TTC TGC-3′	1.9×10^{-7}
DNA_6	5′-C TGG TTC TGC TT-3′	4.3×10^{-7}
DNA_7	5′-GG TTC TGC TTT A-3′	n.d.
DNA_8	5′-TTC TGC TTT AGA-3′	$> 8.5 \times 10^{-7}$

The presumed core binding sequence is highlighted in red. The incorporation of a doubled G residue (orange) enhances the binding. n.d., not determined.

For each of the 12mers an equilibrium dissociation constant was determined. The first (DNA_1) and the last (DNA_8) of the tested oligonucleotides showed only minor binding affinity, the other oligonucleotides were bound with K_d values at levels as previously determined for the 32mer (Table 9; cf. 4.1.1) The binding strength considerably increases upon incorporation of guanine residues (compare DNA_1 and DNA_2). Moreover, a preference for a core sequence composed of 5'-(G)GTTCTG(G)-3' was detected (Table 9). The existence of a guanine pair either at the beginning or at the end of the sequence seems to be advantageous for high affinity binding. An important influence of guanines within the sequence for high affinity binding is consistent with results previously obtained in gel shift experiments (cf. 4.1.1).

4.5.1.2 Influence of *At*GRP7 binding on RNA secondary structure

In a related experiment the influence of secondary structure on the target recognition was studied by PET-FCS. By this method the quenching kinetics of the fluorescent dye on a nanosecond timescale are analysed (Kim *et al.*, 2006). The dye is quenched if it is in close contact to certain residues, such as guanine. Thus, an extended or open structure does not show a quenching, whereas the fluorescence is eliminated in a hairpin loop with a guanine at the end of the stem, opposite of the dye. Based on the the identfied core target sequence (cf. 4.5.1.1), two 13mer oligoribonucleotides containing the core sequence were designed. The first ORN (7-UTR_SL) was predicted to form a hairpin loop, whereas the second (7-UTR_O) should have no significant secondary structures (Figure 38 a). A guanine was introduced at the 5' end of the stem of 7-UTR_SL for an efficient quenching of the MR121 dye that was located a the 3' end. The FCS binding assays showed a binding of *At*GRP7 to both ORNs visible in a shift in diffusion time (Figure 38 b, red and blue line).

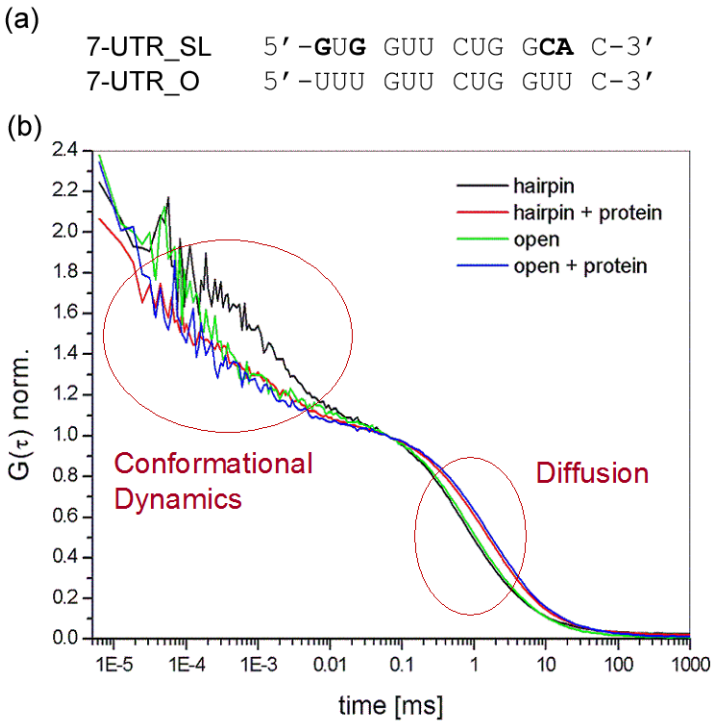

Figure 38: Conformational changes of the *AtGRP7* hairpin upon *At*GRP7 binding. (a) Sequence of the hairpin and the open structured ORNs. The sequences are derived from the identified minimal binding sequence (cf. Table 9). Introduced mutations for the formation of a stable stem are highlighted in boldface. (b) The efficient binding of both ORNs can be observed by an increased diffusion time on the millisecond timescale (right), whereas the conformational changes are visible as quenching effects on the nanosecond timescale (left).

Interestingly, for the hairpin structure the quenching kinetics of the fluorescent dye at a sub millisecond scale changed upon addition of *At*GRP7 (Figure 38 b, compare black and red line). This change in fluorescence intensity implies a conformational change of the RNA from a closed to an open structure since the efficient quenching is abolished and the correlation function of the bound state resembles the curves of the non-structured ORN. In contrast, the quenching kinetic and thus the conformation of the open structured ORN does not change upon *At*GRP7 binding (Figure 38 b, compare green and blue line).

To verify the impact of a change in RNA secondary structure on the protein binding affinity three more ORNs with elongated and thus more stable stems were designed (Table 10).

Table 10: Influence of the secondary structure of the ORN on the binding affinity of *At*GRP7.

Name	Sequence	ΔG [kcal/mol]	Relative Binding
7-UTR_O	UUUGUUCUGGUUC	1.0	+++
7-UTR_SL	**GUG**GUUCUGG**CA**C	-1.8	+++
7-UTR_UA	**G**UU**G**GUUCUGG**CAA**C	-3.0	++
7-UTR_GC	**GGUG**GUUCUGG**CAC**C	-5.2	+
7-UTR_$(GC)_2$	**GGGUG**GUUCUGG**CACCC**	-8.6	-

Mutated or introduced bases in comparison to the wild type sequence from the *AtGRP7* 3'UTR are printed in boldface. The free energy of the secondary structure of the predicted secondary structures was calulated with mfold (Zuker, 2003). The binding affinity of *At*GRP7 is given relativ to the 7-UTR_O ORN.

The FCS experiments showed a clear negative correlation between stem stability and binding affinity. With increasing length and GC-content of the stem the binding affinity to the *At*GRP7 protein was reduced (Table 10).

Thus, the FCS experiments indicate a requirement of a single-stranded nucleotide sequence in an open conformation for target recognition. Stable stem-loop structures interfere with stable RNA-protein complex formation, whereas short stems can be broken up upon protein binding. Additionally, the equilibrium of open and closed ORN conformation is shifted towards the extended secondary structure upon *At*GRP7 binding.

4.5.2 Analysis of the *At*GRP8 binding at the single molecule level

Atomic force microscopy based force spectroscopy had previously been used for the analysis of DNA-protein complexes (Bartels *et al.*, 2007). Based on the results obtained for the DNA-protein interaction the system had to be modified for the examination of RNA-protein complexes that exhibit a high degree of secondary and tertiary structure. The measurements performed by Alexander Fuhrmann (Department of Experimental Biophysics and Applied NanoSciences, Bielefeld University) pointed to the specificity of the *At*GRP8-RNA complex formation and the determination of specific rate constants, such as off-rates and mean life-time of the complexes.

4.5.2.1 Two modes of interaction during the *At*GRP8 binding process

For the AFM-FS measurements synthetic ORNs derived from the 3' UTR of *AtGRP8* were designed. The ORNs were tagged with a thiol linker at the 3' end for coupling of the ORN to the silicon nitride tip of the AFM. Bandshift assays demonstrated that the attached thiol tag had no influence on binding of GST-*At*GRP8 (Figure 39). Likewise, the tag did not change the sequence specificity since a G-mutated ORN showed a reduced binding (Figure 39).

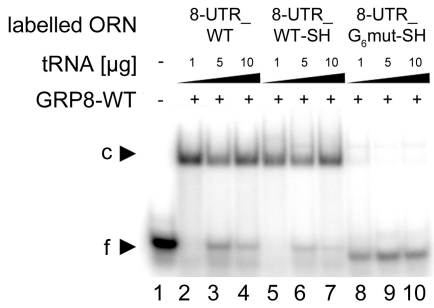

Figure 39: Attachment of a C_3-thiol linker to synthetic ORNs from the *AtGRP8* 3'UTR has no influence on *At*GRP8 binding affinity or sequence specificity. GST-*At*GRP8 protein was incubated with labelled 8-UTR_WT ORN (lane 2-4), 8-UTR_WT-SH ORN (lanes 5-7) and 8-UTR-G_6mut-SH ORN (lanes 8-10) in the presence of 1 µg of tRNA. Lane 1, free 8-UTR_WT ORN.

GST-fusion proteins were immobilised on a mica surface via a BS3 linker (cf. 3.6.1). For a first test of the setup different RNA-protein combinations were tested (Figure 40). The GST tag itself did not show obvious binding to the 8-UTR_WT-SH sequence. Also no binding could be detected in case of a completely artificial poly(A) ORN and GST-*At*GRP8. Almost no interactions with GST-*At*GRP8 could be determined in case of a

poly(U) ORN. Only a few rupture events could be observed in case of the 8-UTR-G_6mut-SH ORN. The GST-*At*GRP8-RQ mutant protein showed a broad distribution of rupture events, however without specific peaks. In contrast, strong complex formation was recorded if the wild type protein and the 8-UTR_WT-SH ORN were used. Moreover, for this combination two distinct events with separate peaks in the force-stiffness plot were observed (Figure 40).

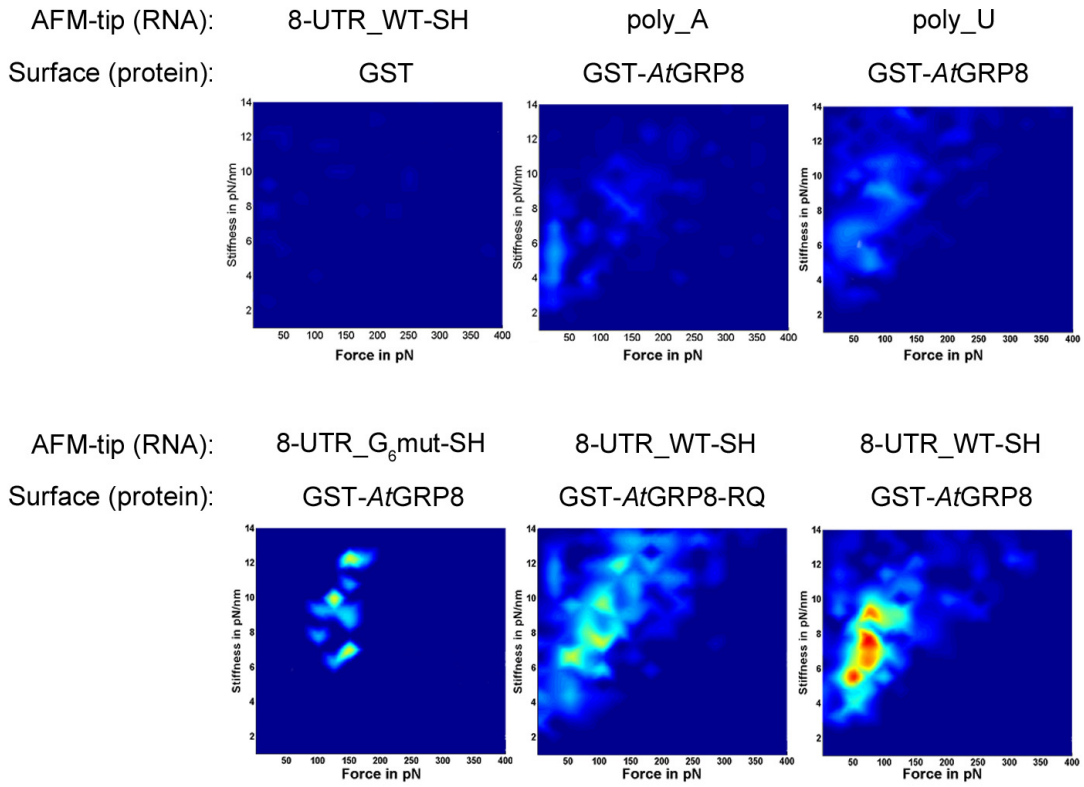

Figure 40: Specific and unspecific binding events are detectable by AFM-FS. The thiol tagged ORNs were coupled to the AFM-tip, GST-fusion proteins were immobilised on a mica surface. Normalised 2d-histograms of different binding partners at a pulling velocity of 5,000 nm/s are shown (see text).

The observation of two distinct binding events with higher and lower affinity raised the question whether both events are specific or not. In ensemble measurements usually competition experiments are carried out to discriminate between specific and unspecific binding (cf. 4.1). Thus, it was tested whether a comparable setup could be established to perfom competition assays at a single molecule level. First, binding of GST-*At*GRP8 to 8-UTR_WT-SH without competitor RNA was recorded (Figure 41 a). Then, a homologous competitor was applied to the surface to saturate specifically all binding sites of the proteins and the rupture events were recorded again. It was shown that the addition of the homologous competitor was sufficient to eliminate all high force-stiffness rupture events at

5.0 pN/nm but not the lower force ones at 3.6 pN/nm (Figure 41 b). Finally, the surface was washed extensively with buffer to remove the free ORN and to reconstitute complex formation. After washing of the surface, the peak at 5.0 pN/nm was restored (Figure 41 c). Thus, the rupture events at 5.0 pN/nm are caused by a specific binding of GST-*At*GRP8 to the 8-UTR_WT-SH ORN.

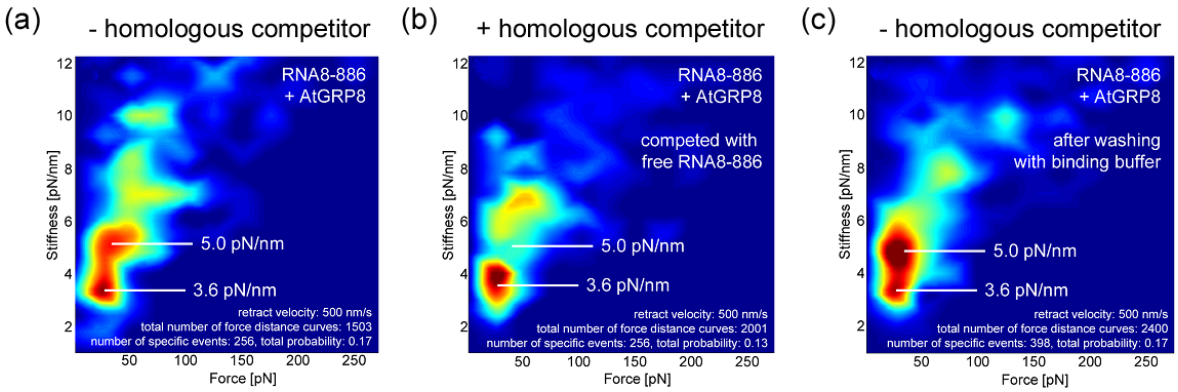

Figure 41: Demonstration of binding specificity by competition experiments. (a) Binding of GST-*At*GRP8 to 8-UTR_WT-SH yielded rupture events with two distinct peaks at 3.6 pN/nm and 5.0 pN/nm, respectively. (b) Application of free 8-UTR_WT ORN to the surface interfered with rupture events at 5.0 pN/nm but not with those at 3.6 pN/nm. (c) Extensive washing of the surface with binding buffer restored the 5.0 pN/nM peak.

The correlation of higher rupture forces with higher binding specificity was supported by the observation that rupture force and stiffness of the *At*GRP8-RNA complex depends on the contact time of the cantilver, the so-called dwell time. A sorting of the rupture events by their dwell time showed that at higher dwell times the number of events with high force-stiffness rates increases (Figure 42).

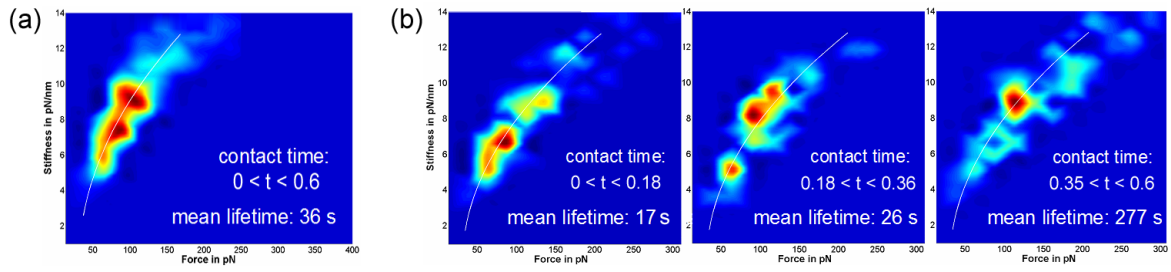

Figure 42: Stability of the *At*GRP8–8-UTR_WT complex increases with longer contact time of the cantilever. (a) Plot of the *At*GRP8-RNA-complex rupture events. (b) Seperation of the different ruptures in (a) according to their dwell time. Low force rupture events predominate at short contact times (left). With increasing contact times between cantilever and surface the stability of the RNA-protein complexes increased, visible in higher rupture forces (middle and right).

Taken together, AFM-FS has been established for the analysis of RNA-protein complexes. The experiments revealed binding specificity and different interactions of *At*GRP8 with its target RNA during the binding process. These different binding modes can be separated into specific and unspecific interactions.

4.6 The rapid turnover of the alternatively spliced *AtGRP7* and *AtGRP8* transcripts is an NMD dependent process

It had previously been detected that the alternatively spliced *AtGRP7* transcript (*as_AtGRP7*) is degraded more rapidly than the mature mRNA. This process may be part of the mechanism underlying the negative regulation. The alternatively spliced transcript contains a pre-mature termination codon (PTC) within the retained first half of the intron. Transcripts with PTCs are often degraded by a pathway called nonsense-mediated decay (NMD). For a long time it had been thought that NMD represents a control mechanism that prevents the translation and accumulation of transcripts with frameshift or nonsense mutations (Maquat, 2002). However, during recent years other regulatory roles have been ascribed to NMD. It was found that NMD is involved in different negative feedback loops as a basic post-transcriptional process regulating normal gene expression (Sureau *et al.*, 2001; Wollerton *et al.*, 2004; Rehwinkel *et al.*, 2006). Additionally, it was shown that at least 10 % of the yeast transcriptome are regulated in a NMD dependent manner also pointing to a more general role of the NMD in the post-transcriptional gene regulation (He *et al.*, 2003; Guan *et al.*, 2006). Three UPF (UP-frameshift) proteins have been identified as key factors of the NMD machinery in mammals. The UPF3 protein is part of the large exon-junction complex (EJC) and is attached to the mRNA during the splicing process in a distance of 20 to 24 nucleotides upstream of the exon-exon boundary. After nuclear export, PTC recognition occurs during a primary round of translation if the stop codon is located upstream of an EJC (Figure 43).

The UPF1 helicase is recruited by translation release factors and interacts with the EJC (Figure 43). This recruitment of UPF1 targets the aberrant transcript for degradation (Chang *et al.*, 2007). This model is well established for animals and yeast. In plants however, the mechanism as well as the *cis*-acting signals are not completely understood yet (Kertesz *et al.*, 2006). Nevertheless, orthologues of UPF1 and UPF3 have been identified and it could be shown that mutant lines for both factors accumulate PTC containing transcripts (Hori & Watanabe, 2005; Arciga-Reyes *et al.*, 2006). Additionally, severe developmental defects were observed for different T-DNA insertion lines of UPF1 and UPF3 (Arciga-Reyes *et al.*, 2006).

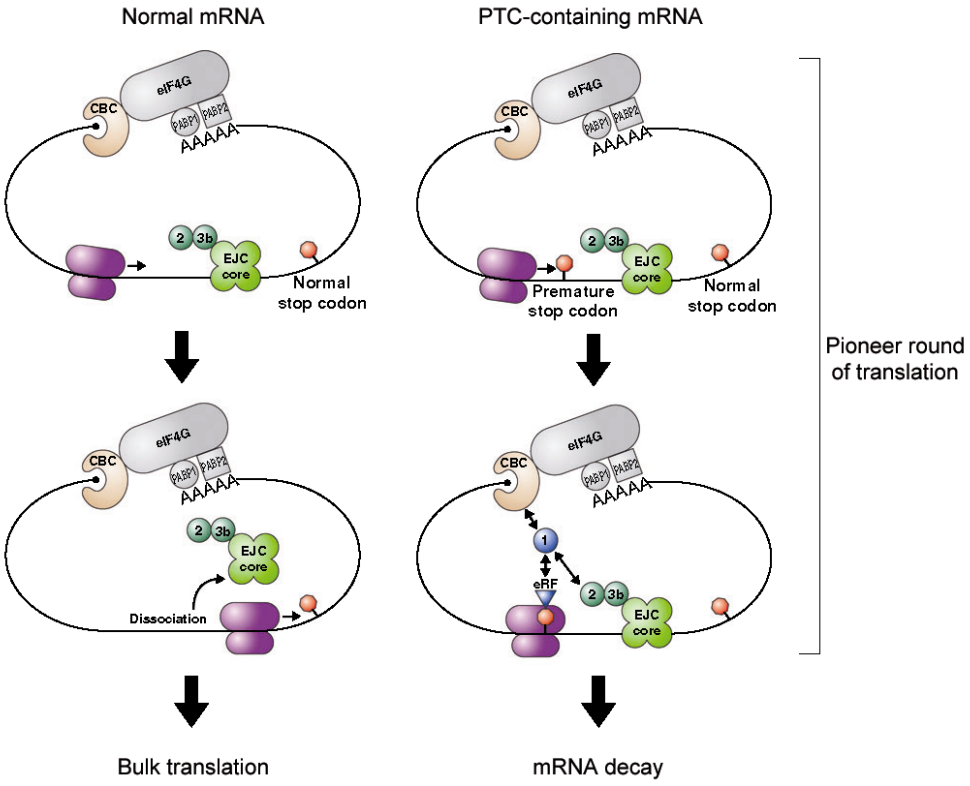

Figure 43: Schematic view of the mammalian nonsense-mediated mRNA decay. In a normal transcript (left panel) all EJCs are located upstream of the stop codon and are displaced by the ribosome during the first round of translation. Subsequently, bulky translation of the mRNA is started. In contrast, the ribosome stops if a PTC is recognised during the "pioneer" round of translation (right panel). UPF-1 is recruited and the transcript is targetd to NMD (Chang *et al.*, 2007).

To see whether the nonsense-mediated decay contributes to the regulation of *AtGRP7* and *AtGRP8,* the levels of *as_AtGRP7* and *as_AtGRP8* were analysed in different *upf1* and *upf3* mutant lines by RT-PCR using specific primer combinations (Table 2). The PCR products were blotted and hybridised with specific, radioactively labelled cDNA probes. The level of *as_AtGRP7* and *as_AtGRP8* are strongly elevated in *upf3-1* and *upf3-2* lines as well as in the *upf1-5* mutant. In *upf1-4* plants the *as_AtGRP7* and *as_AtGRP8* transcripts are only weakly enriched (Figure 44). Constant *ACTIN* levels in all samples served as a control (Figure 44).

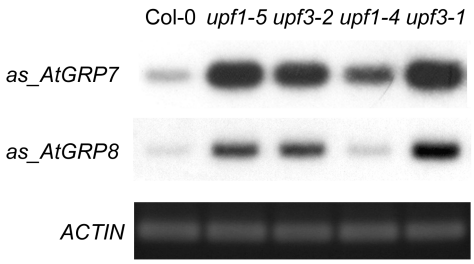

Figure 44: Effect of *upf1* and *upf3* on steady-state abundance of the alternatively spliced *AtGRP7* and *AtGRP8* transcripts. RNA from the mutants and Col WT harvested at ZT10 was reverse-transcribed. PCR amplification of the *as_AtGRP7* and *as_AtGRP8* transcripts was performed using specific primers (Table 2) and 24 cycles. The gel with the PCR products was blotted and hybridised with the *AtGRP7* (top) and *AtGRP8* (middle) cDNAs. Amplification with *ACTIN* primers served as control (bottom).

The RT-PCR results demonstrate a participation of UPF1 and UPF3 in the degradation of the alternatively spliced transcripts that are produced as a consequence of high *At*GRP7 and *At*GRP8 levels. Thus, for the first time a connection has been demonstrated between the nonsense-mediated decay pathway and the circadian system.

5 Discussion

The small glycine-rich RNA-binding protein *At*GRP7 operates within an output pathway from the CCA1-LHY-TOC1 clock. *AtGRP7* is rhythmically transcribed and both the RNA and the protein oscillate with a peak in the subjective evening (Heintzen *et al.*, 1997). At maximum protein levels *At*GRP7 represses its own accumulation and that of the related *At*GRP8 protein by the induction of alternative splicing (Staiger *et al.*, 2003). Moreover, *At*GRP7 is capable to bind its own transcript *in vitro* (Staiger *et al.*, 2003). Due to these findings it has been assumed that *At*GRP7, and probably *At*GRP8, form a secondary oscillator that preserves the signal of the core clockwork and transmits it to an array of proteins in the clock output pathway (Rudolf *et al.*, 2004; Staiger *et al.*, 2006). *At*GRP7 is the first example of a molecular slave oscillator that operates downstream of the clock and exerts its activity at a post-transcriptional level. Thus, the investigation of the molecular mechanism that drives this slave oscillator is of outstanding interst.

In the present work the RNA-binding properties of *At*GRP7 and *At*GRP8 have been studied extensively in ensemble measurements and at a single molecule level. Short binding sequences have been defined in *AtGRP7* and *AtGRP8* that are recognised specifically by the *At*GRP7 and *At*GRP8 proteins *in vitro*. A mutational analysis of the *At*GRP7 and *At*GRP8 RRM has revealed critical residues for binding affinity and target specificity. Moreover, the exchange of a single arginine residue in the RNP1 consensus sequence abolishes the function of *At*GRP7 and *At*GRP8 *in vivo*. A comparison of *At*GRP7 and *At*GRP8 activity *in vivo* uncovered the regulation of common target transcripts as well as a reciprocal regulation of both RNA-binding proteins. Furthermore, the direct binding of *At*GRP7 to its own transcript has been verified *in vivo*. Finally, a connection of the *At*GRP7 and *At*GRP8 feedback loop to the nonsense-mediated decay pathway has been demonstrated.

5.1 Definition of specific binding sites

The exact mapping of the binding site(s) within the target RNA is essential for the determination of base-specific interactions between the RRM and the RNA (Marchand *et al.*, 2005). The binding sites within the *AtGRP7* transcript have previously been narrowed down by deletion analysis (Staiger *et al.*, 2003). One site has been identified in the second half of the intron and a second in the 3' UTR. Based on these results, synthetic oligoribonucleotides covering the presumed target sequences have been designed. The ORNs, 7-UTR_WT and 7-intron_WT, have been tested for binding of *At*GRP7 and *At*GRP8 in electrophoretic mobility shift assays. Both sequences showed a strong complex formation with both *At*GRP7 and *At*GRP8 in the presence of different concentrations of unspecific competitor tRNA. Furthermore, sequence specific binding of *At*GRP7 and *At*GRP8 to the ORNs has been demonstrated in competition experiments with ORNs carrying several G mutations. Likewise, mutated ORNs with several U mutations have been tested for their binding to *At*GRP7 (data not shown). The influence of the U mutations on binding is weaker than that of the G mutations. The strong influence of the guanines on binding implies that these bases are involved in the formation of important base-specific contacts between the RNA and the RRM whereas the uridines may exert a more stabilising function for complex formation. Experiments with *in vitro* transcripts and homoribopolymers had previously revealed some preferences for *At*GRP7 binding to poly(G) and, at a much weaker level, also to poly(U) (Staiger *et al.*, 2003). A binding of homologous RBPs from mustard and tobacco to GU-rich sequences had also been described (Hirose *et al.*, 1993; Staiger *et al.*, 2003).

Similar to *AtGRP7*, the *AtGRP8* transcript is alternatively spliced in *At*GRP7-ox plants and the *as_AtGRP8* transcript is rapidly degraded (Staiger *et al.*, 2003). Thus, it was assumed that *At*GRP7 also binds to sequences within the *AtGRP8* transcript. A bioinformatic approach was chosen for the identification of these binding sites. The sequences of the synthetic ORNs covering the *At*GRP7 binding sites in *AtGRP7* pre-mRNA were used as templates. Regions with a high degree of sequence homology were defined by pair wise alignment of the ORN sequences with the *AtGRP8* pre-mRNA (Thompson *et al.*, 1994; Morgenstern, 2004). Afterwards sequences were discarded that mapped to positions distinct from those of the *AtGRP7* ORNs (e.g. in the 5' UTR). The remaining three potential sequences, 8-intron_WT, 8-UTR_WT, and 8-UTR_938, were analysed for their secondary structure (Zuker, 2003; Steffen *et al.*, 2006). Beside a simple prediction of the

potential ORN structure, the structure of the binding sequences was predicted in context of the complete mRNA. For this purpose both, *AtGRP7* and *AtGRP8*, transcripts were checked for evolutionary conserved secondary structures (in cooperation with Prof. Dr. Irmtraud Meyer, Bioinformatics Centre, University of British Columbia, Vancover, Canada). Surprisingly, large parts of the pre-mRNAs do not show a high degree of secondary structure conservation. However, two regions with conserved structures have been defined. Even more strikingly, the identified binding sites within *AtGRP7* and the predicted binding sites within *AtGRP8* map to these two loci (Figure 22). The secondary structure analysis of the *AtGRP8* sequences revealed a slight preference for the 8-UTR_WT and the 8-intron_WT sequences as target sites since the 8-UTR_983 ORN shows less favourable secondary structure. These preliminary results could be verified by *in vitro* binding assays. Although all three ORNs form complexes with *At*GRP7, the 8-UTR_983 ORN has a significantly higher K_d value. Therefore, the 8-intron_WT and 8-UTR_WT sequences have been defined as target sequences within *AtGRP8*. Sequence specificity of *At*GRP7 and *At*GRP8 binding to the newly defined *AtGRP8* target sequences has been demonstrated in competition experiments.

Thus, the prediction of binding sites by bioinformatic analysis has proved itself as a reliable method in case of the *AtGRP8* transcript. Three parameters have to be considered as extremely important for the good correlation of *in silico* and *in vitro* data: The well characterised template sequences, the knowledge for an identical regulation and the successful prediction of conserved secondary structures in a whole pre-mRNA context.

5.2 Analysis of *At*GRP7 and *At*GRP8 binding affinity

Binding of *At*GRP7 and *At*GRP8 to the identified target sequences was analysed more closely by the determination of equilibrium dissociation constants. K_d values are an important criterion for the comparison of different RNA-binding proteins (Marchand *et al.*, 2005). RNA-binding proteins that are known to bind highly specific to a single target molecule or a to limited number of targets, like U1A, have extremely low K_d values (Law *et al.*, 2005). RBPs with less stringent target patterns, for example hnRNPA1, bind to a broad range of RNA molecules, but with higher K_d values (Abdul-Manan & Williams, 1996).

The *in vitro* binding assays have revealed K_d values in the low micro molar range for *At*GRP7 and *At*GRP8 binding to the intronic sequences (7-intron_WT and 8-intron_WT). For the ORNs derived from the 3'UTRs (7-UTR_WT and 8-UTR_WT) a slightly lower K_d value in the sub-micro molar range was determined.

These K_d values demonstrate an intermediate binding affinity, which is consistent with the K_d values of other RBPs, such as hnRNPA1 and SXL, that bind to a broad range of target transcripts (Samuels *et al.*, 1994; Abdul-Manan & Williams, 1996). Thus, the obtained K_d values strengthen the positioning of *At*GRP7, and probably also *At*GRP8, inside a "slave oscillator" of the *Arabidopsis thaliana* clock that spreads the signal from the central oscillator to an array of downstream targets (Heintzen *et al.*, 1997; Staiger & Heintzen, 1999; Rudolf *et al.*, 2004).

5.3 RNP1 arginine is essential for stable complex formation

Mutations were introduced into the *At*GRP7 and *At*GRP8 RRMs to detect an influence of the mutated residues on the binding affinity. The conserved first amino acid of the *At*GRP7 and *At*GRP8 RNP1 consensus sequence (Arg^{49} and Arg^{47}, respectively) was exchanged for glutamine.

Mutation of the *At*GRP7 Arg^{49} increased the K_d value of *At*GRP7-RQ five- to ninefold towards the four different binding sequences relative to the wild type protein. In case of the *At*GRP8-RQ mutation the K_d values were elevated six- to thirteenfold in comparison to wild type *At*GRP8. Moreover, the reduced binding affinity of the RQ mutant proteins is accompanied by a reduced stability of the complex during the gel run. An improper folding of the *At*GRP7-RQ mutant protein has been excluded by the recording of CD spectra (collaboration with Sven Hennig and Eva Wolf, MPI for Molecular Physiology, Dortmund, Germany). The spectra for wild type *At*GRP7 and *At*GRP7-RQ are almost identical indicating an intact secondary structure of *At*GRP7-RQ. A correct folding can also be assumed for the *At*GRP8-RQ protein variant due to the high homology of *At*GRP7 and *At*GRP8 (cf. 2.1.3).

An influence of the RNP1 arginine upon RNA binding was first discovered for the U1A RRM (Nagai *et al.*, 1990). The replacement of Arg^{52}, the *At*GRP7 Arg^{49} equivalent, by glutamine completely abolished binding of U1A to U1hpII. More detailed analysis suggested contacts of the Arg^{52} residue with the phosphate backbone of the U1hpII by the formation of salt bridges, since the substitution of Arg^{52} by lysine had only a minor influence (Jessen *et al.*, 1991). These assumptions were verified by co-crystallisation and subsequent molecular dynamics simulations of the U1A-U1hpII complex identifying different electrostatic and hydrogen-bonding interactions for Arg^{52} with the RNA (Oubridge *et al.*, 1994; Tang & Nilsson, 1999). Surface plasmon resonance based kinetic analysis by the Laird-Offringa lab implicated Arg^{52} as a key residue during the initiation of the complex formation of U1A and U1hpII (Law *et al.*, 2005; Law *et al.*, 2006a). A likewise important function for the RNP1 arginine has been described for two other well characterised RRM proteins, hnRNP A1 and SXL (Lee *et al.*, 1997; Ding *et al.*, 1999). A comparable function can be assumed for the RNP1 arginine in *At*GRP7 and *At*GRP8 on the basis of the homology modelled tertiary structures of the RRMs (Figure 6), and the reduced binding affinity of the two RQ mutant proteins.

An influence of the RNP1 RQ mutations on sequence specificity was analysed in competition experiments. EMSAs with wild type GST-*At*GRP7 and GST-*At*GRP8 have shown a strong competition by the wild type ORNs, but almost no competition by addition of the same amount of the G-mutated ORNs (cf. 5.1). Similar experiments have been performed with the GST-*At*GRP7-RQ and GST-*At*GRP8-RQ proteins. The residual binding of both protein variants to the different wild type ORNs can also be competed by addition of ORNs with homologous sequences, but not by the corresponding G mutated ORNs. This result suggests that the RNP1 arginine has an important function during complex formation and for complex stability but not for target selection.

5.4 Influence of loop 1 and loop 3 residues on *At*GRP7 binding

Although several prominent RNA-binding proteins are well characterised on the molecular level, only little is known about the process of target discrimination. Since the highly conserved nature of the RNP consensus sequences precludes a major role in target discrimination, the less conserved loop regions surrounding the binding interface on the β-sheet are thought to be predominant determinants of the target specificity of individual RRM proteins (Tang & Nilsson, 1999; Katsamba *et al.*, 2002).

To identify residues that are critical for the target discrimination of *At*GRP7, two less conserved residues within the loop regions of the *At*GRP7 RRM have been mutated. Trp^{17} within the first loop region was replaced by arginine and Glu^{44} in loop 3 was substituted by lysine. Co-crystallisation experiments and molecular dynamics simulations proposed direct contacts of U1A Glu^{19} and U1A Arg^{47} to U1hpII, which occupy analogous positions to Trp^{17} and Glu^{44} in *At*GRP7 (Oubridge *et al.*, 1994; Tang & Nilsson, 1999). Moreover, an important function of the U1A Arg^{47} had been reported for the structural organisation of the RRM during target recognition (Law *et al.*, 2006a). Arg^{47} stabilises Arg^{52} in a favourable position for the interaction with the incoming U1hpII. Additionally, the Arg^{47}-Arg^{52} interaction increases the net positive charge in this area of the binding motif (Law *et al.*, 2006a). Thus, a general role of the loop 1 and loop 3 regions during the first steps in U1hpII binding was assumed including a potential role of these residues in target recognition and discrimination (Boelens *et al.*, 1991; Oubridge *et al.*, 1994; Tang & Nilsson, 1999; Katsamba *et al.*, 2002; Law *et al.*, 2006a).

In contrast to the *At*GRP-RQ mutant proteins no distinct differences in binding affinity towards the 7-UTR_WT ORN have been observed in case of the two *At*GRP7 loop mutants. The amount of retarded complex is slightly reduced compared to the wild type protein for both, GST-*At*GRP7-$E^{44}K$ and GST-*At*GRP7-$W^{17}R$. This result had been expected since a requirement of the two mutated residues had been assumed for target discrimination and not for complex stability. Likewise, only minor effects on binding affinity had been reported in case of a replacement of U1A Glu^{19}, the *At*GRP7 Trp^{17} homologue, by serine (Boelens *et al.*, 1991).

The influence of the *At*GRP7-$W^{17}R$ and *At*GRP7-$E^{44}K$ mutations upon target discrimination was tested with three mutated, permutated or artificial sequences derived from the 7-UTR_WT ORN. The GST-*At*GRP7-$E^{44}K$ mutant shows a slightly, but not significantly, reduced binding to all three ORNs in comparison to wild type GST-*At*GRP7.

Differences in binding have also not been detected between the wild type GST-*At*GRP7 and the GST-*At*GRP7-$W^{17}R$ loop mutant protein towards the 7-UTR_Permut and 7-UTR_UG. However, complex formation of the GST-*At*GRP7-$W^{17}R$ protein variant with the 7-UTR_G_4mut-SH ORN is somewhat elevated compared to the wild type. This points to a slightly reduced sensitivity in target selection of the $W^{17}R$ mutant protein, especially in connection with a lower binding affinity of *At*GRP7-$W^{17}R$ towards the 7-UTR_WT ORN (see above).

Nevertheless, a strong influence of the introduced point mutations on binding affinity or target specificity could neither be verified for *At*GRP7-$W^{17}R$ nor for *At*GRP7-$E^{44}K$. This implicates an involvement of larger regions in the target recognition process as it has been described for U1A and U2B´´ (Scherly *et al.*, 1990). The spliceosomal proteins U1A and U2B'' show a 77 % sequence identity and a 99 % sequence homology for their RRM containing N-terminus (AAs 7-101 of U1A and AAs 4-98 of U2B´´). Moreover, they have identical RNP sequences except for a single residue at the last position of the less conserved RNP2 hexapeptide. Nevertheless, both proteins bind specifically to distinct target sequences. U1A binds to U1hpII whereas U2B´´ binds to the fourth hairpin of the U2 snRNA with extremely high affinities (Lutz-Freyermuth *et al.*, 1990; Scherly *et al.*, 1990; Boelens *et al.*, 1991; Katsamba *et al.*, 2001). U1A and U2B´´ domain-swap mutants have been established and identified a longer, less conserved region of β_2 and loop3 as responsible for the target discrimination (Scherly *et al.*, 1990). Thus, a minor influence of single amino acids on target selection is consistent with the binding mechanism described for prominent RRM proteins.

5.5 New methods for the analysis of RNA-protein interactions at the single molecule level

The gel shift experiments yielded valuable information about the *At*GRP7 and *At*GRP8 RNA-binding process. However, these ensemble measurements have a limited resolution and sensitivity since they only display the result of the complex formation but not the process itself. Thus, new techniques have been developed for the detailed investigation of the *At*GRP7 and *At*GRP8 protein-RNA interaction in solution. FCS and PET-FCS as well as AFM-FS have been adapted to the special requirements for the analysis of RNA containing complexes on the single molecule level.

FCS has been established by analysing the well-characterised binding of *At*GRP7 to its own 3' UTR. The determined K_d values are comparable to those previously calculated on the basis of gel shift experiments and demonstrate the reliability of the new technique. Further investigation revealed the binding of *At*GRP7 to homologous single-stranded DNA sequences. The binding affinities of RNA and DNA oligonucleotides are almost identical. This dual capacity to bind both, RNA and DNA targets of the same sequence resembles hnRNP A1 (Buvoli *et al.*, 1990). For hnRNP A1 binding to telomeric DNA sequences and their RNA analogues had been demonstrated (Abdul-Manan & Williams, 1996).

Additionally, FCS has been used to narrow down the *At*GRP7 core binding sequence to seven nucleotides ((G)GUUCUG(G)). Interestingly, a guanine pair increases the binding affinity, regardless whether it is located at the beginning or at the end of the sequence. This implies that the ORN can possibly be bound by the RRM in two directions: 5' → 3' and 3' → 5'. In EMSAs a delineation of the sequence down to thirteen nucleotides has been achieved (data not shown), however complex formation is severely reduced. Obviously, interactions between the additional nucleotides and the protein surface are necessary to prevent dissociation of the complex by friction during the gel run. The identification of the core binding sequence holds an enormous potential, as a precise characterisation of essential nucleotides for a stable binding by mutational analysis is a prerequisite for the identification of target transcripts *in silico* (Zheng *et al.*, 2007). Moreover, in connection with the mutational analysis of the RRM (cf. 5.3 & 5.4) the short binding sequence will allow a more detailed view on the RRM-ORN interaction, like for example the definition of direct nucleotide – amino acid interactions.

To gain a deeper insight into the binding process itself, the PET-FCS technique has been used. PET-FCS has previously been proved to yield information about the secondary

structure of oligonucleotides in solution (Kim *et al.*, 2006). Thus, the binding of *At*GRP7 to two ORNs that contained the core binding sequence but had a different secondary structure, hairpin and linear, has been examined. Both ORNs were bound by *At*GRP7 with almost the same affinity. However, the quenching kinetics of the fluorescent MR121 dye on a sub-millisecond timescale revealed a change of the secondary structure of the hairpin ORN upon *At*GRP7 binding. The requirement of an extended structure for *At*GRP7 binding was demonstrated since the binding affinity of *At*GRP7 decreases if the breathing of the stem loop structure is prevented by lengthening the stem. It is known that DNA and RNA hairpins form a dynamic equilibrium with open and closed conformations including several intermediate states (Wallace *et al.*, 2001; Li *et al.*, 2004; Kim *et al.*, 2006; Van Orden & Jung, 2007). This implies that *At*GRP7 binds to the ORN if an open confirmation is present and arrests the ORN in this extended structure (Figure 45). Thus, secondary structures of the target RNA can be stabilised or possibly rearranged by *At*GRP7 during the binding process, if the core binding sequence is accessible.

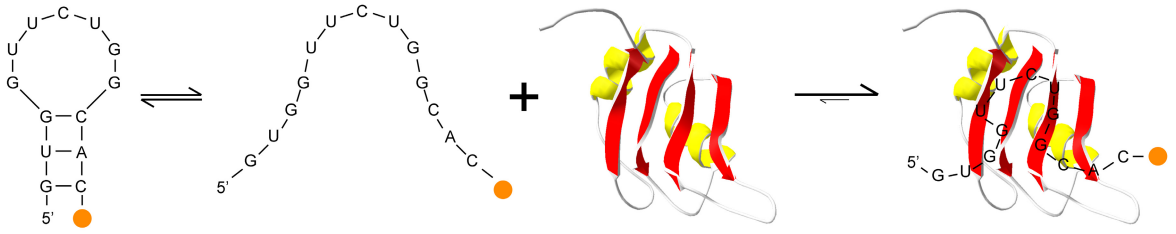

Figure 45: Binding of *At*GRP7 stabilises an extended secondary structure of the 7-UTR_SL ORN. The hairpin and open conformation of the 7-UTR_SL ORN form a dynamic equilibrium. *At*GRP7 is only able to bind to the open structured ORN and stabilises the extended secondary structure. No binding of *At*GRP7 was observed to stable stem-loop structures. Thus, *At*GRP7 can be omitted in the left part of the figure.

A conformational change of the *AtGRP7* RNA upon *At*GRP7 binding could uncover regions essential for the recruitment of splicing factors that subsequently perform the alternative splicing of the transcript (cf. 5.9). Thus, the PET-FCS experiments have strengthened the hypothesis that *At*GRP7 directly triggers its negative auto-regulation by binding to its own transcript.

For the detailed analysis of the *At*GRP8 binding mechanism another single molecule technique has been developed. AFM-FS measurements yielded a deeper insight into the process of contact formation of *At*GRP8 with its target RNAs. The specificity of the method has been proved in experiments demonstrating no or reduced binding of unspecific or mutated RNAs by the wild type protein or a lack of rupture events in case of an unrelated protein. For binding of *At*GRP8 to a sequence derived from the *AtGRP8* 3'UTR

two distinct rupture events could be detected. Competition experiments show a clear correlation between the stiffness of the complex, indicating stability, and the specificity of the detected rupture events. The binding events responsible for the high stiffness peak can be competed by free RNA, whereas the binding events with a lower stiffness cannot be competed. This shows that two discriminable events take place during complex formation. It can be assumed that an unspecific, electrostatic adhesion of the RNA to the positively charged protein surface occurs, presumably followed by several re-binding events until the RNA hits the binding site at the β-sheet of the RRM. The tight binding of the RNA by the RRM is defined by the second peak. The stepwise incorporation of the RNA into a stable RNP complex has also been demonstrated by a separation of the rupture events by the dwell time of the tip. The dwell time defines the contact time of the tip at the surface. With longer contact times the stability of the complex increases, visible in higher stiffness and rupture force.

The idea of a two-step mechanism is also supported by the analysis of the *At*GRP8-RQ mutant. The introduction of the $R^{47}Q$ mutation abolishes the peak at high rupture forces that defines the specific binding, whereas rupture events at low forces persist (cf. Figure 40). Thus, unspecific adhesion of the RNA to the protein surface of the *At*GRP8-RQ mutant is still possible but the incorporation into a fixed, and thus stable complex is impaired.

These results imply an induced fit mechanism for the *At*GRP8-RNA complex formation as it has been proposed for the RNA binding of U1A (Allain *et al.*, 1996). When the U1 snRNA and the U1A protein come into a close range at the binding site of the RRM, the RNA is captured by the RNP1 arginine. Afterwards several re-arrangements of the RRM structure occur until the β_2-β_3 loop protrudes from the U1hpII loop (Law *et al.*, 2006a). Likewise, target RNAs have to come into a close contact to the *At*GRP8 Arg^{47} to induce a stable complex formation.

In conclusion, the newly developed single molecule techniques have resolved the *At*GRP-RNA complex formation at a higher level. A more detailed insight was gained into the intra- and intermolecular dynamics during the binding process, demonstrating the high potential of these methods as general tools for the RNA-protein interaction analysis.

5.6 Reciprocal regulation of *At*GRP7 and *At*GRP8 *in vivo*

The *At*GRP7 protein induces negative auto-regulation and down regulation of the *AtGRP8* transcript presumably by direct binding to the respective pre-mRNAs. As it could be shown within this thesis that *At*GRP8 is sufficient to bind to its own transcript *in vitro* (cf. 4.4.1 and discussion above) it was assumed that *At*GRP8 might also feature negative auto-regulation upon overexpression *in vivo*. Therefore, transgenic *Arabidopsis* lines constitutively overexpressing *At*GRP8 have been generated. In *At*GRP8-ox plants the endogenous *AtGRP8* transcript is severely reduced. Moreover, an alternatively spliced *AtGRP8* transcript, which is also detectable upon *At*GRP7 overexpression, appears at the expense of the mature mRNA. No effect, however, could be detected on the rhythmic expression pattern of *AtGRP8*. Thus, *At*GRP8 overexpression induces negative auto-regulation. The mechanism for the shift in splice site selection is presumably the same as described for the *At*GRP7 overexpression since the size of the alternatively spliced *AtGRP8* transcript is identical (Staiger *et al.*, 2003). Presumably, *At*GRP8 binds at high protein levels to sequences within the second half of the intron and the 3'UTR of its own transcript (cf. 5.1). This binding potentially triggers the recruitment of splice factors and yields the alternative splicing of the *AtGRP8* RNA. Therefore, *At*GRP7 and *At*GRP8 are not only able to bind identical sequences *in vitro*, they also show an identical autoregulatory mechanism *in vivo*.

The identification of a stable binding of *At*GRP8 to sequences within the *AtGRP7* transcript and vice versa pointed to a reciprocal regulation of both proteins (cf. 5.2). *At*GRP8-ox plants have been analysed for the expression of *AtGRP7*. No mature *AtGRP7* mRNA is detectable upon *At*GRP8 overexpression; only a faint band representing the alternatively spliced *AtGRP7* RNA is visible. Correspondingly, the amount of *At*GRP7 protein is severely reduced in *At*GRP8-ox lines. Thus, high *At*GRP8 concentrations repress the accumulation of functional *At*GRP7 by the induction of alternative splicing. These results demonstrate a reciprocal regulation of *At*GRP7 and *At*GRP8 on a post-transcriptional level (Figure 46). This cross-regulation of *At*GRP7 and *At*GRP8 presumably helps to stabilise and sharpen the rhythmic expression pattern of both proteins. Such an interlocked feedback loop of the two RNA-binding proteins had previously been suggested by Heintzen and Staiger (Staiger & Heintzen, 1999). However, the results described above are the first experimental evidence for a circadian feedback loop primarily driven by post-transcriptional control.

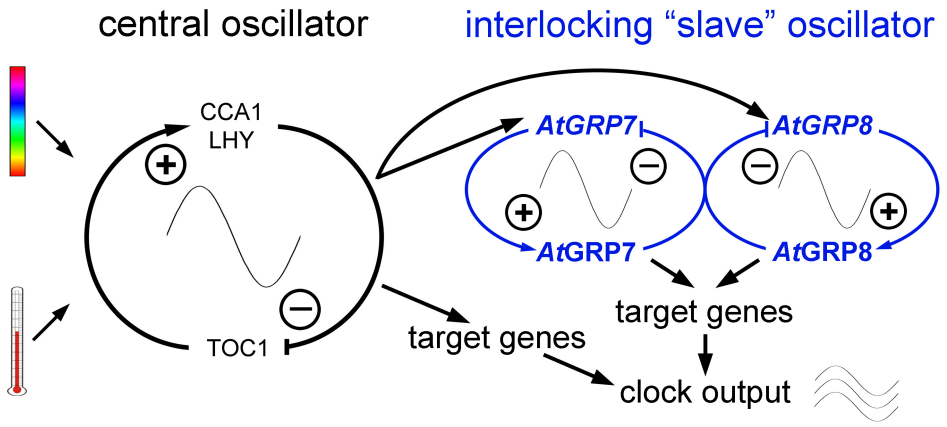

Figure 46: Model of the *At*GRP7/*At*GRP8 interlocking feedback loop in the *Arabidopsis thaliana* circadian system. Environmental information is perceived, e.g. by photoreceptors, and transmitted towards the central oscillator (cf. 2.1.2). The oscillator transduces rhythmicity to *AtGRP7* and *AtGRP8* by transcriptional control. At high levels *At*GRP7 and *At*GRP8 perform negative auto-regulation. Additionally, the two RBPs reciprocally regulate their expression at the post-transcriptional level. This interlocking secondary feedback loop stabilises and amplifies the signals from the central oscillator and transduces them to an array of output genes.

Today, the existence of transcriptional interlocking feedback loops in circadian clocks is well established (cf. 2.1.1.1). The *Drosophila* protein dCLK for example activates the transcription of VRI and PDP1. Subsequently, the transcription of dCLK is regulated negatively and positively by VRI and PDP1, respectively. This reciprocal regulation has been proved to be essential for stability in period length and rhythmicity (Glossop *et al.*, 1999; Cyran *et al.*, 2003; Glossop *et al.*, 2003). Recently, another negative autoregulatory feedback loop has been described that interferes with the activity of dCLK. The transcription factor Clockwork Orange (CWO) binds, like dCLK, to canonical circadian E-boxes and thus counteracts the activity of dCLK (Matsumoto *et al.*, 2007). This demonstrates that circadian clocks can be composed of a multitude of interlocking and antagonistic feedback loops. The existence of interlocking feedback loops on the basis of pseudo-response regulators has been described for *Arabidopsis thaliana* (cf. 2.1.2.1). These factors control, by a yet unknown post-transcriptional mechanism, the activity of the core clock components CCA1, LHY and TOC1 (Farré *et al.*, 2005; Nakamichi *et al.*, 2005).

In conclusion, the reciprocal regulation of *At*GRP7 and *At*GRP8 identifies a new type of interlocking feedback loop based on a post-transcriptional mechanism (Figure 46). In analogy to the *Drosophila* oscillator and the *Arabidopsis* core clockwork the high degree of regulation in *AtGRP7* and *AtGRP8* expression shows that the generation of stable rhythms and the sharpening of the expression peaks may be essential for the accurate and efficient control of downstream transcripts.

5.7 Regulation of identical target transcripts by *At*GRP7 and *At*GRP8

Common RNA-binding properties and shared functions of *At*GRP7 and *At*GRP8 have been demonstrated by *in vitro* and *in vivo* experiments (see discussion above). Thus, it was examined whether *At*GRP7 and *At*GRP8 regulate identical target transcripts in the cell. Affymetrix® GeneChip experiments with wild type and *At*GRP7-ox plants and subsequent verification by qRT-PCR revealed a suite of candidate *At*GRP7 target transcripts (F. Rudolf, C. Streitner, M. Neuenschwander, J.L. Gómez-Porras and D. Staiger, unpublished). Four of these transcripts have been tested for their response upon *At*GRP8 overexpression. All transcripts analysed are regulated identically in *At*GRP8-ox plants and in an *At*GRP7-ox line. *CK2*, *CuZnSOD2* and a *Cu-Chaperone* are up-regulated in case of high *At*GRP levels, whereas *FAD2* is down-regulated. Thus, it has been demonstrated that, in addition to the reciprocal regulation, *At*GRP7 and *At*GRP8 regulate identical target transcripts *in vivo*. Moreover, an *At*GRP8-ox line with a lower *AtGRP8* level generated in a former transformation experiment (*At*GRP8-ox line 15; D. Staiger, unpublished) shows a reduced influence of the *At*GRP8 overexpression on the target transcripts. Thus, the regulation of target transcripts by *At*GRP8 is dose dependent. This dose dependent regulation that is also assumed for *At*GRP7 may be important for the circadian function of *At*GRP8. Potentially, the *At*GRP8 and/or *At*GRP7 concentration has to reach a certain threshold until the protein is sufficient to feed back to its own expression and on that of its targets.

The importance of thresholds for target regulation has also been described for the CWO feedback loop. The CWO transcription factor competes with dCLK for the E-boxes of circadian regulated promoters (Matsumoto *et al.*, 2007). Accordingly, the respective level of both proteins determines the transcriptional state of the concerned promoters. At high levels the CWO protein represses the transcription, whereas high abundance of dCLK induces transcription (Matsumoto *et al.*, 2007). Thus it is reasonable that also *At*GRP7 and *At*GRP8 have to accumulate to a certain level until they can exhibit their regulatory function.

5.8 RNP1 arginine is essential for *At*GRP7 and *At*GRP8 function *in vivo*

To demonstrate an influence of the reduced binding affinity of *At*GRP7-RQ and *At*GRP8-RQ *in vivo*, transgenic lines overexpressing the mutated proteins were established. The negative autoregulatory function and the reciprocal regulation of both *At*GRP proteins are disturbed since no alternative splicing is induced by overexpression of the RQ mutant proteins (Figure 47). Moreover, the regulation of two target transcripts is impaired in *At*GRP7-RQ-ox plants. The transcripts *At*AILP1 (*Arabidopsis thaliana* aluminium induced like protein) and *At*TLL1 (*Arabidopsis thaliana* triacylglycerol lipase like protein) are negative regulated in *At*GRP7-ox plants (D. Page and M. Furuya, Hitachi Advanced Research Laboratory, Hatoyama, Japan). In contrast, the expression of both transcripts, *At*TLL1 and *At*AILP1, is not affected by overexpression of *At*GRP7-ox (data not shown). Thus, the regulation of both, circadianly (e.g. *At*GRP7, *AtGRP8* and *AtAILP1*) and non-circadianly (*AtTLL1*) expressed transcripts requires an intact *At*GRP RNA-binding motif.

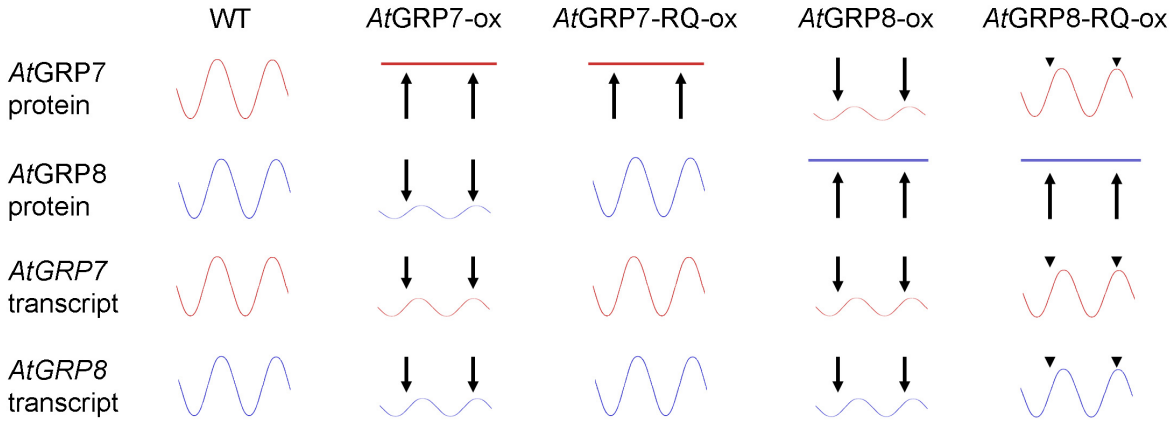

Figure 47: Comparison of the effects of *At*GRP and *At*GRP-RQ overexpression on the RNA and protein abundance. Overexpression of the wild type proteins induces alternative splicing and thus represses the accumulation of the endogenous transcripts and proteins. The overexpression of the RNP1 RQ mutant proteins, however, has no or only modenst influence on the expression of the endogenous *AtGRP* transcripts and proteins.

An *in vivo* approach had previously been described for the *Drosophila* SANSFILLE (SNF) that is homologous to U1A and U2B´´ (Stitzinger *et al.*, 1999). SNF harbours two RRMs and is sufficient to bind both, the U1 and the U2 snRNA. Unexpectedly, a mutation of SNF Arg^{49} to Gln that is analogous to the *At*GRP7-RQ mutation did not have significant effects *in vivo*. The mutated SNF-R^{49}Q was still able to rescue the lethal *snf*^{d210} phenotype and thus to bind U1 and U2 snRNAs. Random mutagenesis screens revealed that the

C-terminal RRM of SNF rescued the abolished binding affinity of the Arg^{49} N-terminal RRM by a still unknown mechanism, although it did not show RNA-binding activity *in vitro* (Stitzinger *et al.*, 1999). Thus, the work on the SNF-R^{49}Q mutant was not able to assign a definite *in vivo* function to the highly conserved RNP1 arginine.

In contrast, the reduced binding affinities of *At*GRP7-RQ and *At*GRP8-RQ directly manifest themselves *in vivo*. Since the mutation of the same arginine residue in *At*GRP7 and *At*GRP8 yields identical molecular phenotypes it can be concluded that the RNP1 arginine indeed makes essential contacts to the RNA *in vivo*. Thus, the mutational analysis of single RRM proteins may be advantagous for the identification of crucial amino acids for the RNA binding *in vivo*, since no additional RNA-binding domain can substitute the mutated RRM.

It should be noted that an influence of secondary factors on the *in vivo* effects of the *At*GRP RNP1 mutations, such as impaired protein-protein interactions, cannot be completely excluded. However, participation of the RNP1 arginine in such interactions has not been reported so far, and the excellent correlation of *in vitro* and *in vivo* data suggest a direct influence of the reduced binding affinity (Maris *et al.*, 2005).

The importance of the RNP1 arginine for *At*GRP7 and *At*GRP8 function in the plant is also interesting from a completely different point of view. *At*GRP7, and also *At*GRP8, have recently been identified as key factors for the virulence of *Pseudomonas syringae* (Fu *et al.*, 2007). The type III effector protein HopU1 is an ADP-ribosyltransferase that modifies *At*GRP7 during the infection process (Fu *et al.*, 2007). Moreover, it could be shown that HopU1 specifically ADP-ribosylates Arg^{49} of *At*GRP7 (J.R. Alfano, Plant Science Initiative and Department of Plant Pathology, University of Nebraska, Lincoln, USA; personal communication). This suggests, that HopU1 may interfere with plant immune responses at a post-transcriptional level by inhibition of *At*GRP7 binding to defense related transcripts. The impaired binding of an Arg^{49} modified *At*GRP7 to target RNAs (cf. 5.3) may thus contribute to plant susceptibility (Figure 48). This view is supported by the phenotype of *atgrp7-1* knock-out plants that show a reduced hypersensitive response (Fu *et al.*, 2007).

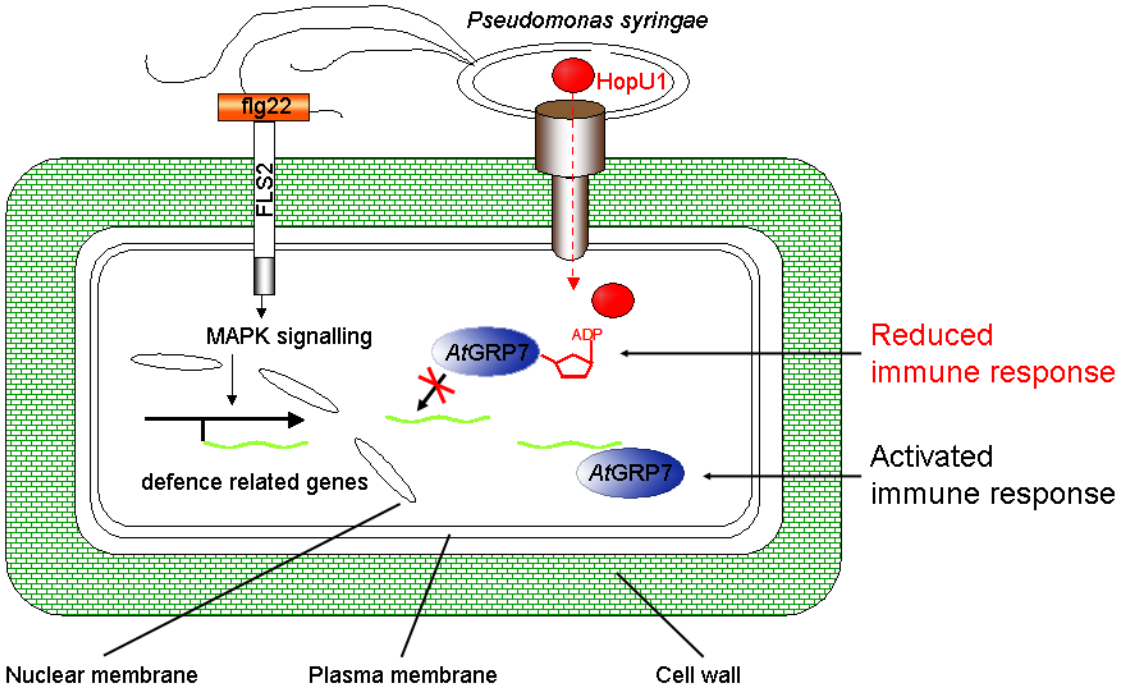

Figure 48: The ADP-ribosylation of the *At*GRP7 Arg[49] interferes with the plant immune response. The type III effector protein HopU1 is injected into the plant cell where it specifically ADP-ribosylates Arg[49] of *At*GRP7. Corresponding to the loss of negative auto-regulation in the *At*GRP7-RQ mutant lines it is likely that the ADP-ribosylation reduces the *At*GRP7 binding to defence related transcripts and thus represses the plant immune response.

In conclusion, the mutational analysis of *At*GRP7 and *At*GRP8 has revealed a requirement of a functional RNA-binding domain for their regulatory role *in vivo*. Moreover, the RNA-binding activity is essential for both, the regulation of transcripts that are clock regulated and of those that are not rhythmically expressed.

5.9 Direct Binding of *At*GRP7 to its own transcript *in vivo*

The analysis of *At*GRP7-RQ-ox and *At*GRP8-RQ-ox plants has demonstrated that the RNA-binding activity is essential for the regulatory function *in vivo*. Potentially, a direct binding of *At*GRP7 to the (pre-)mRNA of its target genes is required to trigger this process. Thus, RNP-immunoprecipitation has been performed to further strengthen this hypothesis. The isolation of intact mRNP complexes from plant tissue is technically challenging since the complexes have to be precipitated under native conditions. Thus, the contamination with and the activity of RNases has to be repressed as far as possible. Moreover, to enable more stringent washing conditions the mRNP complexes have been reversibly cross-linked *in planta* by the infiltration of formaldehyde. Using this method intact full length mRNA could be isolated from the *At*GRP7-RNA-immunoprecipitate.

An direct association of the *AtGRP7* mRNA and the *At*GRP7 protein has been verified by RT-PCR. However, neither the precipitation of *AtGRP8* nor that of other potential target RNAs (cf. 4.4.5 and 5.8) could be demonstrated. The amount of precipitated target RNAs, except for *AtGRP7*, was inconsistent for the replicates (data not shown). This may be due to two reasons: Firstly, *AtGRP7* is one of the most abundant transcripts in *Arabidopsis thaliana*. In connection with a stable binding of the transcript by *At*GRP7, as determined *in vitro* (cf. 5.2), the *AtGRP7* mRNA might displace most of the other transcripts from the complex just by competition. Secondly, the detection of less abundant RNAs is even more difficult due to a high background level of unspecifically precipitated transcripts. This amount of unspecifically co-precipitated RNAs, determined by the amplification of 18S rRNA, is caused by the strategy chosen for the RNP-immunoprecipitation. The monoclonal α-GFP antibody shows a general affinity to nucleic acids, since almost no 18S rRNA can be amplified if the antibody is omitted (cf. Figure 19). Thus, an exchange of the used tag may enhance the sensitivity of the precipitation. Nevertheless, the performed RNP-immunoprecipitation demonstrates a direct binding of *At*GRP7 to its own transcript *in vivo* and thus underlines the results obtained by mutational analysis (cf. 5.8).

The verification of *At*GRP7 RNA-protein interaction *in vivo* supports the idea that *At*GRP7 triggers the negative auto-regulation by binding to its own transcript. Post-transcriptional feedback regulation by alternative splicing has been described for the splice factors TRA-2 from *Drosophila* and SR20 from mice (Ryner & Baker, 1991; Jumaa & Nielsen, 1997). Moreover, the human SR protein SC35 regulates its own expression by the generation of unstable alternative splice forms (Sureau *et al.*, 2001). An influence on splice site

selections has also been shown for the *Arabidopsis thaliana* serine-arginine (SR) rich RNA-binding protein *At*SRP30 and other SR proteins (Lopato *et al.*, 1999; Hastings & Krainer, 2001). However, only co-precipitation of *At*GRP7 with splicing factors from the *AtGRP7* transcript would directly demonstrate the existence of such a mechanism since *At*GRP7 itself is not expected to exhibit splicing activity.

Besides the direct binding to its target transcripts, *At*GRP7 could exert its activity by a completely different mechanism. For several of the described *At*GRP7 and *At*GRP8 target transcripts no alternative splice forms have been described yet. Thus, other mechanisms have to be taken into account for the regulation of these targets. The related mouse RNA-binding protein RBM3 stimulates global gene expression in a post-transcriptional way. It was shown that RBM3 interacts with the large subunit of translating ribosomes (Dresios *et al.*, 2005; Smart *et al.*, 2007). Moreover, the threefold increased protein concentration seems to be associated with a second effect in addition to an enhanced translation initiation. In polysome profiles of RBM3 overexpressing cells a fraction containing microRNAs (miRNAs) was severely reduced (Dresios *et al.*, 2005). It can be speculated that the reduction of miRNAs is responsible for the main part of the translational enhancement. Thus, it is possible that also *At*GRP7 regulates the abundance of different target transcripts by binding to regulatory RNAs or by preventing the hybridisation of small RNAs to these target transcripts.

Nevertheless, the co-precipitation of *AtGRP7* RNA and protein is a strong indication that at least the negative autoregulatory mechanism includes a direct binding of *At*GRP7 to its own transcript.

5.10 UPF1 and UPF3 are involved in degradation of *as_AtGRP7* and *as_AtGRP8*

Alternatively spliced *AtGRP7* and *AtGRP8* transcripts that retain the second half of the intron are generated as a result of *At*GRP7 and *At*GRP8 overexpression. These alternatively spliced transcripts have a shortened half-life (Staiger *et al.*, 2003). Since the transcripts exhibit a premature termination codon in the intronic sequence it was analysed whether they are degraded via the nonsense-mediated decay pathway. To identify critical components for the degradation mechanism, *upf1* and *upf3* mutant plants were analysed for their *as_AtGRP7* and *as_AtGRP8* levels. The UPF proteins (UPF1, UPF2 and UPF3) are critical components of the NMD in yeast, worms, flies and mammals (Chang *et al.*, 2007). Recently, the participation of the *Arabidopsis* UPF1 and UPF3 homologues in the degradation of PTC containing transcripts has been described (Hori & Watanabe, 2005; Arciga-Reyes *et al.*, 2006). Both transcripts *as_AtGRP7* and *as_AtGRP8* are enriched in *upf1-5* and *upf1-4* plants. This demonstrates a participation of UPF1 in the degradation of the alternatively spliced *At*GRP transcripts. Moreover, the observed effect is much stronger in the *upf1-5* line than in *upf1-4* plants consistent with a more reduced *UPF1* level in *upf1-5* (Arciga-Reyes *et al.*, 2006). Likewise results have been obtained for the *upf3-1* and *upf3-2* lines. A knockdown of the UPF3 protein results in higher *as_AtGRP7* and *as_AtGRP8* levels compared to wild type plants. This implies that the rapid degradation of *as_AtGRP7* and *as_AtGRP8* is an NMD dependent process. This result is strengthened by a previous experiment showing that the degradation of the alternatively spliced *AtGRP7* transcript is inhibited by treatment with Cycloheximide (CHX) (Staiger *et al.*, 2003). Thus, the rapid decay of the *as_AtGRP* transcripts requires either translation itself, a short-lived factor that is reduced upon CHX treatment or other processes that are associated with ribosomes. It is known that the inhibition of translation prevents the recognition of the PTC during the first round of translation (Chang *et al.*, 2007). Thus the stabilisation of *as_AtGRP7* by cycloheximide treatment is consistent with the assumed NMD process (Staiger *et al.*, 2003).

The controlled degradation of unproductively spliced mRNAs by NMD had previously been described for the regulation of L3, L7a, L10a, and L12 that encode ribosomal proteins in *C. elegans* (Mitrovich & Anderson, 2000). Analogous to *AtGRP7* and *AtGRP8,* a premature stop codon is generated by the incomplete removal of an intron. Moreover, overexpression of the ribosomal protein L12 enhances alternative splicing and thus induces

negative auto-regulation (Mitrovich & Anderson, 2000). A negative feedback loop on the basis of unstable splice forms that are degraded via the NMD pathway has also been described for the human splice factor SC35 (Sureau *et al.*, 2001). The rapid degradation of a 1.7 kb long PTC containing transcript that is produced upon SC35 overexpression can be prevented by the addition of Cycloheximide (Sureau *et al.*, 2001). Thus, the post-transcriptional regulation of gene expression by generation of alternatively spliced transcripts that are rapidly degraded via the NMD pathway appears to be a common and conserved mechanism.

Moreover, the data obtained for *At*GRP7 and *At*GRP8 show for the first time a connection between circadian regulation and NMD (Figure 49). A widespread regulation of transcripts by NMD has been reported for yeast and is also consistent with the observation of different severe developmental phenotypes in *upf* mutant plants (He *et al.*, 2003; Hori & Watanabe, 2005; Arciga-Reyes *et al.*, 2006).

A post-translational regulation based on the timed degradation of clock proteins via the proteasome has been described (Más *et al.*, 2003). TOC1 and ZTL form complexes during the night. The F-box protein ZTL triggers the ubiquitination of TOC1, which is afterwards degraded in a light-dependent process via the proteasome (Más *et al.*, 2003). Based on the idea of different post-transcriptional and post-translational control mechanism within the plant clock, the timed degradation of clock regulated transcripts by NMD is possibly a new general post-transcriptional mechanism for the shaping and sharpening of circadian oscillations (cf. 5.11; Figure 49).

5.11 Future perspectives

The present work has revealed a reciprocal regulation of the two clock controlled RNA-binding proteins *At*GRP7 and *At*GRP8. This reciprocal regulation, as well as the auto-regulation and the regulation of several target transcripts require a functional RNA-binding domain. Therefore the direct binding of *At*GRP7 and *At*GRP8 to their own (pre-)mRNA and to their targets is likely. Since the direct interaction of *At*GRP7 protein and mRNA has been demonstrated by RNP-immunoprecipitation experiments, this technique is a promising tool to distinguish direct from indirect targets among the candidates identified by transcript profiling and to discover new direct RNA targets in an Ribonomics approach (Tenenbaum *et al.*, 2000). Additionally, the identification of a minimal binding sequence by fluorescence correlation spectroscopy offers the possibility to start an extensive mutational analysis of the target sequence, to define specific interactions of particular nucleotides with the RRM. In connection with the established *At*GRP7 mutant proteins it should be possible to identify single residues that determine sequence specificity. The detailed characterisation of the *At*GRP7-RNA interaction and of the binding mechanism, which has been analysed by AFM-FS, allows a more precise prediction of potential target transcripts *in silico*. The verification of predicted target transcripts can subsequently be performed *in vitro* with EMSAs and the established single molecule techniques.

The *atgrp7-1* mutant that lacks *At*GRP7 protein and RNA due to a T-DNA insertion in the 5´ region represents a novel experimental system to study the physiological functions of *At*GRP7. The *atgrp7-1* mutant is more susceptible to *Pseudomonas syringae* infection (Fu *et al.*, 2007), possibly reflecting an influence of *At*GRP7 on the defense related transcriptome. Moreover, the *atgrp7-1* mutant flowers late due to elevated levels of the *FLOWERING LOCUS C* (*FLC*) transcript encoding the key repressor of flower induction (Streitner, Danisman, Wehrle, Schöning, Staiger; manuscript in preparation). Complementation of *atgrp7-1* plants with wild type *AtGRP7* (pHPT_GRP7-FL) or *AtGRP7-RQ* (pHPT_GRP7RQ-FL) mutant protein (cf. Table 3) has been performed, and the analysis of the offspring will provide insight into the importance of the *At*GRP7 RNA-binding activity for its physiological responses.

Furthermore, a direct connection of the *At*GRP7/*At*GRP8 feedback loop to the nonsense-mediated mRNA decay pathway has been demonstrated. The timed repression of proteins by the generation of alternatively spliced transcripts that are rapidly degraded may be a new type of regulation in the circadian system (Figure 49). In contrast to a proteolytical

degradation this mechanism is faster and more efficient. Thus, it is possible that more oscillating transcripts within the circadian system of *Arabidopsis thaliana* are regulated by the same mechanism. An extended search in *upf* mutant plants for transcripts with altered expression patterns and the subsequent comparison with transcripts altered in clock mutants would identify such transcripts. Moreover, a role for *At*GRP7, and by extension, *At*GRP8 in this process can be analysed.

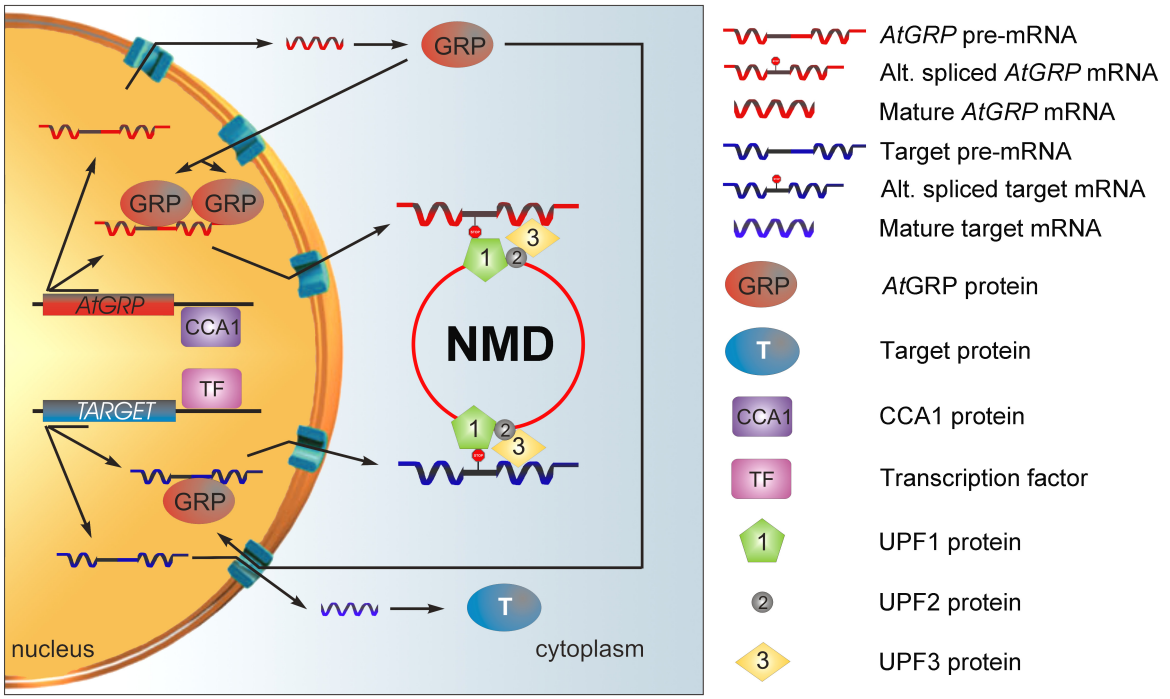

Figure 49: Model for the connection of the *Arabidopsis thaliana* circadian system, the *At*GRP feedback loop and the NMD pathway. The central oscillator of the *Arabidopsis* clock controls the timed transcription of the *AtGRP* genes. The *At*GRP proteins accumulate and subsequently repress post-transcriptionally their own expression and that of other target transcripts. The post-transcriptional control occurs presumably by direct binding of the *At*GRP proteins to the pre-mRNAs, which yields the generation of alternatively spliced transcripts with PTCs. The PTC is recognised during the first round of translation and the alternatively spliced transcripts are degraded via the NMD pathway.

If the assumption is correct that *At*GRP7 is a general factor for the generation of unstable transcripts within the plant circadian system, it is likely that the mechanism of alternative splicing for this regulation is conserved. Splice forms of direct *At*GRP7 targets that are also degraded by NMD should be enriched in *upf* mutant plants as well as in *At*GRP7-ox plants and are therefore identifiable by comparison of these genotypes.

6 References

Abdul-Manan N., Williams K.R. (1996). hnRNP A1 binds promiscuously to oligoribonucleotides: utilization of random and homo-oligonucleotides to discriminate sequence from base-specific binding. *Nucleic Acids Res 24*: 4063-4070.

Alabadi D., Oyama T., Yanovsky M.J., Harmon F.G., Mas P., Kay S.A. (2001). Reciprocal regulation between TOC1 and LHY/CCA1 within the Arabidopsis circadian clock. *Science 293*: 880-883.

Allada R., White N.E., So W.V., Hall J.C., Rosbash M. (1998). A mutant *Drosophila* homolog of mammalian Clock disrupts circadian rhythms and transcription of *period* and *timeless*. *Cell 93*: 791-804.

Allain F.H., Bouvet P., Dieckmann T., Feigon J. (2000). Molecular basis of sequence-specific recognition of pre-ribosomal RNA by nucleolin. *Embo J 19*: 6870-6881.

Allain F.H., Gubser C.C., Howe P.W., Nagai K., Neuhaus D., Varani G. (1996). Specificity of ribonucleoprotein interaction determined by RNA folding during complex formulation. *Nature 380*: 646-650.

Arciga-Reyes L., Wootton L., Kieffer M., Davies B. (2006). UPF1 is required for nonsense-mediated mRNA decay (NMD) and RNAi in Arabidopsis. *Plant J 47*: 480-489.

Bartels F.W., McIntosh M., Fuhrmann A., Metzendorf C., Plattner P., Sewald N., Anselmetti D., Ros R., Becker A. (2007). Effector-stimulated single molecule protein-DNA interactions of a quorum-sensing system in Sinorhizobium meliloti. *Biophys J 92*: 4391-4400.

Binnig G., Quate C.F., Gerber C. (1986). Atomic force microscope. *Phys Rev Lett 56*: 930-933.

Boelens W., Scherly D., Jansen E.J., Kolen K., Mattaj I.W., van Venrooij W.J. (1991). Analysis of in vitro binding of U1-A protein mutants to U1 snRNA. *Nucleic Acids Res 19*: 4611-4618.

Buvoli M., Cobianchi F., Biamonti G., Riva S. (1990). Recombinant hnRNP protein A1 and its N-terminal domain show preferential affinity for oligodeoxynucleotides homologous to intron/exon acceptor sites. *Nucleic Acids Res 18*: 6595-6600.

Cao S., Jiang L., Song S., Jing R., Xu G. (2006). AtGRP7 is involved in the regulation of abscisic acid and stress responses in *Arabidopsis*. *Cell Mol Biol Lett 11*: 526-535.

Carpenter C.D., Kreps J.A., Simon A.E. (1994). Genes encoding glycine-rich Arabidopsis thaliana proteins with RNA-binding motifs are influenced by cold treatment and an endogenous circadian rhythm. *Plant Physiol 104*: 1015-1025.

Chang Y.F., Imam J.S., Wilkinson M.F. (2007). The Nonsense-Mediated Decay RNA Surveillance Pathway. *Annu Rev Biochem 76*: 51-74.

Cyran S.A., Buchsbaum A.M., Reddy K.L., Lin M.C., Glossop N.R., Hardin P.E., Young M.W., Storti R.V., Blau J. (2003). vrille, Pdp1, and dClock Form a SEcond Feedback Loop in the Drosophila Circadian Clock. *Cell 112*: 329-341.

Czechowski T., Stitt M., Altmann T., Udvardi M.K., Scheible W.R. (2005). Genome-wide identification and testing of superior reference genes for transcript normalization in Arabidopsis. *Plant Physiol 139*: 5-17.

Daniel X., Sugano S., Tobin E.M. (2004). CK2 phosphorylation of CCA1 is necessary for its circadian oscillator function in Arabidopsis. *Proc Natl Acad Sci USA 101*: 3292-3297.

Darlington T.K., Wager-Smith K., Ceriani M.F., Staknis D., Gekakis N., Steeves T.D., Weitz C.J., Takahashi J.S., Kay S.A. (1998). Closing the circadian loop: CLOCK-induced transcription of its own inhibitors per and *tim*. *Science 280*: 1599-1603.

de Candolle A.P. (1832). Physiologie Végétale. *Paris*.

de Mairan J. (1729). Observation Botanique. *Hist Acad Roy Sci*: 35-36.

Deo R.C., Bonanno J.B., Sonenberg N., Burley S.K. (1999). Recognition of polyadenylate RNA by the poly(A)-binding protein. *Cell 98*: 835-845.

Ding J., Hayashi M.K., Zhang Y., Manche L., Krainer A.R., Xu R.M. (1999). Crystal structure of the two-RRM domain of hnRNP A1 (UP1) complexed with single-stranded telomeric DNA. *Genes Dev 13*: 1102-1115.

Dodd A.N., Salathia N., Hall A., Kevei E., Toth R., Nagy F., Hibberd J.M., Millar A.J., Webb A.A. (2005). Plant circadian clocks increase photosynthesis, growth, survival, and competitive advantage. *Science 309*: 630-633.

Dresios J., Aschrafi A., Owens G.C., Vanderklish P.W., Edelman G.M., Mauro V.P. (2005). Cold stress-induced protein Rbm3 binds 60S ribosomal subunits, alters microRNA levels, and enhances global protein synthesis. *Proc Natl Acad Sci USA 102*: 1865-1870.

Dunlap J.C., Loros J.J. (2004). The neurospora circadian system. *J Biol Rhythms 19*: 414-424.

Esen A. (1978). A simple method for quantitative, semiquantitative, and qualitative assay of protein. *Anal Biochem 89*: 264-273.

Farré E.M., Harmer S.L., Harmon F.G., Yanovsky M.J., Kay S.A. (2005). Overlapping and Distinct Roles of PRR7 and PRR9 in the Arabidopsis Circadian Clock. *Curr Biol 15*: 47-54.

Fu Z.Q., Guo M., Jeong B.R., Tian F., Elthon T.E., Cerny R.L., Staiger D., Alfano J.R. (2007). A type III effector ADP-ribosylates RNA-binding proteins and quells plant immunity. *Nature 447*: 284-288.

Gallie D.R., Sleat D.E., Watts J.W., Turner P.C., Wilson T.M. (1987). The 5'-leader sequence of tobacco mosaic virus RNA enhances the expression of foreign gene transcripts in vitro and in vivo. *Nucleic Acids Res 15*: 3257-3273.

Glossop N.R., Houl J.H., Zheng H., Ng F.S., Dudek S.M., P.E. H. (2003). VRILLE Feeds Back to Control Circadian Transcription of Clock in the Drosophila Circadian Oscillator. *Neuron 37*: 249-261.

Glossop N.R., Lyons L.C., Hardin P.E. (1999). Interlocked feedback loops within the *Drosophila* circadian oscillator. *Science 286*: 766-768.

Golden S.S., Canales S.R. (2003). Cyanobacterial circadian clocks--timing is everything. *Nat Rev Microbiol 1*: 191-199.

Goodrich J.A., Kugel J.F. (2007). *Binding and Kinetics for Molecular Biologists*. Cold Spring Harbor Laboratory Press, Cold Spring Harbor, New York.

Guan Q., Zheng W., Tang S., Liu X., Zinkel R.A., Tsui K.W., Yandell B.S., Culbertson M.R. (2006). Impact of nonsense-mediated mRNA decay on the global expression profile of budding yeast. *PLoS Genet 2*: e203.

Handa N., Kurimoto K., Kim I., Sakoamoto H., Shimura Y., Muto Y., Yokoyama S. (1999). Structural basis for recognition of the tra mRNA precursor by the Sex-lethal protein. *Nature 398*: 579-584.

Hardin P.E. (2005). The circadian timekeeping system of Drosophila. *Curr Biol 15*: R714-722.

Hardin P.E., Hall J.C., Rosbash M. (1990). Feedback of the *Drosophila period* gene product on circadian cycling of its messenger RNA levels. *Nature 343*: 536-540.

Harms E., Kivimae S., Young M.W., Saez L. (2004). Posttranscriptional and posttranslational regulation of clock genes. *J Biol Rhythms 19*: 361-373.

Hastings M.L., Krainer A.R. (2001). Pre-mRNA splicing in the new millennium. *Curr Opin Cell Biol 13*: 302-309.

He F., Li X., Spatrick P., Casillo R., Dong S., Jacobson A. (2003). Genome-wide analysis of mRNAs regulated by the nonsense-mediated and 5' to 3' mRNA decay pathways in yeast. *Mol Cell 12*: 1439-1452.

Heintzen C., Melzer S., Fischer R., Kappeler S., Apel K., Staiger D. (1994). A light- and temperature-entrained circadian clock controls expression of transcripts encoding nuclear proteins with homology to RNA-binding proteins in meristematic tissue. *Plant J 5*: 799-813.

Heintzen C., Nater M., Apel K., Staiger D. (1997). *At*GRP7, a nuclear RNA-binding protein as a component of a circadian-regulated negative feedback loop in *Arabidopsis thaliana*. *Proc Natl Acad Sci USA 94*: 8515 - 8520.

Hess S.T., Huang S., Heikal A.A., Webb W.W. (2002). Biological and chemical applications of fluorescence correlation spectroscopy: a review. *Biochemistry 41*: 697-705.

Hirose T., Sugita M., Sugiura M. (1993). cDNA structure, expression and nucleic acid-binding properties of three RNA-binding proteins in tobacco: occurrence of tissue-specific alternative splicing. *Nucleic Acids Res 21*: 3981-3987.

Hori K., Watanabe Y. (2005). UPF3 suppresses aberrant spliced mRNA in *Arabidopsis*. *Plant J 43*: 530-540.

Huang Y., Genova G., Roberts M., Jackson F.R. (2007). The LARK RNA-Binding Protein Selectively Regulates the Circadian Eclosion Rhythm by Controlling E74 Protein Expression. *PLoS ONE 2*: e1107.

Jessen T.H., Oubridge C., Teo C.-H., Pritchard C., Nagai K. (1991). Identification of molecular contacts between the U1 A small nuclear ribonucleoprotein and U1 RNA. *EMBO J 10*: 3447-3456.

Jumaa H., Nielsen P.J. (1997). The splicing factor SRp20 modifies splicing of its own mRNA and ASF/SF2 antagonizes this regulation. *Embo J 16*: 5077-5085.

Katsamba P.S., Bayramyan M., Haworth I.S., Myszka D.G., Laird-Offringa I.A. (2002). Complex role of the beta 2-beta 3 loop in the interaction of U1A with U1 hairpin II RNA. *J Biol Chem 277*: 33267-33274.

Katsamba P.S., Myszka D.G., Laird-Offringa I.A. (2001). Two functionally distinct steps mediate high affinity binding of U1A protein to U1 hairpin II RNA. *J Biol Chem 276*: 21476-21481.

Keene J.D. (2001). Ribonucleoprotein infrastructure regulating the flow of genetic information between the genome and the proteome. *Proc Natl Acad Sci USA 98*: 7018-7024.

Kertesz S., Kerenyi Z., Merai Z., Bartos I., Palfy T., Barta E., Silhavy D. (2006). Both introns and long 3'-UTRs operate as cis-acting elements to trigger nonsense-mediated decay in plants. *Nucleic Acids Res 34*: 6147-6157.

Kim J., Doose S., Neuweiler H., Sauer M. (2006). The initial step of DNA hairpin folding: a kinetic analysis using fluorescence correlation spectroscopy. *Nucleic Acids Res 34*: 2516-2527.

Kim W.-Y., Fujiwara S., Suh S.-S., Kim J., Kim Y., Han L., David K., Putterill J., Nam H.G., Somers D.E. (2007). ZEITLUPE is a circadian photoreceptor stabilized by GIGANTEA in blue light. *Nature 449*: 356-360.

Kim W.Y., Geng R., Somers D.E. (2003). Circadian phase-specific degradation of the f-box protein ztl is mediated by the proteasome. *Proc Natl Acad Sci USA 100*: 4933 - 4938.

Kinjo M., Rigler R. (1995). Ultrasensitive hybridization analysis using fluorescence correlation spectroscopy. *Nucleic Acids Res 23*: 1795-1799.

Knippers R. (2001). *Molekulare Genetik*. Georg Thieme Verlag, Stuttgart.

Kojima S., Matsumoto K., Hirose M., Shimada M., Nagano M., Shigeyoshi Y., Hoshino S., Ui-Tei K., Saigo K., Green C.B., Sakaki Y., Tei H. (2007). LARK activates posttranscriptional expression of an essential mammalian clock protein, PERIOD1. *Proc Natl Acad Sci USA 104*: 1859-1864.

Konopka R.J., Benzer S. (1971). Clock mutants of *Drosophila melanogaster*. *Proc Natl Acad Sci USA 68*: 2112-2116.

Laemmli U.K. (1970). Cleavage of structural proteins during the assembly of the head of bacteriophage T4. *Nature 227*: 680-685.

Law M.J., Chambers E.J., Katsamba P.S., Haworth I.S., Laird-Offringa I.A. (2005). Kinetic analysis of the role of the tyrosine 13, phenylalanine 56 and glutamine 54 network in the U1A/U1 hairpin II interaction. *Nucleic Acids Res 33*: 2917-2928.

Law M.J., Linde M.E., Chambers E.J., Oubridge C., Katsamba P.S., Nilsson L., Haworth I.S., Laird-Offringa I.A. (2006a). The role of positively charged amino acids and electrostatic interactions in the complex of U1A protein and U1 hairpin II RNA. *Nucleic Acids Res 34*: 275-285.

Law M.J., Rice A.J., Lin P., Laird-Offringa I.A. (2006b). The role of RNA structure in the interaction of U1A protein with U1 hairpin II RNA. *RNA 12*: 1168-1178.

Lee A.L., Volkman B.F., Robertson S.A., Rudner D.Z., Barbash D.A., Cline T.W., Kanaar R., Rio D.C., Wemmer D.E. (1997). Chemical shift mapping of the RNA-binding interface of the multiple-RBD protein sex-lethal. *Biochemistry 36*: 14306-14317.

Li H., Ren X., Ying L., Balasubramanian S., Klenerman D. (2004). Measuring single-molecule nucleic acid dynamics in solution by two-color filtered ratiometric fluorescence correlation spectroscopy. *Proc Natl Acad Sci USA 101*: 14425-14430.

Lin F.J., Song W., Meyer-Bernstein E., Naidoo N., Sehgal A. (2001). Photic signaling by cryptochrome in the Drosophila circadian system. *Mol Cell Biol 21*: 7287-7294.

Locke J.C., Millar A.J., Turner M.S. (2005a). Modelling genetic networks with noisy and varied experimental data: the circadian clock in *Arabidopsis thaliana*. *J Theor Biol 234*: 383-393.

Locke J.C., Southern M.M., Kozma-Bognar L., Hibberd V., Brown P.E., Turner M.S., Millar A.J. (2005b). Extension of a genetic network model by iterative experimentation and mathematical analysis. *Molecular Systems Biology 1*: E1-E9.

Lopato S., Kalyna M., Dorner S., Kobayashi R., Krainer A.R., Barta A. (1999). atSRp30, one of two SF2/ASF-like proteins from *Arabidopsis thaliana*, regulates splicing of specific plant genes. *Genes Dev 13*: 987-1001.

Lorkovic Z.J., Barta A. (2002). Genome analysis: RNA recognition motif (RRM) and K homology (KH) domain RNA-binding proteins from the flowering plant *Arabidopsis thaliana*. *Nucleic Acids Res 30*: 623-635.

Lund O., Nielsen M., Lundegaard C., Worning P. (2002). CPHmodels 2.0: X3M a Computer Program to Extract 3D Models. *CASP5 conference A102*.

Lutz-Freyermuth C., Query C.C., Keene J.D. (1990). Quantitative determination that one of two potential RNA-binding domains of the A protein component of the U1 small nuclear ribonucleoprotein complex binds with high affinity to stem-loop II of U1 RNA. *Proc Natl Acad Sci USA 87*: 6393-6397.

Madge D. (1976). Chemical kinetics and fluorescence correlation spectroscopy. *Quarterly reviews of biophysics 9*: 35-47.

Maquat L.E. (2002). Nonsense-mediated mRNA decay. *Curr Biol 12*: R196-197.

Marchand V., Mougin A., Méreau A., Branlant C. (2005). Study of RNA-Protein Interactions and RNA Structure in Ribonucleoprotein Particles. In: Hartmann RK, Bindereif A, Schön A, Westhof E, eds. *Handbook of RNA Biochemistry*: pp 172-204. WILEY-VCH, Weinheim.

Margeat E., Poujol N., Boulahtouf A., Chen Y., Muller J.D., Gratton E., Cavailles V., Royer C.A. (2001). The human estrogen receptor alpha dimer binds a single SRC-1 coactivator molecule with an affinity dictated by agonist structure. *J Mol Biol 306*: 433-442.

Maris C., Dominguez C., Allain F.H. (2005). The RNA recognition motif, a plastic RNA-binding platform to regulate post-transcriptional gene expression. *FEBS J 272*: 2118-2131.

Martin-Tryon E.L., Kreps J.A., Harmer S.L. (2006). GIGANTEA acts in blue light signaling and has biochemically separable roles in circadian clock and flowering time regulation. *Plant Physiol 143*: 473-486.

Más P., Kim W.Y., Somers D.E., Kay S.A. (2003). Targeted degradation of TOC1 by ZTL modulates circadian function in Arabidopsis thaliana. *Nature 426*: 567-570.

Mata J., Marguerat S., Bahler J. (2005). Post-transcriptional control of gene expression: a genome-wide perspective. *Trends Biochem Sci 30*: 506-514.

Matsumoto A., Ukai-Tadenuma M., Yamada R.G., Houl J., Uno K.D., Kasukawa T., Dauwalder B., Itoh T.Q., Takahashi K., Ueda R., Hardin P.E., Tanimura T., Ueda H.R. (2007). A functional genomics strategy reveals clockwork orange as a transcriptional regulator in the Drosophila circadian clock. *Genes Dev 21*: 1687-1700.

Matsumoto K., Aoki K., Dohmae N., Takio K., Tsujimoto M. (2000). CIRP2, a major cytoplasmic RNA-binding protein in Xenopus oocytes. *Nucleic Acids Res 28*: 4689-4697.

McClung C.R. (2006). Plant circadian rhythms. *Plant Cell 18*: 792-803.

McNeil G.P., Zhang X., Genova G., Jackson F.R. (1998). A molecular rhythm mediating circadian clock output in *Drosophila*. *Neuron 20*: 297-303.

Meyer P., Saez L., Young M.W. (2006). PER-TIM interactions in living Drosophila cells: an interval timer for the circadian clock. *Science 311*: 226-229.

Michael T.P., McClung C.R. (2002). Phase-specific circadian clock regulatory elements in *Arabidopsis*. *Plant Physiol 130*: 627-638.

Millar A.J., Carré I.A., Strayer C.S., Chua N.-H., Kay S. (1995). Circadian clock mutants in *Arabidopsis* identified by luciferase imaging. *Science 267*: 1161-1163.

Mitrovich Q.M., Anderson P. (2000). Unproductively spliced ribosomal protein mRNAs are natural targets of mRNA surveillance in C. elegans. *Genes Dev 14*: 2173-2184.

Morgenstern B. (2004). DIALIGN: multiple DNA and protein sequence alignment at BiBiServ. *Nucleic Acids Res 32*: W33-36.

Morikis D., Lambris J.D. (2004). Physical methods for structure, dynamics and binding in immunological research. *Trends in immunology 25*: 700-707.

Murashige T., Skoog F. (1962). A revised medium for rapid growth and bio assays with tobacco tissue cultures. *Physiologia plantarum 15*: 473-497.

Nagai K., Oubridge C., Jessen T.H., Li J., Evans P.R. (1990). Crystal structure of the RNA-binding domain of the U1 small nuclear ribonucleoprotein A. *Nature 348*: 515-520.

Nakamichi N., Kita M., Ito S., Yamashino T., Mizuno T. (2005). Pseudo-Response Regulators, PRR9, PRR7, and PRR5, Play Together Essential Roles Close to the Circadian Clock of Arabidopsis thaliana. *Plant Cell Physiology 46*.

Nawathean P., Rosbash M. (2004). The doubletime and CKII kinases collaborate to potentiate Drosophila PER transcriptional repressor activity. *Mol Cell 13*: 213-223.

Neuweiler H., Doose S., Sauer M. (2005). A microscopic view of miniprotein folding: enhanced folding efficiency through formation of an intermediate. *Proc Natl Acad Sci USA 102*: 16650-16655.

Neuweiler H., Sauer M. (2005). Exploring life by single-molecule fluorescence spectroscopy. Molecular characteristics hidden by ensemble experiments can be revealed by fluorescence. *Anal Chem 77*: 179A-185A.

Newby L.M., Jackson F.R. (1996). Regulation of a specific circadian clock output pathway by lark, a putative RNA-binding protein with repressor activity. *J Neurobiol 31*: 117-128.

Niranjanakumari S., Lasda E., Brazas R., Garcia-Blanco M.A. (2002). Reversible cross-linking combined with immunoprecipitation to study RNA-protein interactions in vivo. *Methods 26*: 182-190.

Oubridge C., Ito N., Evans P.R., Teo C.-H., Nagai K. (1994). Crystal structure at 1.92 A resolution of the RNA-binding domain of the U1A spiceosomal protein complexed with an RNA hairpin. *Nature 372*: 432-438.

Pedersen J.S., Meyer I.M., Forsberg R., Simmonds P., Hein J. (2004). A comparative method for finding and folding RNA secondary structures within protein-coding regions. *Nucleic Acids Res 32*: 4925-4936.

Piehler J. (2005). New methodologies for measuring protein interactions in vivo and in vitro. *Curr Opin Struct Biol 15*: 4-14.

Price J.L., Blau J., Rothenfluh A., Abodeely M., Kloss B., Young M.W. (1998a). *double-time* is a novel *Drosophila* clock gene that regulates PERIOD protein accumulation. *Cell 94*: 83-95.

Price S.R., Evans P.R., Nagai K. (1998b). Crystal structure of the spliceosomal U2B"-U2A' protein complex bound to a fragment of U2 small nuclear RNA. *Nature 394*: 645-650.

Reddy P., Zehring W.A., Wheeler D.A., Pirrotta V., Hadfield C., Hall J.C., Rosbash M. (1984). Molecular analysis of the *period* locus in *Drosophila melanogaster* and identification of a transcript involved in biological rhythms. *Cell 38*: 701-710.

Rehwinkel J., Raes J., Izaurralde E. (2006). Nonsense-mediated mRNA decay: Target genes and functional diversification of effectors. *Trends Biochem Sci 31*: 639-646.

Rhee S.Y., Beavis W., Berardini T.Z., Chen G., Dixon D., Doyle A., Garcia-Hernandez M., Huala E., Lander G., Montoya M., Miller N., Mueller L.A., Mundodi S., Reiser L., Tacklind J., Weems D.C., Wu Y., Xu I., Yoo D., Yoon J., Zhang P. (2003). The Arabidopsis Information Resource (TAIR): a model organism database providing a centralized, curated gateway to Arabidopsis biology, research materials and community. *Nucleic Acids Res 31*: 224-228.

Roenneberg T., Merrow M. (2003). The network of time: understanding the molecular circadian system. *Curr Biol 13*: R198-207.

Ros R., Eckel R., Bartels F., Sischka A., Baumgarth B., Wilking S.D., Puhler A., Sewald N., Becker A., Anselmetti D. (2004). Single molecule force spectroscopy on ligand-DNA complexes: from molecular binding mechanisms to biosensor applications. *J Biotechnol 112*: 5-12.

Rudolf F., Wehrle F., Staiger D. (2004). Slave to the rhythm. *The Biochemist 26*: 11-13.

Rutila J.E., Suri V., Le M., So W.V., Rosbash M., Hall J.C. (1998). *CYCLE* is a second *bHLH-PAS* clock protein essential for circadian rhythmicity and transcription of *Drosophila period* and *timeless*. *Cell 93*: 805-814.

Ryner L.C., Baker B.S. (1991). Regulation of doublesex pre-mRNA processing occurs by 3'-splice site activation. *Genes Dev 5*: 2071-2085.

Sachetto-Martins G., Franco L.O., de Oliveira D.E. (2000). Plant glycine-rich proteins: a family or just proteins with a common motif? *Biochim Biophys Acta 1492*: 1-14.

Salome P.A., McClung C.R. (2004). The Arabidopsis thaliana clock. *J Biol Rhythms 19*: 425-435.

Sambrook J., Russel D.W. (2001). *Molecular Cloning: A Laboratory Manual*. Cold Spring Harbor Laboratory Press, Cold Spring Harbor, New York.

Samuels M.E., Bopp D., Colvin R.A., Roscigno R.F., Garcia-Blanco M.A., Schedl P. (1994). RNA binding by Sxl proteins in vitro and in vivo. *Mol Cell Biol 14*: 4975-4990.

Schaffer R., Ramsay N., Samach A., Putterill J., Carre I.A., Coupland G. (1998). The late elongated hypocotyl mutation of *Arabidopsis* disrupts circadian rhythms and the photoperiodic control of flowering. *Cell 93*: 1219-1229.

Scherly D., Boelens W., Dathan N.A., van Venrooij W.J., Mattaj I.W. (1990). Major determinants of the specificity of interaction between small nuclear ribonucleoproteins U1A and U2B" and their cognate RNAs. *Nature 345*: 502-506.

Schöning J.C., Staiger D. (2005). At the pulse of time: protein interactions determine the pace of circadian clocks. *FEBS Lett 579*: 3246-3252.

Schöning J.C., Staiger D. (2006). Being in time: the importance of posttranslational processes in circadian clocks. *BIO TECH international 18*: 12-15.

Schöning J.C., Streitner C., Page D.R., Hennig S., Uchida K., Wolf E., Furuya M., Staiger D. (2007). Autoregulation of the circadian slave oscillator component *At*GRP7 and regulation of its targets is impaired by a single RNA recognition motif point mutation. *Plant J 52*: 1119-1130.

Schöning J.C., Streitner C., Staiger D. (2006). Clockwork Green - the circadian oscillator in *Arabidopsis*. *Biological Rhythm Research 37*: 335-352.

Schuler J., Frank J., Trier U., Schafer-Korting M., Saenger W. (1999). Interaction kinetics of tetramethylrhodamine transferrin with human transferrin receptor studied by fluorescence correlation spectroscopy. *Biochemistry 38*: 8402-8408.

Sehgal A., Price J.L., Man B., Young M.W. (1994). Loss of circadian behavioral rhythms and *per* RNA oscillations in the *Drosophila* mutant *timeless*. *Science 263*: 1603-1606.

Siomi H., Dreyfuss G. (1997). RNA-binding proteins as regulators of gene expression. *Curr Opin Genet Dev 7*: 345-353.

Smart F., Aschrafi A., Atkins A., Owens G.C., Pilotte J., Cunningham B.A., Vanderklish P.W. (2007). Two isoforms of the cold-inducible mRNA-binding protein RBM3 localize to dendrites and promote translation. *J Neurochem 101*: 1367-1379.

Somers D.E., Schultz T.F., Milnamow M., Kay S.A. (2000). ZEITLUPE encodes a novel clock-associated PAS protein from Arabidopsis. *Cell 101*: 319-329.

Staiger D., Apel K. (1999). Circadian clock-regulated expression of an RNA-binding protein in Arabidopsis: characterisation of a minimal promoter element. *Mol Gen Genet 261*: 811-819.

Staiger D., Heintzen C. (1999). The circadian system of Arabidopsis thaliana: forward and reverse genetic approaches. *Chronobiol Int 16*: 1-16.

Staiger D., Streitner C., Rudolf F., Huang X. (2006). Multiple and slave oscillators. In: Hall A, McWatters H, eds. *Endogenous plant rhythms*: pp 57-83. Blackwell Publishers.

Staiger D., Zecca L., Wieczorek Kirk D.A., Apel K., Eckstein L. (2003). The circadian clock regulated RNA-binding protein AtGRP7 autoregulates its expression by influencing alternative splicing of its own pre-mRNA. *Plant J 33*: 361-371.

Steffen P., Voss B., Rehmsmeier M., Reeder J., Giegerich R. (2006). RNAshapes: an integrated RNA analysis package based on abstract shapes. *Bioinformatics 22*: 500-503.

Steitz T.A. (1990). Structural studies of protein-nucleic acid interaction: the sources of sequence-specific binding. *Quarterly reviews of biophysics 23*: 205-280.

Stitzinger S.M., Conrad T.R., Zachlin A.M., Salz H.K. (1999). Functional analysis of SNF, the Drosophila U1A/U2B" homolog: identification of dispensable and indispensable motifs for both snRNP assembly and function in vivo. *RNA 5*: 1440-1450.

Strayer C., Oyama T., Schultz T.F., Raman R., Somers D.E., Mas P., Panda S., Kreps J.A., Kay S.A. (2000). Cloning of the Arabidopsis clock gene TOC1, an autoregulatory response regulator homolog. *Science 289*: 768-771.

Sugano S., Andronis C., Green R.M., Wang Z.-Y., Tobin E.M. (1998). Protein kinase CK2 interacts with and phosphorylates the *Arabidopsis* circadian clock-associated gene 1 protein. *Proc Natl Acad Sci USA 95*: 11020-11025.

Sun L., Doxsee R.A., Harel E., Tobin E.M. (1993). CA-1, a novel phosphoprotein, interacts with the promoter of the cab140 gene in Arabidopsis and is undetectable in det1 mutant seedlings. *Plant Cell 5*: 109-121.

Sureau A., Gattoni R., Dooghe Y., Stévenin J., Soret J. (2001). SC35 autoregulates its expression by promoting splicing events that destabilize its mRNAs. *Embo J 20*: 1785-1796.

Suswam E.A., Li Y.Y., Mahtani H., King P.H. (2005). Novel DNA-binding properties of the RNA-binding protein TIAR. *Nucleic Acids Res 33*: 4507-4518.

Tang Y., Nilsson L. (1999). Molecular dynamics simulations of the complex between human U1A protein and hairpin II of U1 small nuclear RNA and of free RNA in solution. *Biophys J 77*: 1284-1305.

Tenenbaum S.A., Carson C.C., Lager P.J., Keene J.D. (2000). Identifying mRNA subsets in messenger ribonucleoprotein complexes by using cDNA arrays. *Proc Natl Acad Sci U S A 97*: 14085-14090.

Thompson J.D., Higgins D.G., Gibson T.J. (1994). CLUSTAL W: improving the sensitivity of progressive multiple sequence alignment through sequence weighting, position-specific gap penalties and weight matrix choice. *Nucleic Acids Res 22*: 4673-4680.

Töpfer R., Matzeit V., Gronenborn B., Schell J., Steinbiss H.H. (1987). A set plant expression vectors for transcriptional and translational fusions. *Nucl Acids Res 15*: 14.

van Nocker S., Vierstra R.D. (1993). Two cDNAs from Arabidopsis thaliana encode putative RNA binding proteins containing glycine-rich domains. *Plant Mol Biol 21*: 695-699.

Van Orden A., Jung J. (2007). Fluorescence correlation spectroscopy for probing the kinetics and mechanisms of DNA hairpin formation. *Biopolymers*.

Vosshall L.B., Price J.L., Sehgal A., Saez L., Young M.W. (1994). Block in nuclear localization of *period* protein by a second clock mutation, *timeless*. *Science 263*: 1606-1609.

Wallace M.I., Ying L., Balasubramanian S., Klenerman D. (2001). Non-Arrhenius kinetics for the loop closure of a DNA hairpin. *Proc Natl Acad Sci U S A 98*: 5584-5589.

Wang Z.Y., Tobin E.M. (1998). Constitutive expression of the CIRCADIAN CLOCK ASSOCIATED1 (CCA1) gene disrupts circadian rhythms and suppresses its own expression. *Cell 93*: 1207-1217.

Wijnen H., Naef F., Boothroyd C., Claridge-Chang A., Young M.W. (2006). Control of Daily Transcript Oscillations in Drosophila by Light and the Circadian Clock. *PLoS Genet 2*: e39.

Will C.L., Lührmann R. (2001). Spliceosomal UsnRNP biogenesis, structure and function. *Curr Opin Cell Biol 13*: 290-301.

Wohland T., Friedrich K., Hovius R., Vogel H. (1999). Study of ligand-receptor interactions by fluorescence correlation spectroscopy with different fluorophores: evidence that the homopentameric 5-hydroxytryptamine type 3As receptor binds only one ligand. *Biochemistry 38*: 8671-8681.

Wollerton M.C., Gooding C., Wagner E.J., Garcia-Blanco M.A., Smith C.W. (2004). Autoregulation of polypyrimidine tract binding protein by alternative splicing leading to nonsense-mediated decay. *Mol Cell 13*: 91-100.

Xu H., Frank J., Trier U., Hammer S., Schroder W., Behlke J., Schafer-Korting M., Holzwarth J.F., Saenger W. (2001). Interaction of fluorescence labeled single-stranded DNA with hexameric DNA-helicase RepA: a photon and fluorescence correlation spectroscopy study. *Biochemistry 40*: 7211-7218.

Ye G.N., Stone D., Pang S.Z., Creely W., Gonzalez K., Hinchee M. (1999). Arabidopsis ovule is the target for Agrobacterium in planta vacuum infiltration transformation. *Plant J 19*: 249 - 257.

Zheng S., Robertson T.A., Varani G. (2007). A knowledge-based potential function predicts the specificity and relative binding energy of RNA-binding proteins. *FEBS J 274*: 6378-6391.

Zuker M. (2003). Mfold web server for nucleic acid folding and hybridization prediction. *Nucleic Acids Res 31*: 3406-3415.

7 Publications and Abstracts

7.1 Research papers

Jan C. Schöning, Corinna Streitner, Damian R. Page, Sven Hennig, Kenko Uchida, Eva Wolf, Masaki Furuya, Dorothee Staiger (2007). Auto-regulation of the circadian slave oscillator component *At*GRP7 and regulation of its targets is impaired by a single RNA recognition motif point mutation. *The Plant Journal* 52: 1119-1130.

Mark Schüttpelz, **Jan C. Schöning**, Sören Doose, Hannes Neuweiler, Elisabeth Peters, Dorothee Staiger, Markus Sauer (2007). Changes of conformational dynamics of mRNA upon *At*GRP7 binding studied by fluorescence correlation spectroscopy. *Proceedings of the National Academy of Sciences, submitted.*

Corinna Streitner, Selahattin Danisman, Franziska Wehrle, **Jan C. Schöning**, Dorothee Staiger (2007). The small glycine-rich RNA-binding protein *At*GRP7 promotes floral transition in *Arabidopsis thaliana*. *In preparation.*

Jan C. Schöning, Yahong Gao, Corinna Streitner, Dorothee Staiger (2008). The RNA-binding proteins *At*GRP7 and *At*GRP8 form an interlocking feedback loop downstream of the *Arabidopsis thaliana* clock. *In preparation.*

Alexander Fuhrmann[1], **Jan C. Schöning[1]**, Dario Anselmetti, Dorothee Staiger, Robert Ros (2008). Identification of two distinct binding modes of the *At*GRP8 protein by atomic force microscopy based force spectroscopy. *In preparation.*

7.2 Invited reviews and book chapters

Jan C. Schöning, Dorothee Staiger (2007). RNA-protein interaction mediating post-transcriptional regulation in the circadian system. In: *Methods in Molecular Biology,* Thomas Pfannschmidt (ed.), Humana press, Totowa. *In press.*

Jan C. Schöning, Dorothee Staiger (2006). Being in time: the importance of posttranslational processes in circadian clocks. *BIO TECH international* 18(2): 12-15.

Jan C. Schöning, Corinna Streitner, Dorothee Staiger (2006). Clockwork green – the circadian oscillator in *Arabidopsis*. *Biological Rhythm Research* 37: 335-352.

Jan C. Schöning[2], Dorothee Staiger (2005). At the pulse of time: protein interactions determine the pace of circadian clocks. *FEBS Letters* 579: 3246–3252.

7.3 Selected conference abstracts

Jan C. Schöning, Alexander Fuhrmann, Corinna Streitner, Martina Lummer, Dario Anselmetti, Robert Ros, Dorothee Staiger (2007). The RNA-binding protein *At*GRP7 – molecular characterisation and RNA-binding properties. *FEBS Journal* 274 (S1): 87.

Alexander Fuhrmann, **Jan C. Schöning**, Rainer Eckel, Sebastian Getfert, Peter Reimann, Dario Anselmetti, Dorothee Staiger, Robert Ros (2007). Single molecule protein-RNA interactions. 2007 Biophysical Society Meeting Abstracts. *Biophysical Journal*, Supplement, 168a, Abstract, 784-Pos.

[1] Both authors contributed equally to this work.
[2] Corresponding author

8 Appendix

8.1 Constructs for recombinant expression of GST-fusion proteins

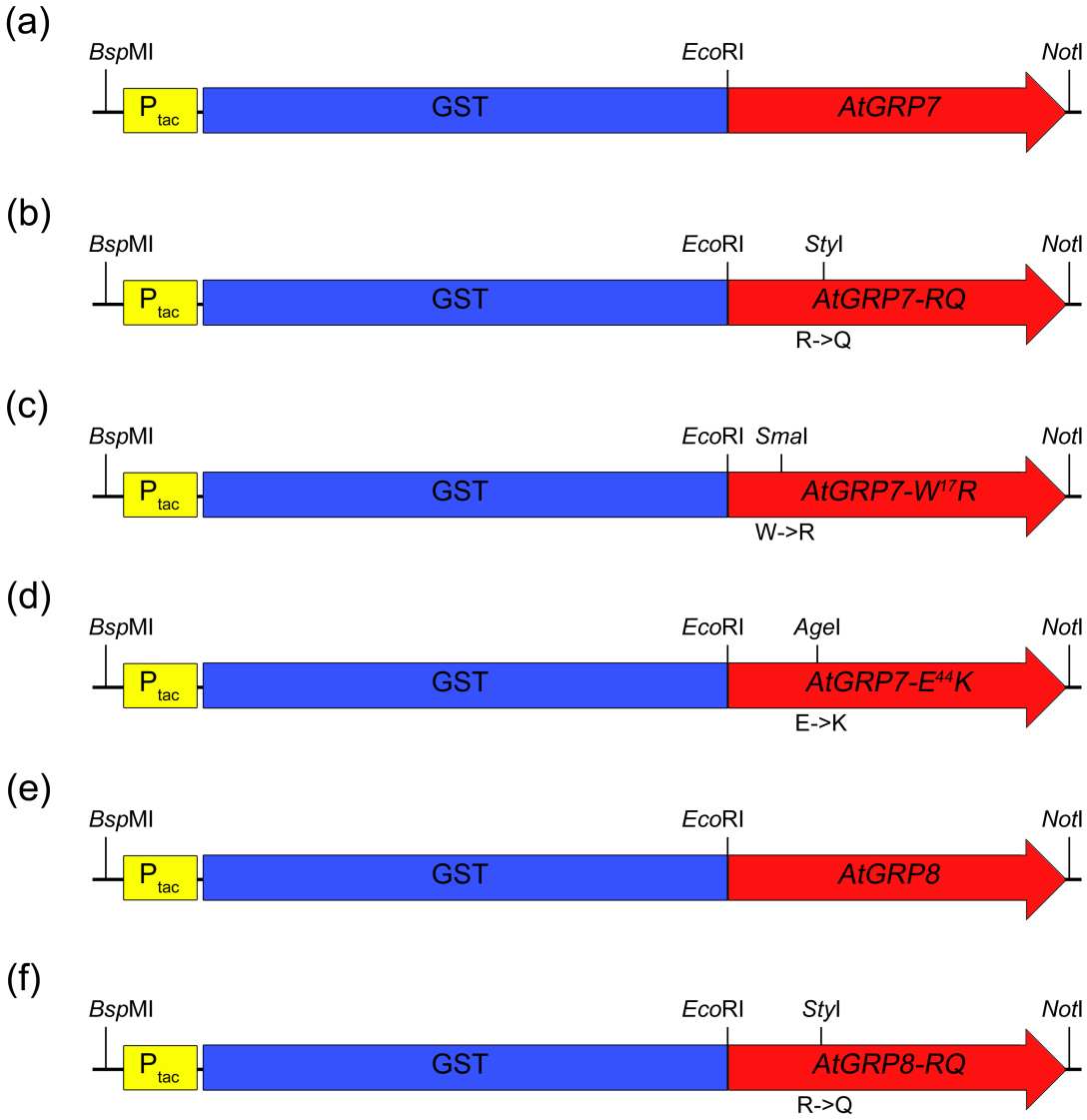

Figure 50: Constructs for the recombinant expression of *At*GRP7 and *At*GRP8 protein variants in *E. coli*. (a-f) Schematic view of the genetic structure of GST-*At*GRP7, -*At*GRP7-RQ, -*At*GRP7-$W^{17}R$, -*At*GRP7-$E^{44}K$, -*At*GRP8 and -*At*GRP-RQ expression vectors, respectively. The origin of replication, the ampicillin resistance gene and the $LacI^q$ encoding region are omitted. The constructs were either generated by the direct cloning of cDNA sequences into the pGEX-6P-1 plasmid (GE Healthcare, Freiburg, Germany) or by site directed mutagenesis PCR (see text). (Diagnostic) restriction sites and the introduced mutations are indicated.

8.2 Prediction of evolutionary conserved RNA secondary structures

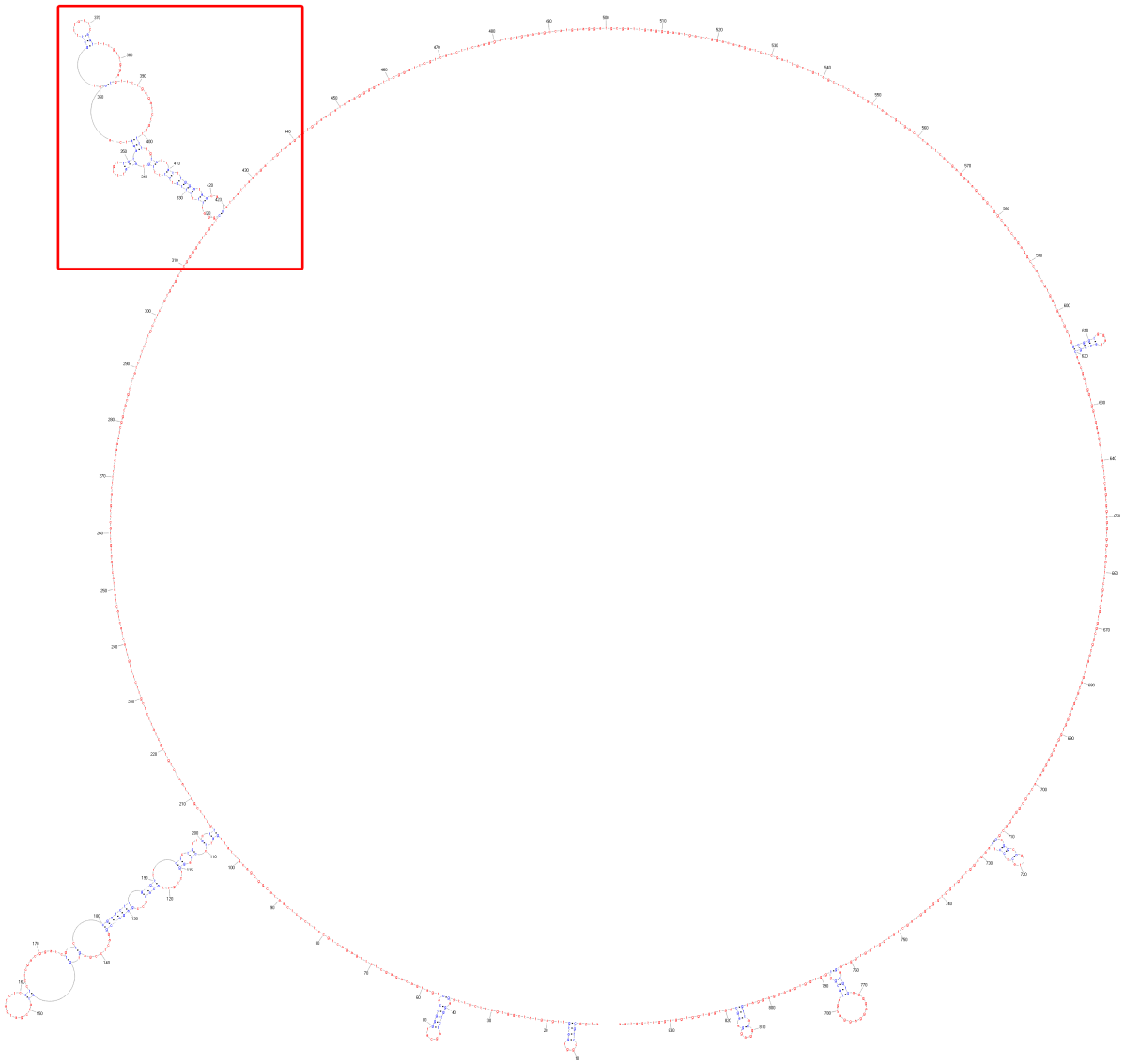

Figure 51: Conserved secondary structure elements of the *AtGRP7* pre-mRNA. Displayed is the sequence from the ATG to the STOP codon including the intronic sequence. A red box indicates the region enlarged in Figure 22.

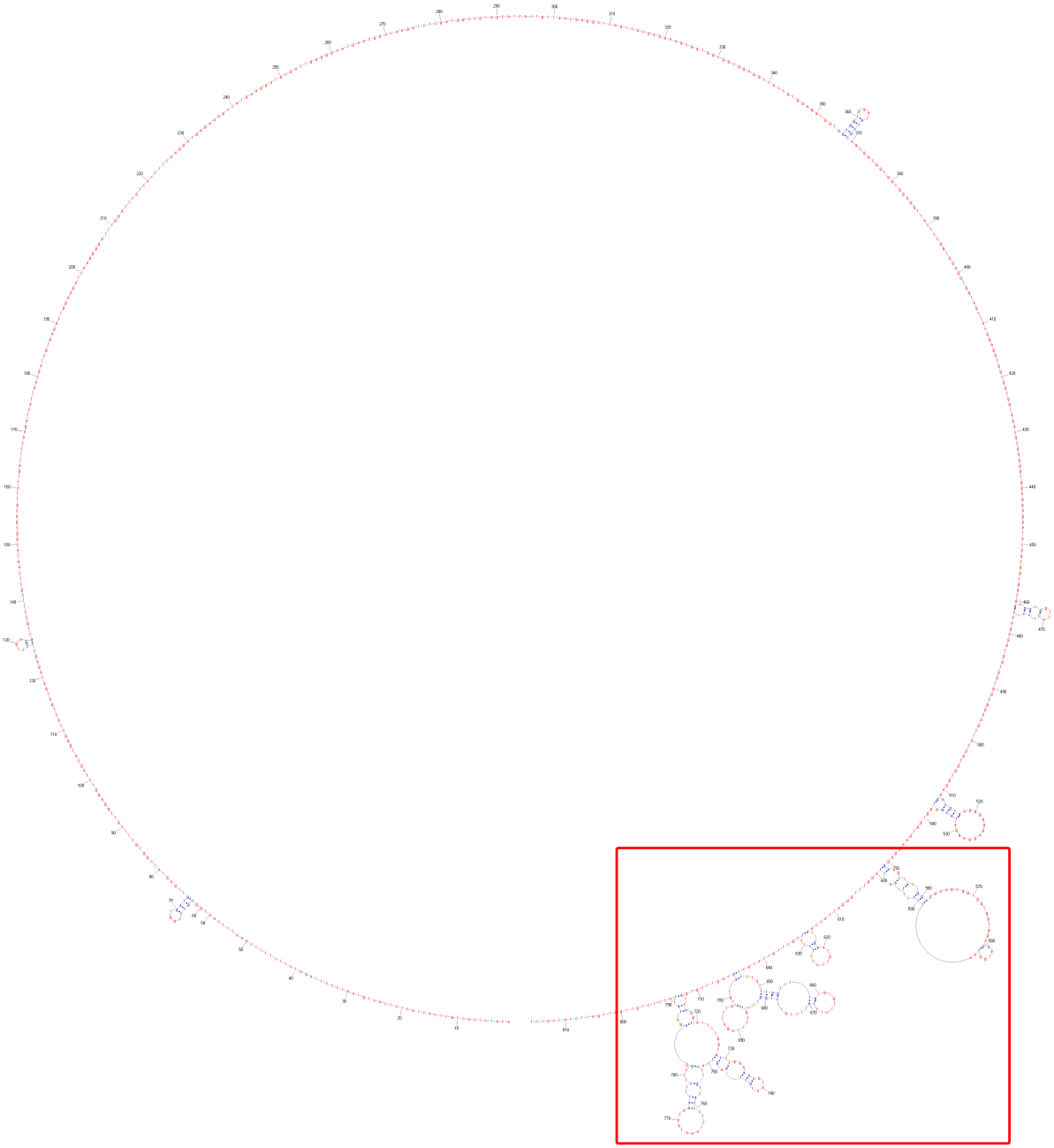

Figure 52: Conserved secondary structure elements of the *AtGRP7* mRNA. Displayed are the coding sequence and the 5' and 3' untranslated regions. A red box indicates the region enlarged in Figure 22.

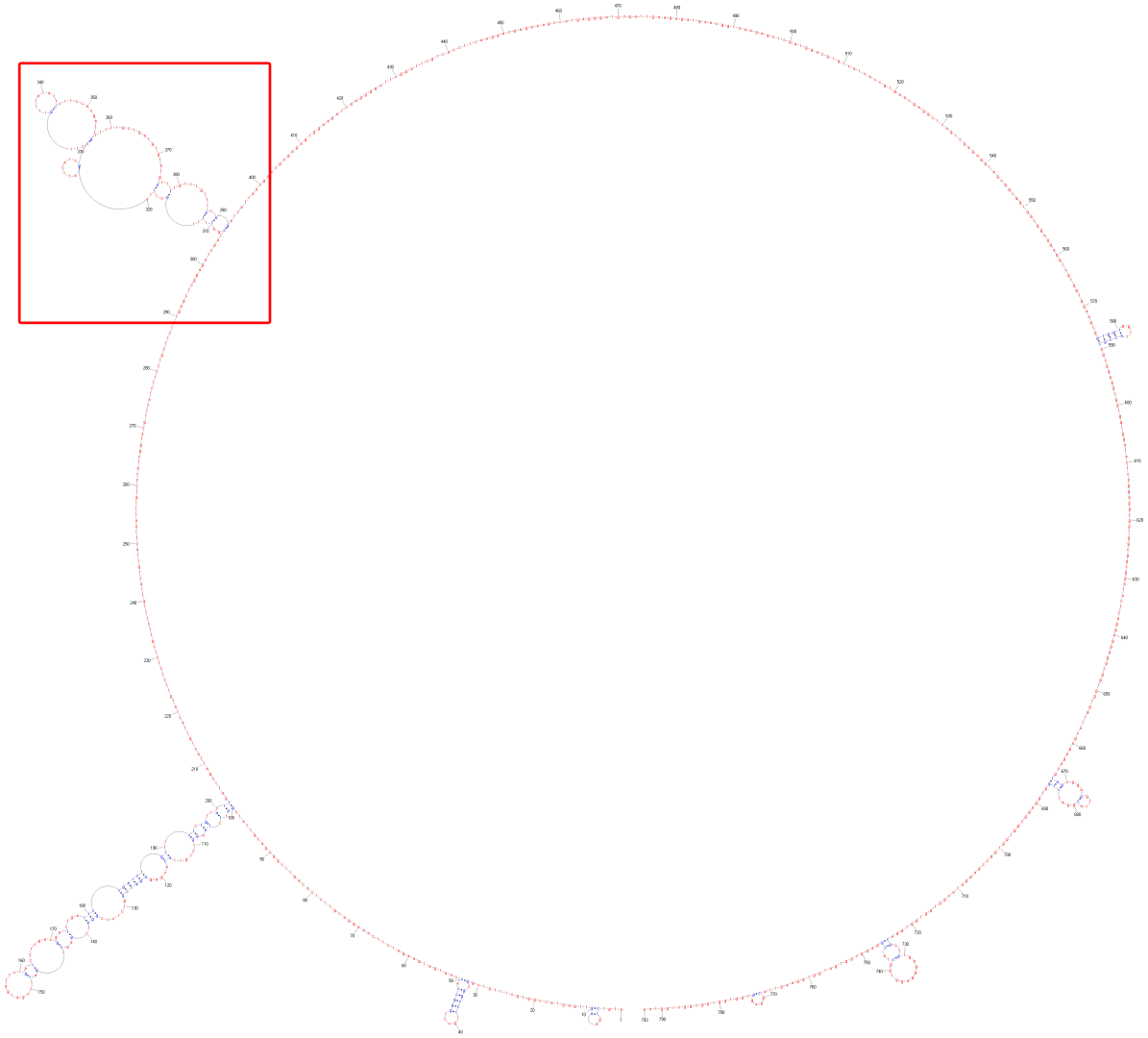

Figure 53: Conserved secondary structure elements of the *AtGRP8* pre-mRNA. Displayed is the sequence from the ATG to the STOP codon including the intronic sequence. A red box indicates the region enlarged in Figure 22.

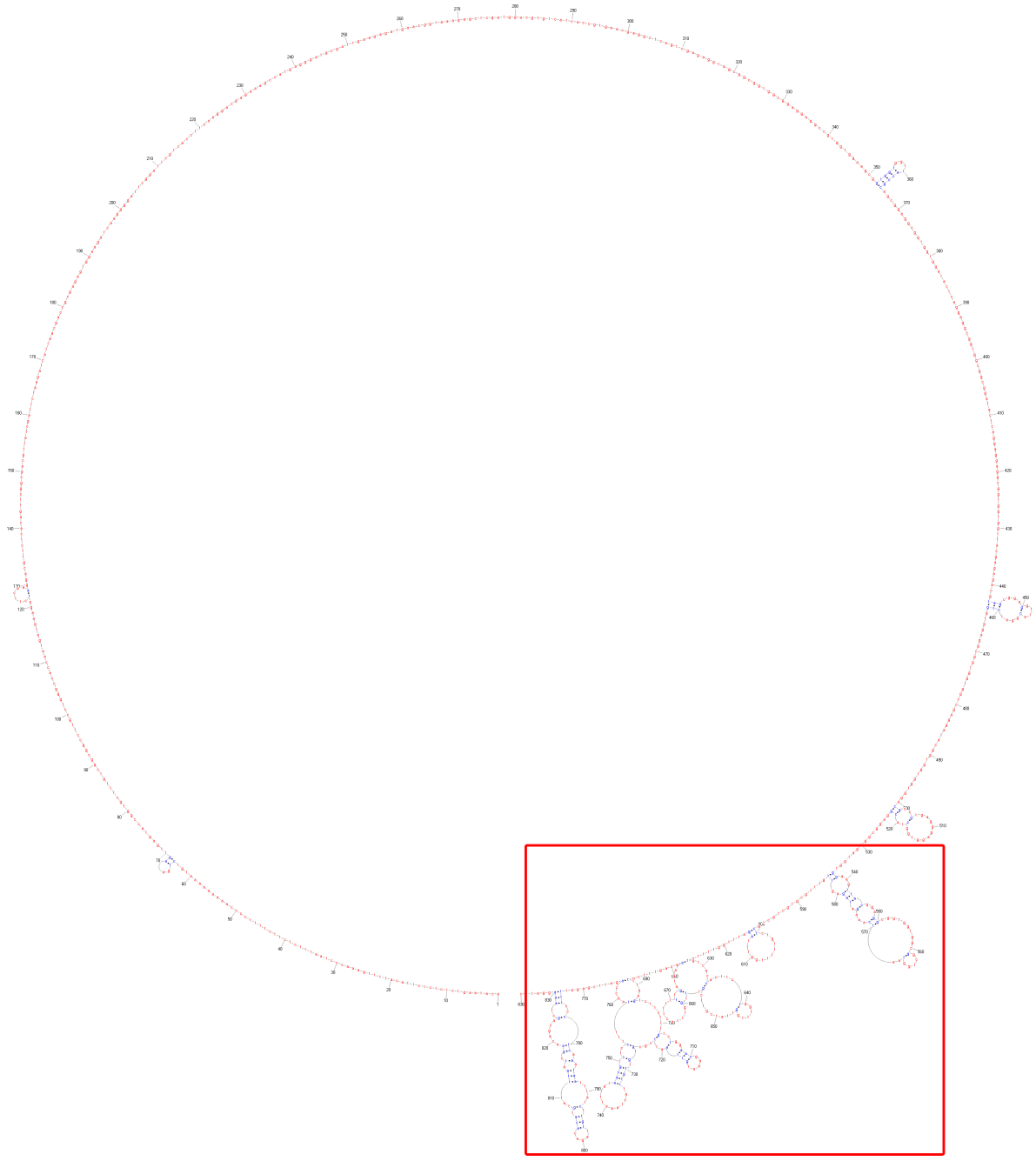

Figure 54: Conserved secondary structure elements of the *AtGRP8* mRNA. Displayed are the coding sequence and the 5' and 3' untranslated regions. A red box indicates the region enlarged in Figure 22.

8.3 Abbreviations

%	Percent
°C	Degree Celsius
AA	Amino acid
AFM	Atomic force microscopy
*At*GRP	*Arabidopsis thaliana* glycine-rich RNA-binding protein
AtGRP	gene / transcript of *Arabidopsis thaliana* glycine-rich RNA-binding protein
as_AtGRP	alternatively spliced *AtGRP* transcript
*At*GRP-ox	*At*GRP overexpressing
*At*GRP-RQ-ox	*At*GRP-RQ overexpressing
ATP	Adenosine-5'-triphosphate
BSA	Bovine Serum Albumin
CBS	CCA1 binding site
CD	Circular dichroism
Col	Columbia
dATP	2'-deoxy-adenosine-5'-triphosphate
DNA	Deoxyribonucleic acid
ds	Double-stranded
EDTA	Ethylendiaminetatraacetic Acid
EE	Evening element
EJC	Exon-junction complex
EMSA	Electrophoretic mobility shift assay
EtBR	Ethidium-bromide
FCS	Fluorescence correlation spectroscopy
FRET	Fluorescence resonance energy transfer
FS	Force spectroscopy
g	Gramme
GFP	Green fluorescent protein
GRP	Glycine-rich RNA-binding protein
GST	Glutathione-S-transferase
HPLC	High-performance liquid chromatography
HRP	Horse radish peroxidase
IPTG	Isopropyl β-D-1- thiogalactopyranoside
K_d	Equilibrium dissociation constant
L	Litre
LOV	Light-oxygen-voltage
M	Molar
mg	Milligramme
mL	Millilitre
mM	Millimolar

mol	Mole
µg	Microgramme
µL	Microlitre
µM	Micromolar
µm	Micrometer
µmol	Micromole
MS	Murashige & Skoog
nM	Nanomolar
nm	Nanometer
NMD	Nonsense-mediated decay
nmol	Nanomole
NMR	Nuclear magnetic resonance
NP40	Nonidet P40
nt	nucleotide(s)
OD_{600}	Optical density at 600 nanometer
ORN	Oligoribonucleotide
PAS	PER-ARNT-SIM
PBS	Phosphate-buffered saline
PCR	Polymerase chain reaction
PEG	Polyethylene Glycol
PET	Photoinduced electron transfer
PI	PhosphoImager
pmol	Picomole
pN	Piconewton
PTC	Premature termination codon
qRT-PCR	Quantitative RT-PCR
RBP	RNA-binding protein
RNA	Ribonucleic acid
RNP	Ribonucleoprotein
RRM	RNA recognition motif
RT-PCR	Reverse-transcribed PCR
RVC	Ribonucleoside Vanadyl Complex
s	Second
SDS	Sodium Dodecyl Sulfate
ss	Single-stranded
U1hpII	U1 snRNA hairpin II
UTR	Untranslated region
v/v	Volume per volume
w/v	Weight per volume
× g	Fold gravity
ZT	Zeitgeber time (hours after light on)

9 Danksagung

Nachdem der wissenschaftliche Teil dieser Arbeit nun abgehandelt ist, ist es an der Zeit, mich bei all den Menschen zu bedanken, die einen großen Anteil an dem Gelingen dieser Arbeit haben:

Zunächst möchte ich mich ganz herzlich bei Frau **Professorin Dr. Dorothee Staiger** bedanken, die mir die Bearbeitung dieses interessanten Themas angeboten hat und mich in die faszinierenden Geheimnisse der RNA-Welt eingeweiht hat. Auch für ihre stete Unterstützung in allen wissenschaftlichen und nichtwissenschaftlichen Belangen bin ich ihr besonders dankbar.

Des Weiteren möchte ich Herrn **Professor Dr. Norbert Sewald** danken, dass er trotz vieler anderweitiger Verpflichtungen das Zweitgutachten für diese Arbeit übernommen hat und dass er während meiner Zeit als Stipendiat der Studienstiftung ein hervorragender Vetrauensdozent gewesen ist.

Ein ganz besonderer Dank gilt meinen Kooperationspartnern **Alexander Fuhrmann**, **Dr. Mark Schüttpelz**, **Sven Hennig**, **Prof.'in Dr. Irmtraud Meyer**, **Prof.'in Dr. Eva Wolf**, **Prof. Dr. Dario Anselmetti**, **Prof. Dr. Markus Sauer** und **Prof. Dr. Robert Ros**, die mir sowohl durch ihre Experimente geholfen haben als auch durch viele nützliche Diskussionen. Eine unvoreingenommene Meinung ist oft mehr wert als hundert Bücher!

Allen Mitgliedern der **Arbeitsgruppe Molekulare Zellphysiologie** möchte ich für tolle drei Jahre danken, in denen ich viel Spaß hatte. **Elisabeth Detring**, **Kristina Neudorf** und **Barbara Fuchs** danke ich für exzellente technische Assistenz. Ein besonderer Dank geht an **Daniel Pietsch** für das Korrekturlesen dieser Arbeit und diverse Badminton-Abende. Bei **Martina Lummer** bedanke ich mich für ihre notorisch gute Laune – eine bessere Büro- und Laborkollegin hätte ich mir nicht wünschen können! **Benjamin Sommer** und der **AG Fermentationstechnik** danke ich für schöne Mittags- und Kaffeepausen.

Weiterhin möchte ich mich bei der **Studienstiftung des Deutschen Volkes** für die finanzielle und ideelle Förderung während dieser Doktorarbeit bedanken.

Einen Dank für viele schöne Abende schulde ich **Josi**, **Willi**, **Margeritta** und **Florian**. Letzterem besonders auch für die Übernachtungsmöglichkeit bei Flugreisen...

Einen wesentlichen Anteil an meiner wissenschaftlichen Karriere haben **meine Eltern**. Sie haben mir mein Studium ermöglicht und mich fortwährend unterstützt. Auch für das Korrekturlesen dieser Arbeit möchte ich mich ausdrücklich bedanken. Es gut zu wissen, dass ihr immer hinter mir steht!

Schließlich möchte ich mich bei meiner Freundin **Caterina** für sieben tolle Jahre bedanken. Zwei Naturwissenschaftler unter einen Hut zu bringen, ist sicher keine leichte Sache. Um so schöner finde ich es, dass wir es geschafft haben und du mein Leben bereicherst. Ich liebe dich!

Hiermit versichere ich, dass ich die vorliegende Arbeit ohne fremde Hilfe selbstständig verfasst und nur die angegebenen Quellen und Hilfsmittel benutzt habe. Wörtlich oder dem Sinn nach aus Werken entnommene Stellen sind unter Angabe der Quellen kenntlich gemacht.

Bielefeld, im Dezember 2007

Jan C. Schöning